# Cosmic Origins (COR)

# Program Technology Development

# 2018

# Program Technology Development Quad Charts

## UV/Vis/IR



## Far-IR

# Advanced FUV/UV/Visible Photon-Counting and Ultralow-Noise Detectors

PI: Shouleh Nikzad / JPL

## Objectives and Key Challenges:

- Develop and advance TRL of solar-blind (SB), high-efficiency, photon-counting, and ultralow-noise solid-state detectors, especially in FUV ( $\lambda$ < 200 nm)
- SB silicon, large-format arrays, reliable and stable high response in FUV

## Significance of Work:

- Key innovations are high and stable UV response through atomic-level control of surface and interfaces; the breakthrough in rendering Si detectors with optimized in-band response and out-of-band rejection; versatility with CMOS and CCD

Edge of conduction band for SL doped silicon

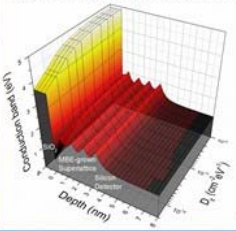


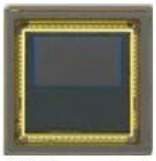

sCMOS example of ultralow-noise CMOS

Superlattice doped EMCCD

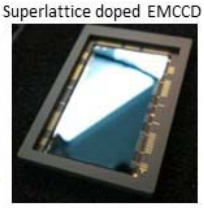

## Approach:

- Fabricate and process UV detectors by superlattice (SL) doping Electron Multiplying CCDs (EMCCDs) and ultralow-noise CMOS wafers
- Develop multi-stack, integrated, SB filters using atomic-layer deposition (ALD)
- Combine integrated SB filters and SL with sCMOS and EMCCDs
- Characterize and validate

## Key Collaborators:

- Chris Martin (Caltech)
- David Schiminovich (Columbia University)
- Michael Hoenk (JPL)
- Teledyne-e2v, Andor , SRI, AMS-CMOSIS, Alacron, STA

## Current Funded Period of Performance:

Jan 2016 – Dec 2018

## Recent Accomplishments:

- ✓ EMCCD wafers processed by SL-doping and coatings
- ✓ Visible-blind filters on functional SL-doped EMCCDs
- ✓ FIREBall detector re checked tested in prep for flight
- ✓ Partnership with CMOS vendors (CMOSIS 7/17, Andor 5/18, SRI 4/17)
- ✓ Radiation testing plan modified following WFIRST protocol
- ✓ Room temperature proton radiation testing on one device

## Next Milestones:

- Optimize detector-integrated filters into functional SLD EMCCDs (July 2018)
- Complete processing: Next batch of SL doped EMCCDs (July 2018)
- Characterize devices pre radiation (July 2018)
- Radiation testing (Aug 2018)
- Process first batch of ultralow noise CMOS wafers (Sep 2018)

## Applications:

- LUVOIR, HabEx, Lynx
- Probes, Explorers, CubeSats

sCMOS $TRL_{In} = 3$ $TRL_{Current} = 3$ $TRL_{Target} = 4\text{-}5$

EMCCD $TRL_{In} = 4$ $TRL_{Current} = 4$ $TRL_{Target} = 5\text{-}6$

Note: TRLs assessed for 2-D, w/integrated filters

# Development of Digital Micro-Mirror Device Arrays for Use in Future Space Missions

PI: Zoran Ninkov / Rochester Institute of Technology

## Objectives and Key Challenges:

- There is a need for a technology to allow for selection of targets in a field of view that can be input to an imaging spectrometer for use in remote sensing and astronomy
- We are looking to modify and develop Digital Micromirror Devices (DMD) for this application

## Significance of Work:

- Existing DMDs need to have the commercial windows replaced with appropriate windows for the scientific application desired. Devices were tested to test for ability to be used in space

Postdoc Vorobiev prepares DMDs for UV scattering measurements at NASA GSFC

## Approach:

- Use available 0.7 XGA DMD devices to develop window removal procedures and then replace delivered window with a hermetically sealed UV transmissive one of Magnesium Fluoride, HEM Sapphire, and fused silica
- Test and evaluate such devices and also Cinema DMDs

## Key Collaborators:

- Sally Heap, Manuel Quijada, Jonny Pellish, and Tim Schwartz (NASA/GSFC)
- Massimo Robberto (STScI)
- Alan Raisanen and Dmitry Vorobiev (RIT)

## Current Funded Period of Performance:

May 2014 – May 2018

## Recent Accomplishments:

- ✓ XGA devices re-windowed successfully
- ✓ Radiation, low temperature and vibration testing shows good results
- ✓ Contrast measurements indicate high contrast
- ✓ Preparations for NASA GSFSC Gamma testing
- ✓ Recoat DMD devices and test

## Next Milestone:

- TRL review (Nov 2018)

## Applications:

- Proposed for Probe mission ATLAS (Astrophysics Telescope for Large Area Spectroscopy) and ISCEA (Infrared SmallSat for Cluster Evolution Astrophysics)

$TRL_{In} = 4$ $TRL_{PI\text{-}Asserted} = 5$ $TRL_{Target} = 5$

# Ultra-Stable Structures: Development and Characterization Using Spatial Dynamic Metrology

PI: Babak N. Saif/GSFC

## Objectives and Key Challenges:

- Develop picometer-level surface metrology of mirrors and structures
- Develop structures and mirrors with controlled dynamics at picometer levels

## Significance of Work:

- Stability and dynamics of large structures and mirrors are required for large space missions such as ATLAST and Exoplanet missions

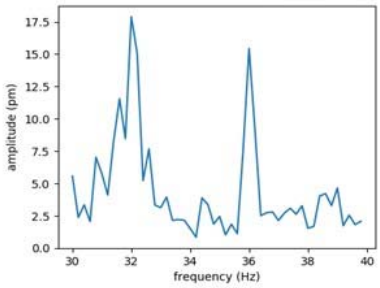


16-pm carbon-fiber motion at 36 Hz

## Approach:

- Work with a vendor to develop a Dynamical Digital Speckle Pattern Interferometer with picometer precision
- Develop an isolated table-top setup to measure dynamics and drift of material and small structures
- Redesign and model dynamics of = measured material/structures

## Key Collaborators:

- Lee Feinberg (GSFC)
- Dave Chaney (Ball Aerospace)
- Marcel Bluth (SGT)
- Perry Greenfield (STSCI)

## Current Funded Period of Performance:

Feb 2016 – Feb 2019

## Recent Accomplishments:

- ✓ ULE® temperature-controlled subsystem delivered to GSFC
- ✓ Completed 16-pm amplitude measurement of carbon fiber

## Next Milestones:

- Measure drift of ULE® subsystem in the chamber
- Develop robust algorithm for drift measurements
- Characterize different carbon-fiber material in thermal vacuum

## Application:

- Future large astronomy/astrophysics missions
- Exoplanet missions

$TRL_{In} = 3$ $TRL_{Current} = 3$ $TRL_{Target} = 4$

# Improving Ultraviolet Coatings and Filters Using Innovative Materials Deposited by ALD

PI: Paul Scowen / ASU

## Objectives and Key Challenges:

- Use a range of oxide and fluoride materials to build stable optical layers using Plasma-Enhanced Atomic Layer Deposition (PEALD) to reduce adsorption, scattering, and impurities
- Layers will be suitable for protective overcoats with high UV reflectivity and unprecedented uniformity (compared to thermal Atomic Layer Deposition, ALD)
- Development of single-chamber system to deposit metal oxide and dielectric layers without breaking vacuum

## Significance of Work:

- The improved ALD capability can help leverage innovative UV/optical filter construction

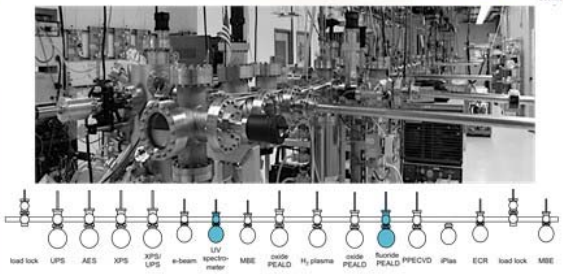


Photograph and schematic of UHV system. The chamber highlighted in blue were constructed for this project. The fluoride PEALD will support oxygen-free deposition and processing, and is in the final stages of assembly.

## Approach:

- Develop existing PEALD system to a single-chamber model
- Demonstrate Al-film deposition
- Demonstrate fluoride deposition on top of Al films
- Demonstrate VUV reflectivity, uniformity, and stability

## Key Collaborators:

- Paul Scowen, Robert Nemanich, Brianna Eller, Daniel Messina, Zheng Ju, Franz Koeck, Hongbin Yu (ASU)
- Tom Mooney (Materion)
- Matt Beasley (Planetary Resources, Inc.)

## Current Funded Period of Performance:

Dec 2015 – Nov 2018

## Recent Accomplishments:

✓ RF plasma system successfully tested on PEALD

## Next Milestone:

- Complete PEALD system (Aug 2018)
- Demonstrate deposition of Al films using PEALD and measure UV reflectivity to better than 3% accuracy (Aug 2018)
- Upgrade in-situ VUV spectrometer to measure performance from 254 nm to 90 nm (Sep 2018)

## Applications:

- LUVOIR / HDST / ATLAST / HabEx

$TRL_{In} = 3$ $TRL_{Current} = 3$ $TRL_{Target} = 4$

# High-Performance Sealed-Tube Cross-Strip Photon-Counting Sensors for UV-Vis Astrophysics Instruments

PI: Oswald Siegmund / UC Berkeley

## Objectives and Key Challenges:

- Exploit developments in atomic-layer-deposited microchannel plates (MCPs), photocathodes, and cross strip (XS) readout techniques to implement a new generation of enhanced-performance sealed-tube photon-counting sensors that span the 115-nm-to-400-nm regime; subcomponent areas have achieved considerable technical development, but putting them into a robust, integrated package, advancing the TRL from 4 to 6 for the next UV-Vis astrophysics instruments has not yet been attempted

## Significance of Work:

- Format, performance, and capabilities of the scheme is directly relevant to the requirements specified for CETUS, LUVOIR and HABEX, as well as SMEX and SmallSat efforts

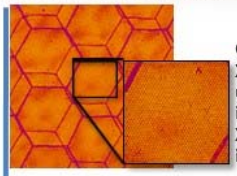

Commissioning of MCP test system with 50-mm XS anode; a pair of ALD MCPs with 20-μm pores used to detect 185-nm UV (~$1 \times 10^9$ photons); image shows MCP hexagonal packing structure; XS anode and PXS-2 electronics resolves the individual 20-μm MCP pores over the whole FOV

CsI opaque photocathode deposited onto ALD 33-mm MCP for cathode evaluation

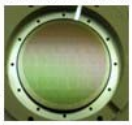

## Approach:

- Adopt current Photonis Planacon 50-mm device and implement the new technologies within this envelope
  - Implement UV $MgF_2$ entrance window and UV-optimized bialkali semitransparent photocathode with narrow (~200-μm) proximity gap
  - Replace standard MCPs with two ALD MCPs, depositing an opaque UV photocathode onto MCP input surface
  - Replace pad-array anode with XS anode readout

## Key Collaborators:

- Incom Inc, Photonis USA, Elcon

## Current Funded Period of Performance:

Jan 2018 – Dec 2020

## Recent Achievements:

- ✓ Atomic layer deposited MCPs: visited MCP fab facility; reviewed and set production parameters; Ordered large-area-format ALD MCPs with 10-μm pores
- ✓ XS anodes and electronics: commissioned 50-mm test system with electronics; resolved 20-μm ALD MCP pores; ordered and received initial batch of 47-mm XS anodes for sealed tubes
- ✓ Photocathodes in the UV-VIS: multialkali UV photocathode trials on $MgF_2$ windows in tank, process underway; alkali-halide opaque photocathode deposited on ALD MCP and in testing
- ✓ Sealed tubes: met vendor, set process sequences, placed initial order

## Next Milestones:

- Test 10-μm pore sample MCPs
- Measure bialkali and alkali-halide photocathode performance
- Planacon body-anode seal tests and XS anode validations

## Applications:

- Explorer, Probe class (CETUS), Flagship (LUVOIR, HABEX), Suborbital
- Planetary and Earth-observing missions
- Homeland security, biological imaging, high energy physics

$TRL_{In} = 4$ $TRL_{Current} = 4$ $TRL_{Target} = 6$

# Advanced UVOIR Mirror Technology Development for Very Large Space Telescopes

PI: H. Philip Stahl/MSFC

## Objectives and Key Challenges:

- Advance TRL of key technology challenges for the primary mirror of future large-aperture Cosmic Origins UVOIR space telescopes
- Enable monolithic and segmented mirror design paths
- Conduct prototype development, testing, and modeling
- Trace metrics to science mission error budget

## Significance of Work:

- Deep-core manufacturing method enables 4-m-class mirrors with 20-30% lower cost and risk
- Design tools increase speed and reduce cost of trade studies
- Integrated modeling tools enable better definition of system and component engineering specifications

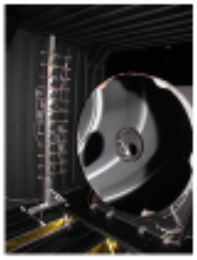

1.5m Harris testing in XRCF

Schott mirror testing in XRCF

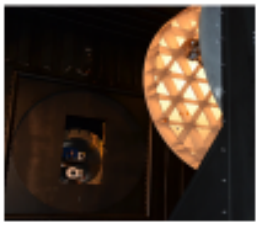

## Approach:

- Science-driven systems engineering
- Mature technologies required to enable highest-priority science and result in high-performance, low-cost, low-risk system
- Provide options to science community by developing technology enabling both monolithic- and segmented-aperture telescopes
- Mature technology in support of 2020 Decadal process

## Key Collaborators:

- AMTD team at MSFC
- Stuart Shaklan (JPL)
- Carl Rosati, Rob Egerman, and Katie Hannon (Harris)
- Steve Sokach (Schott)
- Tony Hull (UNM)
- Martin Valente (AOS)
- Gary Mosier (GSFC)

## Funded Period of Performance:

Sep 2011 – Dec 2017

## Accomplishments:

- ✓ Demonstrated stacked-core process at Harris Corp by making a 0.4m dia x 0.4m thick cut out of 4m mirror and a 1.5m ULE® mirror.
- ✓ Learned lessons about slumping thick mirrors.
- ✓ Made as-built finite element models of both mirrors using Computed Tomography of internal structure and CTE map data.
- ✓ Validated and correlated model by thermal and mechanical test.
- ✓ Thermal and modal characterization of Schott & Harris mirrors
- ✓ Characterized flight traceable mirror mounts for WFIRST.
- ✓ Created Arnold Mirror Modeler and transferred it to industry.
- ✓ Created tool to analyze interaction between optical telescope wavefront stability and coronagraph contrast leakage.
- ✓ Created Thermal MTF tool for designing thermally stable telescope.

## Applications:

- Flagship optical missions; Explorer-type optical missions
- Department of Defense and commercial observations

$TRL_{In} = 3$ $TRL_{Current} = 3$ $TMB_{Final} = 4$

*(values depend on specific technology)*

# Predictive Thermal Control (PTC) Technology to Enable Thermally Stable Telescopes

PI: H. Philip Stahl / MSFC

## Objectives and Key Challenges:

- Validate models that predict thermal optical performance of real mirrors and structure based on their structural designs and constituent material properties, i.e. CTE distribution, thermal conductivity, thermal mass, etc.
- Derive thermal system stability specifications from science-driven wavefront-stability requirement
- Demonstrate utility of PTC system for achieving thermal stability

## Significance of Work:

- Thermally stable space telescopes enable the desired science of potential HabEx and LUVOIR missions
- Integrated modeling tools enable better definition of system and component engineering specifications

Testing surface shape response of 1.5-m ULE® mirror to thermal lamp array inside X-Ray & Cryogenic Facility (XRCF)

## Approach:

- Science-driven systems engineering
- Mature technologies required to enable highest-priority science and result in high-performance, low-cost, low-risk system
- Mature technology in support of 2020 Decadal process

## Key Collaborators:

- Thomas Brooks, Richard Siler and Ron Eng (MSFC)
- Carl Rosoti, Keith Harvey, and Rob Egerman (Harris Corp)

## Current Funded Period of Performance:

Jan 2017 – Sept 2020

## Recent Accomplishments:

- ✓ Created high-fidelity model of 1.5-m ULE® mirror using X-Ray CT dimensional data and Corning CTE map
- ✓ Tested 1.5-m ULE® mirror with lamp array and correlated with model
- ✓ Specified and designed PTC heater system for 1.5-m ULE® mirror
- ✓ Presented progress results at Tech Days 2017

## Next Milestones:

- Initiate PTC rear heater system fabrication (7/2018)
- Design and fabricate forward cold sink (9/2018)
- Potentially initiate an Aluminum Test Mirror (8/2018)

## Applications:

- Flagship optical missions; Explorer-type optical missions
- Department of Defense and commercial observations

$TRL_{In} = 3$ $TRL_{Current} = 3$ $TRL_{Target} = 4 - 5$

*(values depend on specific technology)*

# Development of Large-Area (100 cm$^2$) Photon-Counting UV Detectors

PI: John Vallerga / UC Berkeley

## Objectives and Key Challenges:

- A 50 mm x 50 mm XS MCP photon-counting UV detector was previously developed, achieving high spatial resolution (15 µm) at low gain (500k) and high input flux (MHz). The detector was then environmentally qualified. Two ASICs (CSAv3 and HG2) were also fabricated to improve this performance. This program continues development by scaling the detector format to 100 mm x 100 mm while updating the ASICs for lower power and simpler layout.
- Combining our two existing ASIC designs into one ASIC ("GRAPH") using 130-nm CMOS technology
- Maintaining noise performance with analog and digital circuits on same die
- Developing a new 100 mm x 100 mm MCP detector with the new electronics and testing it environmentally

## Significance of Work:

- Allow high-speed, photon-counting UV detection in package small enough and low enough power and mass to be usable in space

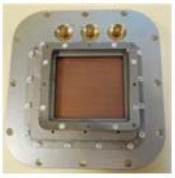

Existing 50-mm detector (without MCPs)

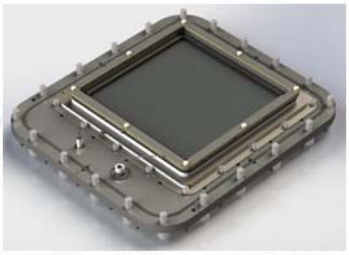

100-mm MCP detector with ASIC electronics qualified for flight

## Approach:

- Scale up the 50 mm x 50 mm detector design by a factor of two to create a flight-qualified 100 mm x 100 mm design that can be environmentally tested for thermal and vibration stability
- Test the sensitivity of both ASICs to radiation, both total ionizing dose and single event upsets
- Convert the HG2 ASIC design into 130-nm CMOS technology and combine with the existing CSAv3 design into a single die
- In parallel, design and construct an FPGA readout circuit for these new ASICs

## Key Collaborators:

- Prof. Gary Varner (U. Hawaii)
- Dr. Oswald Siegmund (U.C. Berkeley)

## Current Funded Period of Performance:

Apr 2016 – Mar 2019

## Recent Accomplishments:

- ✓ 100-mm detector fabricated
- ✓ Detector imaging performance with PXS electronics
- ✓ Vibration-tested 100-mm detector
- ✓ Converted HG2 design to GRAPH in 130-nm CMOS

## Next Milestones:

- Submit GRAPH ASIC to foundry (July 2018)
- Fabrication and performance testing of GRAPH (fall 2018)
- GRAPH ASIC integration with control FPGA boards (winter 2018)
- Test full ASIC electronics with detector (winter 2018)

## Applications:

- High performance UV (1-300 nm) detector for astrophysics (LUVOIR, ANUBIS, CETUS), planetary, solar, heliospheric, or aeronomy missions
- Particle or time-of-flight detector for space physics missions
- Neutron radiography/tomography for material science

$TRL_{In} = 4$ $TRL_{Current} = 4$ $TRL_{Target} = 5$

# Ultra-Sensitive Bolometers for Far-IR Spectroscopy at the Background Limit

PI: C.M. (Matt) Bradford / JPL

## Objectives and Key Challenges:

- Demonstrate readiness with a far-IR detector system which can operate at or near the natural space-borne backgrounds for moderate-resolution spectroscopy with large pixel formats
- Targeting large arrays of detectors with sensitivity of $1\times10^{-19}$ $WHz^{-1/2}$; goal is to obtain $3\times10^{-20}$ W $Hz^{-1/2}$.

## Significance of Work:

- The far-IR is a scientifically vital but technically underserved waveband for astrophysics; no commercial or industrial detector options exist
- A robust high-performance far-IR detector system is the primary tall pole enabling powerful future far-IR missions
- Observing speed improvements of $>10^6$ are possible just with a cold telescope, a simple spectrometer, and suitable detector arrays

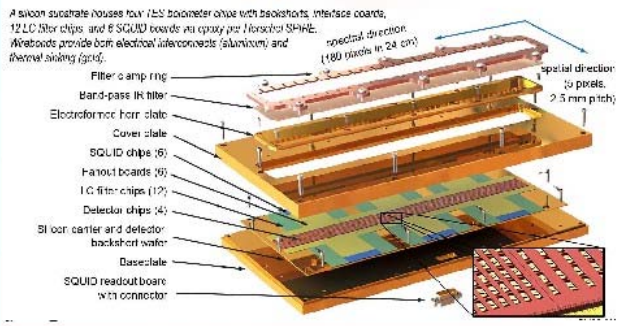


## Approach:

- We are building on our success with transition-edge-sensed (TES) bolometers in APRA and internally funded programs at JPL
- We have demonstrated the required sensitivity, but our devices are too slow due to the dry-etch processing; other processing techniques exist and can be implemented
- We will implement a frequency-domain multiplexing readout system developed by our collaborators at the Space Research Organization of the Netherlands (SRON)

## Key Collaborators:

- M. Kenyon, M. Runyan, and P. Echternach (JPL)
- D. Audley, R. Hijmering, P. Khosropanah, and P. Roelfsema (SRON)

## Current Funded Period of Performance:

Dec 2017 – Oct 2020

## Recent Accomplishments:

- ✓ Dilution refrigerator specified and ordered (arriving July)
- ✓ Designed test array with various approaches to TES suspension
- ✓ Developed new wet-release process for suspended bolometers, demonstrating released devices with geometry suitable for $1\times10^{-19}$ $WHz^{-1/2}$ NEP

## Next Milestones:

- Bring fridge online (Sep 2018)
- Design and assemble 50-mK test assembly accommodating bolometers, LC MUX chips, SQUID, and filters (Jan 2019)
- Add metal layers to prototype detector arrays (Jan 2019)

## Applications:

- Space Infrared Telescope for Cosmology and Astrophysics (SPICA)
- Origins Space Telescope (OST)
- Far-IR Probe-class missions, e.g. the Galaxy Evolution Probe (GEP)

$TRL_{In} = 4$ $TRL_{Current} = 4$ $TRL_{Target} = 6$

# Raising the Technology Readiness Level of 4.7-THz Local Oscillators

PI: Qing Hu / MIT

## Objectives and Key Challenges:

- This project seeks to raise the TRL of 4.7-THz local oscillators (LOs) based on THz quantum-cascade lasers
- The key challenges are to increase the output power level from the current level of <1 mW to 5 mW, and to increase the operating temperature from a lab-demonstrated ~10 K to ~40 K that can be provided in a space-based or suborbital observatory

## Significance of Work:

- The 4.744 THz [OI] fine-structure line is the dominant cooling line of warm, dense, neutral atomic gas; observation of this line will provide valuable information for studies of cosmic origins
- This project will be important to the recently initiated GUSTO project

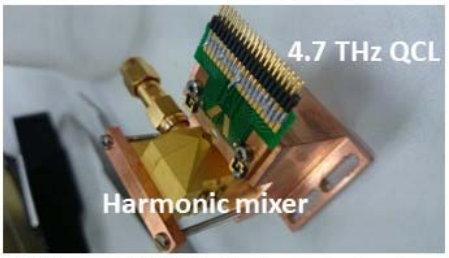


Array of DFB lasers at ~4.7 THz. The harmonic mixer is used to phase-lock the QCL LO.

## Approach:

- Develop perfectly phase-matched 3rd-order DFB structures at 4.7 THz with robust single-mode operations with good beam patterns
- Develop phase-matched 3rd-order DFB structures coupled with integrated antennae to increase the output power level to ~5 mW, and to increase the wall-plug power efficiency to 0.5%

## Key Collaborators:

- J.L. Reno (Sandia Nat'l Lab)
- J.R. Gao (SRON/Delft)

## Current Funded Period of Performance:

Mar 2016 – Feb 2019

## Recent Accomplishments:

- ✓ Fabricated perfectly phase-matched 3rd-order DFB lasers around 4.7 THz
- ✓ Developed a novel scheme to electrically tune the frequency by ~10 GHz (at a center frequency of ~3.9 THz, but the method can be applied to 4.7 THz once the gain medium is available)

## Next Milestones:

- Characterize the power, frequency, and beam patterns of the fabricated devices (Feb 2019)

## Application:

- GUSTO (The Gal/xgal U/LDB Spectroscopic/Stratospheric THz Observatory)

$TRL_{In} = 3$ $TRL_{PI\text{-}Asserted} = 4$ $TRL_{Target} = 5$

# Advancing Focal Plane TRL for LiteBIRD and other Next Generation CMB Space Missions

PI: Adrian Lee / Berkeley, SSL

## Objectives and Key Challenges:

- Advance TRL for US contribution to JAXA LiteBIRD CMB Mission
  - Develop flight specification arrays
  - Cosmic-ray deadtime mitigation
  - Launch vibration survival
  - Develop flight specification cold readout
  - Simulate detector performance in mission

## Significance of Work:

- Science goal to understand the physics of the Big Bang
- JAXA Main Mission with US Mission of Opportunity
- US detectors/readout are key technologies
- Applicable to any space mission from far-IR to mm-wave bands

Drawing of LiteBIRD focal planes behind low- and high-frequency telescopes. Focal plane 30 × 40 $cm^2$ in size

## Approach:

- Detector Array Fabrication at U.C. Berkeley and NIST
- Colorado and Stanford: Array Testing
- UCSD: Cold Readout Development + Test
- SSL/LBNL: Full Mission Data Simulation

## Key Collaborators:

- Julian Borrill, Toki Suzuki, Ellen Taylor, Dave Curtis (Berkeley, SSL)
- Nils Halverson (University of Colorado, Boulder)
- Hannes Hubmayr, Gene Hilton (NIST)
- Kam Arnold (UCSD)
- Chao-lin Kuo and Keith Thompson (Stanford University)

## Current Funded Period of Performance:

Oct 2017 to Oct 2020

## Recent Accomplishments:

- ✓ Demonstrated low response to radioactive source
- ✓ Demonstrated mission-specific TES detectors

## Next Milestones:

- Further cosmic-ray susceptibility tests with radioactive sources (Jan 2019)
- Achieve flight specification single pixels (Sep 2019)
- Measure resonance frequencies of detector modules (Sep 2019)
- Test flight-specification SQUID amplifiers (Sep 2019)
- Simulate one month of flight data (Sep 2019)

## Applications:

- LiteBIRD
- PICO (US Probe study)
- Other far-IR or sub-mm missions

$TRL_{In} = 3$ $TRL_{Current} = 3$ $TRL_{Target} = 5\text{-}6$

# Development of a Robust, Efficient Process to Produce Scalable, Superconducting Kilopixel Far-IR Detector Arrays

PI: Johannes Staguhn / JHU & GSFC

## Objectives and Key Challenges:

- Demonstrate a versatile scheme to connect 2-dimensional superconducting detectors and cold readout electronics through a separate silicon structure with superconducting through-wafer vias
- Reduction in complexity of individual components in detector arrays for astronomy applications
- Need to identify problem sources such as metal-to-metal interfaces

## Significance of Work:

- An important step in enabling large detector arrays for major suborbital and space-based Far-IR observatories, such as the Origins Space telescope (OST)

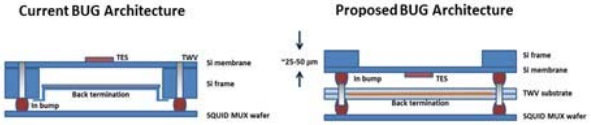


Cross-section view schematics of current and proposed Backshort Under Grid (BUG) detector architecture; in the current embodiment, the through-wafer vias are integrated in the array wafer, but are in a separate wafer in the proposed architecture

## Approach:

- Reduce complexity of individual components in superconducting arrays for Far-IR astronomy
- Systematic studies of component interface issues
- Development of test plan that allows separate tests for each potential failure mode

## Key Collaborators:

- S. Harvey Moseley, Ari Brown, Ed Wollack, Karwan Rostem, Elmer Sharp and Steve Maher (NASA/GSFC)
- Gene Holton (NIST-Boulder)
- Kent Irwin (Stanford)

## Current Funded Period of Performance:

Jan 2018 – Dec 2019

## Recent Accomplishments:

- ✓ Finished layout of test wafer and started production
- ✓ Refined design of multiplexer readout board
- ✓ Designed test detector pixels and detector array, started preparations for production

## Next Milestones:

- Develop through-wafer via substrate fabrication process, refine double bond hybridization, and prepare for device tests
- First iteration of detector fabrication and tests/characterization; delivery of uWave SQUID multiplexers (Dec 2018)

## Applications:

- Super Hirmes for SOFIA
- Origins Space Telescope (OST)

$TRL_{In} = 3$ $TRL_{Current} = 3$ $TRL_{Target} = 5$

# High-Efficiency Continuous Cooling for Cryogenic Instruments and sub-Kelvin Detectors

PI: James Tuttle / GSFC

## Objectives and Key Challenges:

- Bring to TRL 6 a cooling system that provides:
  - Continuous cooling at T < 50 mK; rejecting heat at 10 K
  - Cooling power > 10 times that of current flight Adiabatic Demagnetization Refrigerator (ADR) at 50 mK
  - Continuous cooling at 4 K for telescopes, optics, etc.
  - Low external magnetic field: |B| < 5 μT
  - Simple, efficient, vibration-free operation
  - Proven reliability; no moving parts

## Significance of Work:

- System will exceed requirements of currently conceived cryogenic detector arrays

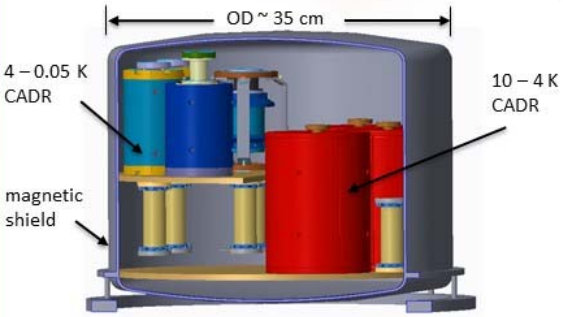


## Approach:

- Adiabatic Demagnetization Refrigerator
  - Paramagnetic salts heated/cooled by changing magnetic field
  - Heat pumped between stages separated by heat switches
  - Control of heat transfer provides continuous cooling at selected stages (50 mK, 4 K); continuous ADR (CADR)
  - Advanced magnetic shielding eliminates stray fields

## Key Collaborators:

- Amir Jahromi, Ed Canavan, Hudson DeLee, Mike DiPirro, Mark Kimball, Peter Shirron, Dan Sullivan, and Eric Switzer (NASA/GSFC)

## Current Funded Period of Performance:

Jan 2017 – Dec 2019

## Recent Accomplishments:

- ✓ Assembled a designed-for-flight single-stage 10 – 4 K ADR
- ✓ Measured ADR's cooling capability and recycle time
- ✓ Performed extensive analysis based on ADR test results
- ✓ Made minor design modification based on analysis
- ✓ Continued procurement of parts, supplies and equipment
- ✓ Began parallel study of vibration-heating in Kevlar suspension

## Next Milestones:

- Demonstrate 10-to-4-K CADR (Dec 2018)
- Demonstrate pre-vibe 10-to-0.05-K CADR (Sep 2019)
- Demonstrate post-vibe 10-to-0.05-K CADR (Dec 2019)

## Applications:

- OST (FIP, OSS and MISC instruments), Lynx, PICO, GEP
- Possibly LiteBIRD

$TRL_{In} = 3 - 5$ $TRL_{Current} = 3 - 5$ $TRL_{Target} = 6$

# Program Technology Development Status

## UV/Vis/IR



## Far-IR

# Advanced FUVUV/Visible Photon Counting and Ultralow Noise Detectors

Prepared by: Shouleh Nikzad (PI; JPL), Chris Martin (Caltech), David Schiminovich (Columbia U), and Michael Hoenk (JPL)

## Summary

In this three-year SAT effort that began in January 2016, we develop and advance the technology readiness level (TRL) of solar-blind, high-efficiency, photon-counting, low-noise solid-state detectors in ultraviolet (UV) with emphasis on far ultraviolet (far-UV) with λ < 200 nm. We combine superlattice doping (SL, Fig. 1), integrated solar blind (SB) filters (Fig. 2), antireflection (AR) coatings, and ultra-low-noise scientific CMOS (e.g., sCMOS) and large format electron multiplying CCDs (EMCCDs). We fabricate, characterize, and validate these detectors in a relevant space environment.

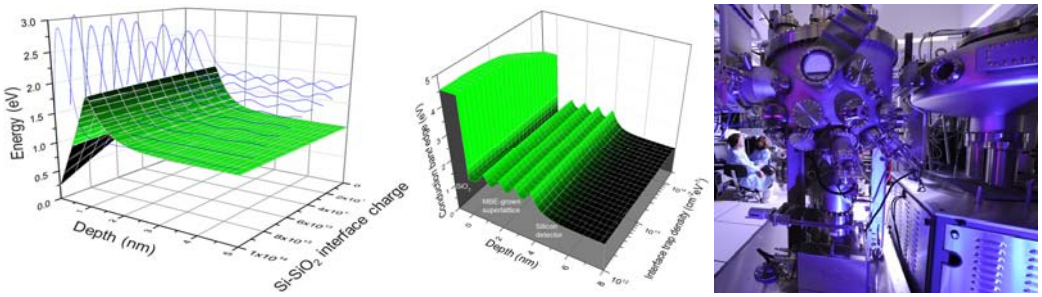


***Fig. 1.*** Left and Middle: *Band diagram of delta-doped and superlattice-doped silicon surfaces.* Right: *Superlattice doping is a molecular beam epitaxy (MBE) process performed in the 8"-wafer-capacity silicon MBE at JPL.*

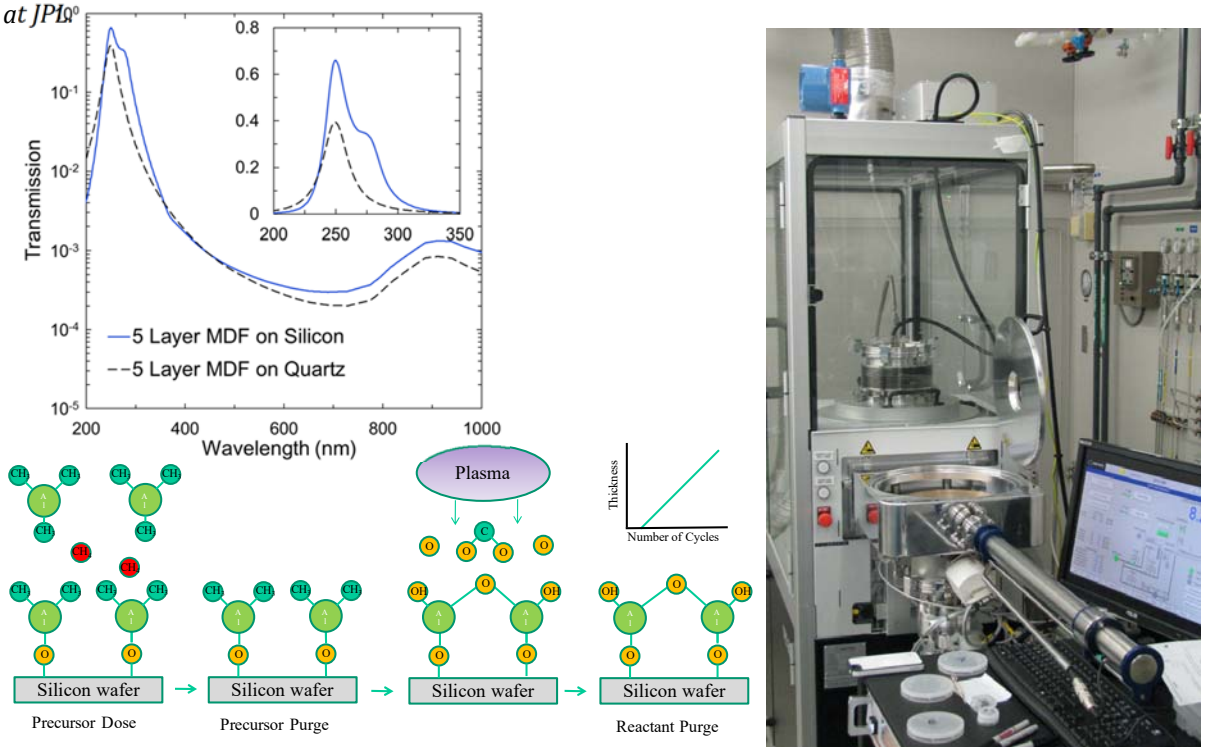

***Fig. 2.*** Top Left: C*alculated performance of a five-layer metal-dielectric filter on Si or quartz substrates, showing in-band QE > 60% and out-of-band rejection approaching $10^{-4}$. This is an example of detector-integrated filters that can render silicon "solar blind."* Bottom Left: *Diagram of ALD process showing its layer-by-layer-controlled nature.* Right: JPL *ALD system used for deposition of these metal-dielectric layers.*

The detectors under development in this effort offer potentially game-changing performance and capabilities, directly addressing the Technology development for Cosmic Origins (TCOR) requirements outlined in the SAT call for detectors with high quantum efficiency (QE) in $\lambda < 200$ nm, large format, photon-counting capability, and ultra-low noise. High-performance UV detector and coating technologies will be an essential part of the Large UV/Optical/Infrared (LUVOIR) Surveyor, a leading contender to be one of NASA's next astrophysics flagship missions. Additionally, the photon-counting capability and ultralow noise in either UV or visible will have a high impact on the Habitable Exoplanet Observatory (HabEx). Because of the dramatic efficiency increase in the detector, flagship-class science will be possible with smaller size apertures. This effort is also likely to have a great impact on future Probe- and Explorer-class missions. Our coating processes, with films prepared by atomic layer deposition (ALD), also advance UV coatings for optics.

Superlattice doping (or multilayer delta doping, Fig. 1) was invented at JPL [1] and proven to achieve high internal QE on electron EMCCDs and CMOS arrays [2-6]. Superlattice-doped EMCCDs and superlattice-doped CMOS are at TRL 4. Integrated visible-rejection filters have been demonstrated and proven on avalanche photodiodes and extensively tested [7]; they are at TRL 3. The resulting combination of these superlattice-doped, AR-coated (SLAR) and Solar-Blind (SB) EMCCD [8, 9] and sCMOS arrays is at TRL 3. Furthermore, we will extend the capability to $\lambda < 200$ nm. All devices will be produced to meet our QE, noise, and visible rejection requirements; will be thermally cycled and characterized; and validated in a relevant radiation environment to raise them to TRL 4-5 by the end of this three-year effort.

Our team comprises members with complementary expertise in materials, detectors, instrument building, and observational science. The team is uniquely qualified to carry out the proposed work. By forming alliances between technology developers, instrument builders, and mission Principal Investigators (PIs) such as Prof. Schiminovich and Prof. Martin (PIs of GALEX as well as suborbital missions such as FIREBALL), our team has a natural path for TRL advancement and flight insertion.

## Background

The 2010 Decadal Survey, "*New Worlds, New Horizons in Astronomy and Astrophysics*" (NWNH) [10] recommends, as a priority, path-finding work towards a 4m+ UV/Optical flagship mission as a successor to the HST. Great emphasis on Explorer missions is also anticipated in this decade.

Recently, mid-decadal studies have been ongoing that build on the work of the NWNH. These studies have consistently set forth technology development goals aimed at enabling a future large-aperture, UVOIR flagship mission as a successor to the Hubble Space Telescope, and increasing the scientific reach of smaller missions in this decade. The Cosmic Origins Program Analysis Group (COPAG) is now evaluating and recommending technology investments towards these goals through Science Interest Groups (SIGs). In addition, a new Technology Interest Group (TIG) is reviewing technology gaps. In these scientific focus areas, single-photon-counting or ultra-low-noise detectors are a priority. Furthermore, these recommendations set as a goal, very-large-format (100 Megapixel to Gigapixel), high-QE, UV-sensitive detectors**.** These recommendations reflect the new understanding of the scientific opportunities enabled by technological breakthroughs in large-scale detector fabrication.

Our objectives are tied to the needs of and recommendations for future missions mentioned in NWNH, guided by mid-decadal studies being carried out by COPAG and the Association of Universities for Research in Astronomy (AURA), and updated per the needs of flagship concepts such as LUVOIR and HabEx.

Frontier astrophysical investigations are necessarily conducted at the limits of resolution, etendue, and sensitivity. A future 10-m UV/Optical telescope mission will require significant detector advances beyond HST, GALEX, and FUSE detector technologies, particularly in QE, spectral responsivity in the UV, resolution, and pixel count. Our primary performance metric, detector QE in the UV, represents a dramatic increase (5-10x) over previous missions. Dramatically increasing detector efficiency could allow Explorer-class or Probe-class missions to perform flagship-mission science.

A solid-state detector with high efficiency and photon counting offers scalability and reliability that are necessary and attractive features for reliable, high-performance, and cost-effective instruments. LUVOIR's requirements are directly applicable to the objectives of this effort. Additionally, detectors developed under this SAT but optimized for visible light would also have a high impact on HabEx.

## Objectives and Milestones

Table 1 shows the project's milestones and schedule.

| Milestone | Year 1 | | | | Year 2 | Year 3 |
|---|---|---|---|---|---|---|
| | Q1 | Q2 | Q3 | Q4 | | |
| **Demonstrate solar-blind, SLAR EMCCD** | | | | | | |
| Procure wafers of standard larger-format EMCCDs | Δ | | | | | |
| Thin, bond, and SL-dope wafers | | | | | | |
| Incorporate advanced ALD filters (200-240 nm) | | | | | | |
| **Demonstrate solar-blind, SLAR, low-noise CMOS** | | | | | | |
| Select low-noise CMOS design | | | | | | |
| Procure wafers of low-noise CMOS (e.g., sCMOS) | | | | | | |
| Thin, bond, and SL-dope sCMOS | | | | | | |
| Incorporate advanced ALD filters (200-240 nm) | | | | | | |
| **Extend visible-blind filter to FUV** | | | | | | |
| Extend multilayer design to center at 140 or 150 nm | | | | | | |
| Integrate with SLAR EMCCD | | | | | | |
| Integrate with SLAR sCMOS | | | | | | |
| **Validation and environmental testing** | | | | | | |
| Test noise and QE with temperature and illumination. Lifetime testing. | | | | | | |

***Table 1.*** *Project milestones and schedule.*

## Progress and Accomplishments

Progress in all aspects of development milestones are discussed here. These include fabricating and producing delta/superlattice-doped EMCCDs, superlattice-doped CMOS, out-of-band-rejection integrated filters, environmental testing for TRL advancement, and suborbital and orbital flight-path planning and progress is discussed. In addition to technical progress detailed below, publication,

programmatic activities, professional society activities, and professional honors and awards are also included in this report.

EMCCD wafers were procured and received. These wafers were used to produce the superlattice-doped, coated and uncoated EMCCDs using the process outlined in Fig. 3. This included bonding to "handle" or "support" wafer sprior to thinning—final thickness decisions depends on the extent of depletion region and passivation capability for dark-noise reduction. In the first batch of wafers, we implemented on one wafer superlattice doping and single-layer $Al_2O_3$ coating designed for the Faint Intergalactic Redshifted Emission Balloon (FIREBall) balloon experiment, funded by the Astrophysics Research and Analysis (APRA) Program. Several devices were subsequently coated with multilayer dielectrics after they were diced. All devices were packaged, and detailed characterization was performed to determine optimal performance. Testing and characterizations were performed both at JPL and Caltech (in photon-counting mode) and as a team, cross-checking results and verifying performance measured previously on superlattice-doped devices at e2v. As part of validation, devices were taken to Palomar for on-sky data validation using the Cosmic Web Imager (CWI). Photon-counting, low-noise, and QE performance were verified.

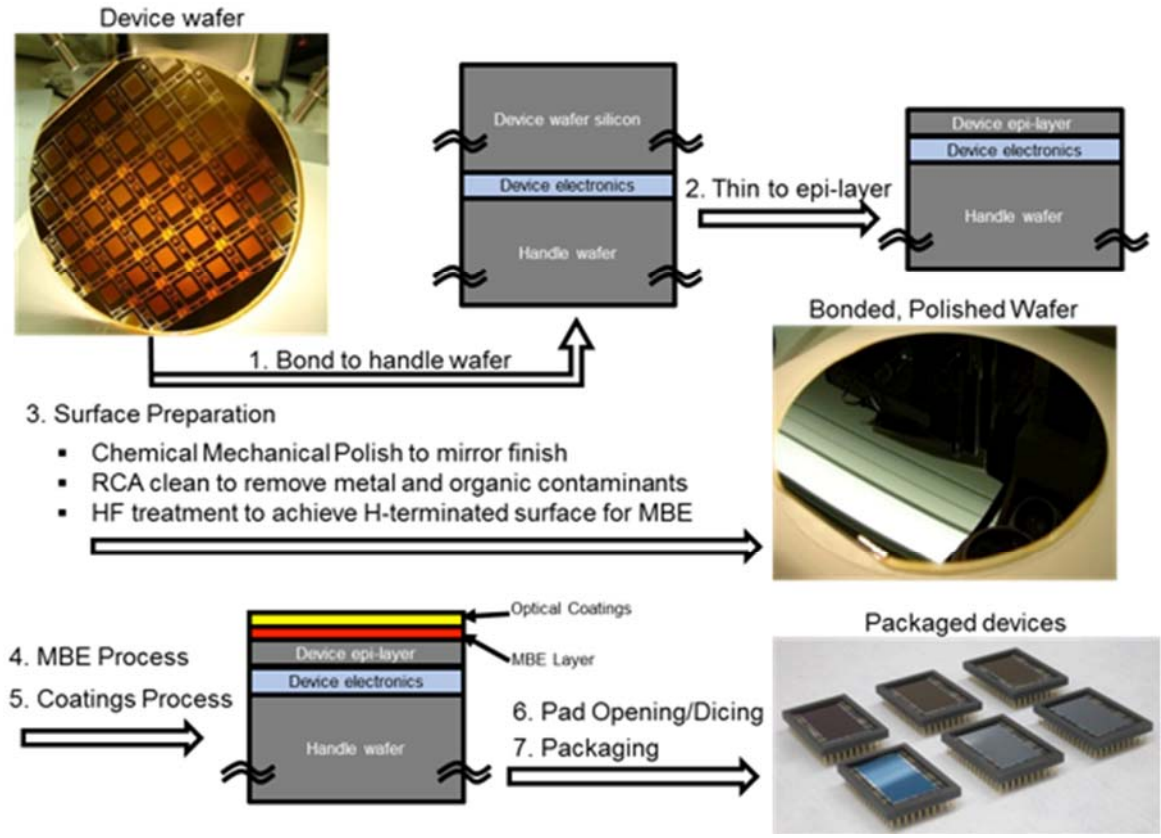


***Fig. 3.*** *End-to-end post-fabrication processing shown for EMCCD device wafer. Results of some of these were published [12,13].*

Upon receipt of full funding for 2017, discussions resumed with Andor, Sarnoff, and potentially e2v regarding acquiring wafers containing sCMOS or other low-noise CMOS devices. We had contacted top groups in ultra-low-noise CMOS development such as Fairchild for sCMOS, Celeaste, e2V, Sarnoff, AMS-CMOSIS, and Rutherford Appleton Laboratory (RAL) regarding wafer procurement and collaboration. NDA were executed with Sarnoff, Andor, AMS-CMOSIS, and others as potential CMOS suppliers. Wafers and wafer fractions from two vendors have been received. Because some of these

wafers were not fabricated for back illumination (BI), extra processing steps and additional NDAs with foundries were required. These activities are well underway.

Metal dielectric filters for enhancement in the 140-150 nm wavelength range were designed. In collaboration with end users, the 150-175 nm band was identified as potentially useful. The latter design was implemented in a silicon wafer. The designed layers were also implemented in non-functional superlattice-doped EMCCDs to check for and address mechanical issues. These designs are ready for integration into functional superlattice-doped EMCCDs.
Prototype devices have been fabricated with five-layer $Al/AlF_3$ model dielectric function (MDF). Reflectance measurements show good agreement with the model (Fig. 4), as do relative QE measurements (Fig. 5).

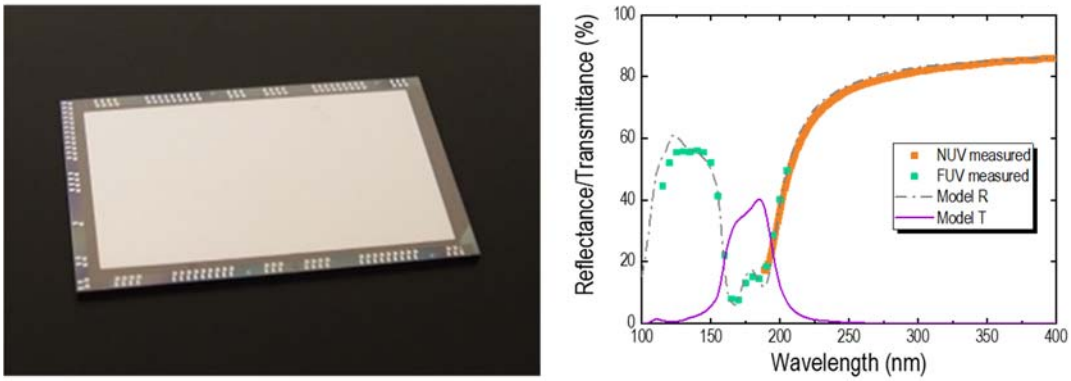


***Fig. 4.*** Left: *Prototype device with an integrated, five-layer, $Al/AlF_3$ MDF.* Right: *Reflectance measurement from the sample on the left showing good agreement with the model.*

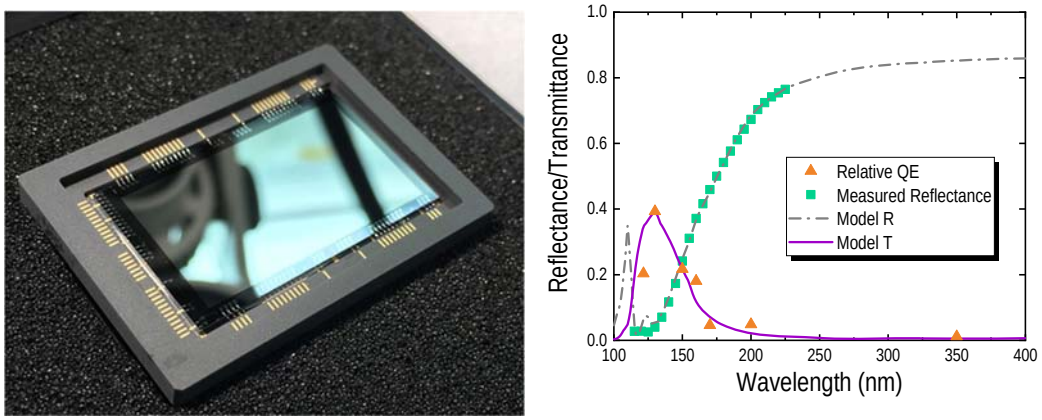


***Fig. 5.*** Left: *Prototype device with an integrated, five-layer, $Al/AlF_3$ MDF.* Right: *Relative QE measurements show out-of-band rejection that agrees with the model.*

Our TRL advancement plan uses environmental testing, and suborbital and small-sat flights. Superlattice-doped and AR-coated devices are due to fly on FIREBall-2 (Fig. 6) in September 2018, and superlattice-doped devices with out-of-band-rejection integrated filters are due to fly on SHIELDS (Fig. 7), a heliophysics sounding rocket in the fall of 2019.

***Fig. 6.*** Left: *FIREBall undergoing on-sky calibration in Ft. Sumner, NM.* Left: *FIREBall detector with three-layer dielectric delivering QE > 60%.*

***Fig. 7.*** *SHIELDS rocket at University of Arizona. The superlattice-doped device with integrated out-of-band-rejection filter is under development and is planned to fly on this rocket in the fall of 2019.*

SHIELDS is a funded sounding rocket led by Prof. Walter Harris at the University of Arizona. Professor Harris in part of the LUVOIR Science and Technology Definition Team (STDT). A superlattice EMCCD with detector-integrated filters optimized for 120-140 nm ($10^{-3}$ out-of-band rejection) is under fabrication and optimization.

Environmental testing is part of this effort. Thermal cycling has been an ongoing part of device characterization as devices are cycled from room temperature to cold (down to -100°C). This year, we also focused on radiation testing. We chose the test protocol of the Wide-Field Infrared Survey Telescope (WFIRST). In early June 2017, one superlattice-doped EMCCD was taken along with several WFIRST EMCCDs to a Loma Linda local hospital's radiation facility for room-temperature testing. Several devices were selected and are under characterization for FIREBall-2, an APRA-funded balloon-borne experiment to study emissions from intergalactic medium and circum-galactic medium. FIREBall-2 depends on high-efficiency photon-counting detectors. A superlattice-doped device was delivered in the previous reporting period, custom-coated with three dielectric layers optimized for FIREBall's narrow atmospheric UV window centered on 205 nm. The detector was tested at Prof. Martin's Caltech lab, at Palomar for photon counting capability, and at system level by the FIREBall-2 team using the entire FIREBall-2 spectrograph system. The detector was tested to show photon-counting, and nearly 60% QE (5× better than FIREBall's MCP detector response). A device with three-layer coatings was selected for flight for good cosmetics and excellent performance. The FIREBall team was ready to fly in September 2017 but unfortunately due to weather and safety concerns unrelated to FIREBall, only one balloon flew that month. This

year, the FIREBall team began measurements and calibrations in preparation for a September 2018 flight. According to the project lead and project scientist, the detector has been unchanged over nearly a year with no adjustment necessary.

Additionally, Star-Planet Activity Research CubeSat (SPARCS) has baselined two 2D-doped CCDs. SPARCS is a 6U cube-sat designed to monitor M-type stars in two photometric bands in the near-UV and far-UV (S-NUV, 260-300 nm; S-FUV, 150-170 nm), and is planned for 2021 flight. The FUV detector will also have a detector-integrated filter. SPARCS has baselined a dichroic design that allows for simultaneous S-NUV and S-FUV observation. SPARCS would advance 2D-doped detectors and detector-integrated out-of-band-rejection filter technologies for potential application in future mission concepts such as LUVOIR and HabEx.

## Path Forward

We will complete further wafer processing and produce several 2-megapixel arrays in part in preparation for radiation testing. We will analyze data from room-temperature, unbiased radiation testing of coated and uncoated superlattice-doped 2-megapixel EMCCDs. Informed by the room-temperature results, we will optimize our low-temperature biased radiation testing plan. We will complete these tests in the fall of 2018. We will evaluate and characterize the QE, dark noise, and uniformity of these devices before and after radiation following WFIRST protocol. In parallel, we will implement another design of metal-dielectric films into superlattice EMCCDs. We will continue working with the SHIELDS team (Walt Harris; PI, U. of Arizona). Further optimization (design and processing) of out-of-band-rejection filters might be necessary based on lab feedback and for testing by the SHIELDS team. In order to get closer to the absolute value of the QE, we are verifying the measured QE in other systems. The Caltech group also characterizes devices in photon-counting mode. We will resume our discussions with CMOS vendors and work on procuring wafers from our selected vendors.

## References


[1] "*Growth of a Delta-Doped Silicon Layer by Molecular-Beam Epitaxy on a Charge-Coupled Device for Reflection-Limited Ultraviolet Quantum Efficiency*," M.E. Hoenk, P.J. Grunthaner, F.J. Grunthaner, M. Fattahi, H-F. Tseng and R.W. Terhune, Appl. Phys. Lett., 61, 1084 (1992).

[2] "*Delta-doped CCDs: High QE with Long-term Stability at UV and Visible Wavelengths*," S. Nikzad, M.E. Hoenk, P.J. Grunthaner, R.W. Terhune, F.J. Grunthaner, R. Winzenread, M. Fattahi, and H-F. Tseng, Proc. of SPIE, 2198, 907 (1994).

[3] "*Near-100% Quantum Efficiency of Delta Doped Large-Format UV-NIR Silicon Imagers*," J. Blacksberg, S. Nikzad, M.E. Hoenk, S.E. Holland, and W. Kolbe, IEEE Trans. On Electron Devices 55 3402, (2008).

[4] "*Delta-doped back-illuminated CMOS imaging arrays: Progress and prospects*," M. E. Hoenk, T. J. Jones, M. R. Dickie, F. Greer, T. J. Cunningham, E. R. Blazejewski and Shouleh Nikzad, Proceedings of the SPIE 74190 74190-74115 (2009).

[5] "*Silicon Detector Arrays with Absolute Quantum Efficiency over 50% in the Far Ultraviolet for Single Photon Counting Applications*," S. Nikzad, M.E. Hoenk, F. Greer, E. Hamden, J. Blacksberg, B. Jacquot, S. Monacos, Chris Martin, D. Schiminovich, P. Morrissey, Applied Optics, 51, 365 (2012)

[6] "*Delta-doped CCDs As Stable, High Sensitivity, High Resolution UV Imaging Arrays*," S. Nikzad, M.E. Hoenk, P.J. Grunthaner, R.W. Terhune, R. Winzenread, M. Fattahi, H-F. Tseng, and F.J. Grunthaner, Proc. of SPIE, 2217, 355 (1994).

[7] "*Antireflection Coatings Designs for use in UV Imagers*," E. Hamden, F. Greer, M.E. Hoenk, J. Blacksberg, T.J. Jones, M. Dickie, B. Jacquot, S. Monacos, C. Martin, P. Morrissey, D. Schiminovich, S. Nikzad, Applied Optics, 50, 4180-4188 (2011).

[8] "*LLLCCD—Low Light Level Imaging without the need for an intensifier*," P. Jarram, P. Pool, R. Bell, D. Burt, S. Bowring, S. Spencer, Proc. SPIE 4306, 178 (2001).

[9] "*Impactron – A New Solid State Image Intensifier*," J. Hynecek, IEEE Transaction on Electron Devices, 48 No. 10, 2238-2241 (2001).

[10] "*New Worlds, New Horizons in Astronomy and Astrophysics*," Blandford et al., National Academy of Sciences, (2010).

[11] "Parametric Cost Models for Space Telescopes", H.P. Stahl, T. Henrichs, C. Dollinger, International Conference on Space Optics, Rhodes, Greece, October 2010.

[12] "*UV photon-counting CCD detectors that enable the next generation of UV spectroscopy missions: AR coatings that can achieve 80-90% QE*," E. Hamden, D. Schiminovich, S. Nikzad, and C. Martin, Proceedings of the SPIE, 8453, High Energy, Optical, and Infrared Detectors for Astronomy V, 845309 (2012).

[13] "*Delta doped Electron Multiplied CCD with Absolute Quantum Efficiency over 50% in the near to far Ultraviolet Range for Single Photon Counting Applications",* Shouleh Nikzad, Michael E. Hoenk, Frank Greer, Blake Jacquot, Steve Monacos, Todd Jones, J. Blacksberg, Erika Hamden, David Schiminovich, Chris Martin, and Patrick Morrissey, *Applied Optics*, **51**, 365 (2012).

## Publications, Presentations, and Professional Society Leadership Roles

Nikzad was honored by election and subsequent induction into the National Academy of Inventors as a fellow.

*Shouleh Nikzad in the induction ceremony at the National Academy of Inventors flanked by the President of NAI and the Commissioner for Patents for the U.S. Patent and Trademark Office*

Two papers were presented as oral presentation at the 2017 International Image Sensor Workshop (2017 IISW) by S. Nikzad and M.E. Hoenk. These were published as peer-reviewed papers in the proceedings of IISW. S. Nikzad also served as the technical program committee member on IISW.

Two papers were presented at the Scientific Detector Workshop (SDW), Baltimore MD, in September 2017 by S. Nikzad and M.E. Hoenk. S. Nikzad served as a panel member on the detector needs for the future astrophysics flagship missions, as well as on the Scientific Organizing Committee.

S. Nikzad served as conference co-chair and proceedings co-editor for the SPIE Astronomical Telescopes and Instrumentations: Gamma Ray to Ultraviolet meeting.

M.E. Hoenk served on the program committee of the SPIE High Energy, Optical and Infrared Detectors for Astronomy VIII meeting.

Seven papers were presented or co-authored by the team at the SPIE Astronomical Telescopes + Instrumentation, Austin, Texas, June 2018 Astronomical Telescopes and Instrumentations: Gamma Ray to Ultraviolet and High Energy, Optical and Infrared Detectors for Astronomy VIII.


*Photographs of participants and presenters at the SPIE conference co chaired by Nikzad on Astronomical Telescopes + Instrumentations: Gamma Ray to Ultraviolet*

1. S. Nikzad, A.D. Jewell, M.E. Hoenk, T.J. Jones, J. Hennessy, T. Goodsall, A.G. Carver, C. Shapiro, S.R. Cheng, E.T. Hamden, G. Kyne, D.C. Martin, D. Schiminovich, P. Scowen, K. France, S. McCandliss, and R.E. Lupu, "*High-efficiency UV/optical/NIR detectors for large aperture telescopes and UV explorer missions:*

*development of and field observations with delta-doped arrays*," JATIS **3**(3), 036002 (2017), doi: 10.1117/1.JATIS.3.3.036002.
2. S. Nikzad et al., "*Overview of High Efficiency and Low Noise Solid State Detectors for Future Missions including the Flagship Concepts: The Habitable Exoplanet Imaging Mission*," SDW, Baltimore MD (September 2017)
3. M.E. Hoenk et al., "*Efficiency and Stability of 2D-doped Silicon Detectors,*" SDW, Baltimore MD (September 2017)
4. S. Nikzad, J. Hennessy, M.E. Hoenk, A. Kiessling, M.R. Bolcar, D.F. Figer, S. Martin, and R. Morgan, "*Solid state detectors for the Habitable Exoplanet imaging mission (HabEx) and the large UV/optical/infrared (LUVOIR) surveyor mission concepts*," SPIE Astronomical Telescopes + Instrumentation, Austin, Texas (June 2018)
5. Y. Yatsu, T. Ozawa, H. Mamiya, N. Kawai, Y. Kikuya, M. Matsushita, S. Matunaga, P. Bilgi, S. Nikzad, S.R. Kulkarni, N. Tominaga, M. Tanaka, T. Morokuma, N. Takeyama, A. Enokuchi, and K. Sasaki, "*Conceptual design of a wide-field near UV transient survey in a 6U CubeSat*," SPIE Astronomical Telescopes + Instrumentation, Austin, Texas (June 2018)
6. A.D. Jewell, J. Hennessy, T. Jones, S. Cheng, A. Carver, D. Ardila, E. Shkolnik, M.E. Hoenk, and S. Nikzad, "*Ultraviolet detectors for astrophysics missions: a case study with SPARCS*," SPIE Astronomical Telescopes + Instrumentation, Austin, Texas (June 2018)
7. J. Hennessy, C.S. Moore, K. Balasubramanian, A.D. Jewell, K. France, and S. Nikzad, "*Ultrathin protective coatings by atomic layer engineering for far ultraviolet aluminum mirrors*," SPIE Astronomical Telescopes + Instrumentation, Austin, Texas (June 2018)
8. P.A. Scowen, E. Shkolnik, D. Ardila, J. Bowman, D. Jacobs, A. Jewell, M. Beasley, T. Berman, V. Gorjian, J. Llama, V. Meadows, S. Nikzad, M. Swain, and R. Zellem, "*Monitoring the high-energy radiation environment of exoplanets around low-mass stars with SPARCS (star-planet activity research CubeSat)*," SPIE Astronomical Telescopes + Instrumentation, Austin, Texas (June 2018)
9. R.M. Morgan, K. Warfield, H.P. Stahl, B. Mennesson, S. Nikzad, J. Nissen, K. Balasubramanian, S. Shaklan, J. Krist, D. Mawet, K. Stapelfeldt, and S. Warwick, "*Technology maturity for the habitable-zone exoplanet imaging mission (HabEx) concept*," SPIE Astronomical Telescopes + Instrumentation, Austin, Texas (June 2018)
10. M.E. Hoenk, A.D. Jewell, S. Nikzad, Q. Looker, B.D. Tierney, and M.O. Sanchez, "*Superlattice-doped detectors with high stable quantum efficiency in high radiation environments*," SPIE Astronomical Telescopes + Instrumentation, Austin, Texas (June 2018)

**For additional information, contact Shouleh Nikzad: Shouleh.Nikzad@jpl.nasa.gov**

# Development of DMD Arrays for Use in Future Space Missions

Prepared by: Zoran Ninkov (PI; Rochester Institute of Technology, RIT); Sally Heap and Manuel Quijada (NASA/GSFC); Massimo Robberto (STScI); and Alan Raisanen, Dmitry Vorobiev, and Anton Travinsky (RIT)

## Summary

This NASA Strategic Astrophysics Technology (SAT) project began in May 2014. The project seeks to investigate the feasibility of using a digital micro-mirror device (DMD) as the slit mask for a multi-object spectrograph (MOS) system for a variety of future NASA space missions. In particular, we are investigating a number of key operating parameters for Texas Instruments (TI) commercial-off-the-shelf DMDs including: replacing the borosilicate window with windows transmissive at ultraviolet (UV) and infrared (IR) wavelengths, tolerance to particle-radiation effects, ability to survive the vibrational conditions of launch, and non-specular scattering properties of the DMDs. The team includes Sally Heap at NASA/GSFC, who provides us with insight into the connection between astronomical measurement requirements and our laboratory testing; Massimo Robberto at the Space Telescope Science Institute (STScI), who provides test design guidance and has previous experience with proposed DMD used by the European Space Agency (ESA); Manuel Quijada at GSFC, who provides considerable optics experience and the use of the Carey 5000 Spectrometer at GSFC; and Alan Raisanen at RIT, who provides the necessary microsystems experience to allow for replacement of DMD windows in the RIT cleanroom. Additionally, we have worked with Jonny Pellish (GSFC Code 561) to conduct heavy-ion radiation testing of DMDs at Texas A&M and Tim Schwartz (GSFC Code 549) for vibration and shock testing. The project has made significant progress this year, including an improved measurement of light scattering from the TI DMD, a second round of heavy-ion testing on the DMDs at the Texas A&M University Cyclotron, vibrational and shock testing of DMDs in re-windowed and standard packages, extensive low-temperature testing with our collaborators at Johns Hopkins University (JHU), and re-coating a DMD with high-purity aluminum at GSFC.

## Background

Our ultimate objective is to address two key questions of NASA's Cosmic Origins (COR) Program:

1. How did galaxies evolve from the very first systems to the elliptical and spiral types we observe today?
2. How did super-massive black holes affect the lives of galaxies in which they reside, and vice versa?

Ground-based telescopes and the Hubble Space Telescope (HST) have shown us that the Hubble sequence of elliptical and spiral galaxies was in place by redshift $z = 1$. However, what physical processes drove $z > 1$ galaxies to join the Hubble sequence? To understand galaxy evolution, we need to carry out a large spectroscopic survey of the sky with a particular focus on galaxies at redshifts of $z = 1 \sim 2$. Experience with the Sloan Digital Sky Survey [1] indicates that several hundred thousand galaxies need be observed in order to distinguish among the many possible drivers of galaxy evolution (e.g., accretion, mergers, star formation, stellar evolution and feedback, growth of black holes, etc.).

A large spectroscopic survey requires a MOS able to record the spectra of hundreds of galaxies in a single exposure. The MOS must have adjustable slits to eliminate confusion with nearby sources and to block out unwanted zodiacal background, which would otherwise swamp the light from these faint galaxies. The MOS should have access to the far UV (1200 - 2000 Å) radiation emitted by a $z \sim 1$ galaxy because this spectral region has a rich set of diagnostics of stars, gas, and dust in the galaxy. Access to the blue-red spectral regions (2000 – 8000 Å) is also essential for determining the precise redshift

of a galaxy, its stellar mass, and its elemental abundances; and for characterizing dust extinction. Because the light from a z~1 galaxy is redshifted before reaching us, a large spectroscopic survey should be sensitive over the spectral interval 2000 - 16000 Å.

***The Problem***: No existing MOS has such a wide spectral range, let alone access to the UV. TI's DMD would make an excellent slit selector for a spectrograph if it were sensitive in the UV. However, commercial DMD windows block UV light.

***Scientific Impact***: A UV-transmitting DMD window enables a breakthrough in observational power sufficient to address two key COR science issues. No other telescope, ground- or space-based, present or planned, can accomplish this investigation, because it can't observe all the spectral diagnostics from Ly $\alpha$ (~1200 Å) to H$\alpha$ + [N II] (~6600 Å) in the same high-redshift galaxy.

Our project intends to investigate the applicability of DMDs to this and other space-based applications by testing the radiation hardness and light-scattering properties of these devices. In addition, our project will look at approaches to replacing the commercially provided windows on DMDs.

***The Solution***: We therefore propose to optimize the performance of DMDs for the UV region. This requires replacing the DMD window with a UV-transmitting window (> 2000 Å) with an anti-reflection coating on each side, optimized for the UV, optical, and IR. Because the target galaxies are at a redshift of z~1, the observed spectrum of a galaxy over 0.2 – 1.6 μm records the light emitted by the galaxy in the spectral range 0.1 – 0.8 μm. This wavelength region contains virtually all the important spectral diagnostics of stars, gas, and dust in the galaxy.

## Objectives and Milestones

Table 1 provides the major milestones of this project. Our project started more slowly than expected, principally because it took longer than expected to identify vendors for the needed components (e.g., windows, DMDs) and services (L-1 Standards & Technology). There was also a long delay in getting purchase orders through the GSFC system. Finally, although we received a quote from a US-based distributor to acquire TI Cinema DMDs when we submitted the proposal, it turned out they could not resell those in the US. The only way to get these DMDs was through TI's European distributor, at a higher-than-budgeted cost. STScI provided the additional funds, but there was a delay in placing the sub-contract and thus the order.

| Milestone | Vendor / Work Location | Dates | Comments |
|---|---|---|---|
| Proton-testing of DMD and data analysis | LBNL 88" Cyclotron | Completed 2014 | Results published |
| Receipt of $MgF_2$ and Heat Exchanger Method (HEM) Sapphire windows | Photonics Solutions Group, Blue Ridge Optics, GT Crystal Systems | Received Sep 2015 | After many delays from vendors, we received all of the windows; all windows met our specifications |
| Replacement of TI DMDs window | L-1 Standards & Technology | Received Dec 2015 | Devices all accepted |
| Receipt of Cinema DMDs + drive electronics | VISITECH, Germany | Received Jan 2016 | Final quote for these items was higher than budgeted; supplemental funding allowed order to proceed |
| Replacement of TI DMD windows with custom windows | Semiconductor & Microsystem Fabrication Laboratory, RIT | Aug 2015 & Jan 2016 | DMDs with Sapphire and $MgF_2$ windows have been fabricated as have devices with Kapton and Mica windows for heavy-ion testing |

| | | | |
|---|---|---|---|
| Vibration and shock testing | NASA GSFC Code 549 | Testing completed May 2016; Analysis completed Feb 2017 | Results accepted by Journal of Astronomical Telescopes, Instruments, and Systems |
| Measurement of light scattering from eXtended Graphics Array (XGA) DMD | RIT, Carey 5000 at GSFC Code 551 | May 2016 Mar 2017 | High signal-to-noise ratio (SNR) measurements of standard DMDs; Final measurements of bare DMDs with original coating and new Al coating |
| Heavy-ion testing of DMD and data analysis | Texas A&M Radiation Effects Facility | Tests Aug 2015 & Apr 2016; Analysis completed Feb 2017 | On-orbit event rates estimated; Results accepted by Journal of Astronomical Telescopes, Instruments, and Systems |
| Recoating of DMDs with high-reflectivity aluminum | NASA GSFC Code 551 | Feb 2017 | Coated a section of a functioning XGA DMD with high reflectivity aluminum; DMD remained operational |
| Low-temperature testing of DMDs | Instrument Development Group at JHU | May 2017 | Supplied DMDs with re-windowed & original packages for testing at 77 K |
| Gamma-ray testing | NASA GSFC | June 2018 | Tests of multiple DMD devices |
| Extended-time low-temperature testing | JHU/APL | November 2017 | Hold DMD patterns for typical astronomical observation times at low temperature |
| Optical modeling module | RIT | June 2018 | Permit inclusion of DMD scattering in standard software packages |

***Table 1.*** *Milestones of this SAT project.*

## Progress and Accomplishments

For DMD arrays to be suitable for future NASA missions, a number of performance issues must be addressed. This project attempts to investigate these questions, and to improve DMDs to make them more suitable for such instrumentation requirements. The two commercially available DMDs we will be evaluating are the 0.7 XGA 1024 × 768 13.6-µm pixel pitch and the Cinema 2048 × 1080 13.6-µm pixel pitch DMD.

***Radiation Testing***: The heavy-ion radiation testing was performed at the Cyclotron Institute of the Texas A&M University. The facility is equipped with three beam types: 15, 25, and 40 MeV/amu. Over the two rounds of testing, we used the 25 MeV/amu beam with four different ions – neon, argon, krypton, and xenon. DMDs were re-windowed with 2-µm-thick pellicle and tested under accelerated heavy-ion radiation (control electronics shielded from radiation), focusing on detection of single-event effects (SEEs) including latch-up events. Testing showed that while DMDs are sensitive to non-destructive ion-induced state changes, all SEEs were cleared with a soft reset (that is, sending a new pattern to the device). The DMDs did not experience single-event-induced permanent damage or functional changes that required a hard reset (power cycle), even at high ion fluence. The proton and heavy-ion testing suggests that the SEE-rate burden will be manageable for a DMD-based instrument when exposed to solar-particle fluxes and cosmic rays in orbit. Using the 95% confidence bounds obtained from the fitted model (Fig. 1) we calculate lower and upper values for the predicted worst-case in-orbit single-event upset (SEU) rate to be 3.42 and 11.7 micromirrors in 24 hours, for an XGA DMD with 1024 × 768 mirrors.

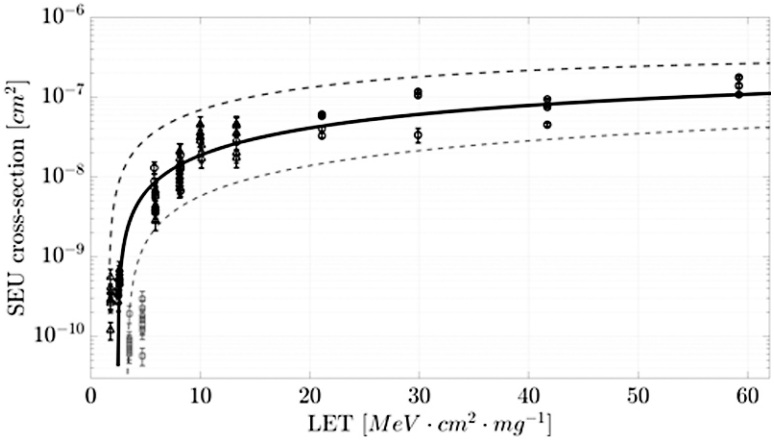


***Fig. 1.*** *Measured SEU cross-section as a function of linear energy transfer (LET) of incident ions from both runs. The Weibull cumulative distribution fit and 95%-confidence-level bounds are represented by solid and dotted lines, respectively.*

***Low-Temperature Testing***: We have collaborated with colleagues at the Instrument Development Group at JHU to build on our previous efforts to test DMD performance at cryogenic temperatures. At RIT, we used a modified Infrared Laboratories liquid nitrogen dewar to test the DMD at temperatures as low as 130 K [2]. This is the lowest temperature we could achieve, because the DMD control electronics had to be housed in the dewar. The commercial formatter board dissipated too much heat to allow us to reach 77 K.

At JHU, together with our collaborators, we have used a much larger dewar with a cryo-cooler (Fig. 2), which allowed us to reach a temperature of 77K, even while using the same formatter board. Several XGA DMDs with HEM Sapphire, fused silica, and original TI windows were used in extensive testing. Among the tests performed were high-duty-cycle tests (where the DMD mirrors are flipped many times, rapidly at low temperature) and "operational conditions" tests (where the DMD mirrors are latched in the same state for about 20 minutes at a time, as would be done in a spectrograph). These tests have been completed and the results have been published. The DMD devices worked without problem at the low temperatures. The only issues noted were with contaminants introduced during the re-windowing.

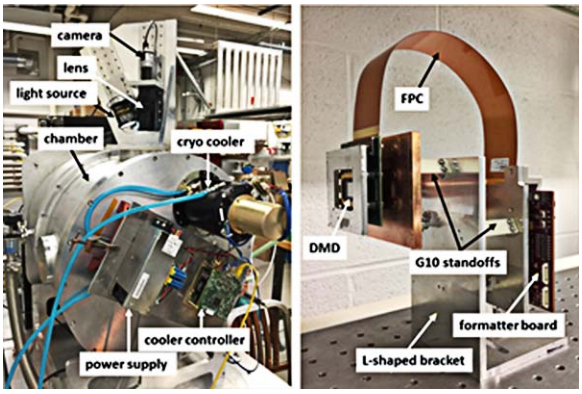


***Fig. 2.*** Left: *Test chamber and optical setup used for cryogenic DMD operability testing.* Right: *DMD and formatter board mounted to the chamber interface bracket (FPC, Flexible Printed Circuit).*

***Re-Coating DMDs with Al:*** Replacing the standard borosilicate window with a UV-transmissive material ($MgF_2$, HEM Sapphire, fused silica) extends the operational range of the DMD to approximately 200 nm. The UV reflectance of the DMD (ignoring losses due to fill factor and diffraction) is less than

that of pure aluminum, because the DMD mirrors are made with an aluminum alloy. Below about 200 nm, the DMD reflectance drops rapidly (Fig. 3, Right). This decrease is seen for all aluminum (and aluminum-alloy) mirrors if they are not protected against the formation of an aluminum oxide layer. In the last year, we attempted to extend the use of the DMD to approximately 100 nm, by recoating the DMD with high-purity aluminum and protecting it with a thin film of LiF or $AlF_3$.

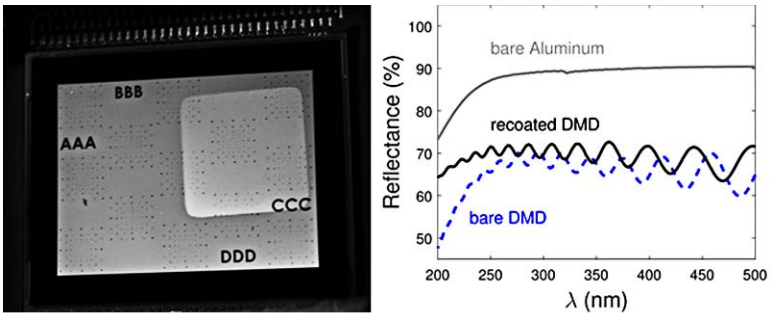


***Fig. 3.*** Left: *We re-coated a section of a TI XGA DMD with high-purity aluminum at NASA GSFC (lighter-color square). The DMD remained operational after the coating process.* Right: *Reflectance of the re-coated region increased across the visible range, with significant improvements in the UV.*

The re-coated DMD remained operational (Fig. 3, Left), with no obvious differences between the coated and original regions, except improved reflectance. The re-coated region showed a reflectance improvement of several percent across the visible range, with more significant gains in the UV; at 200 nm, the reflectance increased from 48% to 65%. At this wavelength, the reflectance difference between the re-coated DMD and a standard aluminum mirror is due to the 92% fill-factor of the DMD. At longer wavelengths, diffraction creates additional losses, as well as the "ringing" structure seen in the blue curve. Neither the re-coated DMD nor the witness mirror sample was protected against oxidation in this experiment, so the reflectance drop-off near 200 nm persists. However, our initial tests show that DMDs can survive this type of re-coating, suggesting that DMDs can be made usable in the 100 – 400 nm range, if the coating is protected with a fluoride film. Lithium fluoride windows can be used to protect the DMD using the re-windowing techniques we developed as part of this SAT program, to allow operation in the 108 – 3000 nm range. Furthermore, we are investigating the use of DMDs without protective windows, to extend the usable range to 91.2 nm (rest-frame Lyman limit), which is near the current state-of-the-art aluminum coatings [3, 4].

In addition, scattering measurements on the re-windowed XGA devices at wavelengths down to 200 nm have been completed and published. A new process has been developed and prototyped for re-windowing DMDs without epoxy but rather using laser welding, and devices have been manufactured that are as hermetic as the original devices from TI. The gamma-ray radiation testing of DMDs at GSFC will be done 19-21 June 2018, and those results will be used to determine total in-orbit upset rates.

## Path Forward

Given the robustness of the DMDs in all tests performed within the scope of this AST program, we believe the devices are ready for actual deployment. Our goal is to propose their use in a sub-orbital program proposal for final vindication as to thir survivability and utility.

## References

[1] J.E. Gunn et al., "*The 2.5-m Telescope of the Sloan Digital Sky Survey*," The Astronomical Journal, **131**, Issue 4, 2332-2359 (2006)

[2] K. Fourspring, Z. Ninkov, S. Heap, M. Robberto, and A. Kim, "*Testing of digital micromirror devices for space-based applications*," Proc. SPIE, **8618**, Emerging Digital Micromirror Device Based Systems and Applications V, id. 86180B (2013)

[3] M.A. Quijada, J. Del Hoyo, and S. Rice, "*Enhanced far-ultraviolet reflectance of $MgF_2$ and LiF over-coated Al mirrors*," Proc. SPIE, **9144**, 91444G (2014)

[4] K. Balasubramanian, J. Hennessy, N. Raouf, S. Nikzad, M. Ayala, S. Shaklan, P. Scowen, J. Del Hoyo, and M. Quijada, "*Aluminum mirror coatings for UVOIR telescope optics including the far UV*," Proc. SPIE, **9602**, 96020I (2015)

## Publications

1. A. Travinsky, D. Vorobiev, Z. Ninkov, A.D. Raisanen, J. Pellish, M. Robberto, and S. Heap, "*Effects of heavy ion radiation on digital micromirror device performance*," Optical Engineering, **55** (9), 094107 (2016)
2. A. Travinsky, D. Vorobiev, Z. Ninkov, A.D. Raisanen, M. Quijada, S. Smee, J. Pellish, T. Schwartz, M. Robberto, S. Heap, D. Conley, C. Benavides, N. Garcia, Z. Bredl, and S. Yllanes, "*Evaluation of Digital Micromirror Devices for use in space-based Multi-Object Spectrometer application*," J. Astron. Telesc. Syst., **3** (3), 035003, doi:10.1117/1.JATIS.3.3.035003 (2017)
3. D. Vorobiev, A. Travinsky, Z. Ninkov, and M. Quijada, *"Development of digital micromirror devices for us in the far-ultraviolet regime*," Proc. SPIE 10706-211 (2018)
4. A. Travinsky, D. Vorobiev, K. Oram, G. M. Nero, and Z. Ninkov "*On-sky performance evaluation of RITMOS, a micromirror-based multi-object spectrometer*," Proc. SPIE 10702-59 (2018)
5. R. Content, Australian Astronomical Observatory (Australia); Y. Wang, IPAC, Caltech (United States); M. Robberto, Space Telescope Science Institute (United States); R. Barkhouser, Johns Hopkins Univ. (United States); Z. Ninkov, Rochester Institute of Technology (United States); S. Smee, Johns Hopkins Univ. (United States); M. Dickinson, National Optical Astronomy Observatory (United States); H.C. Ferguson, Space Telescope Science Institute (United States); L. Hillenbrand, Caltech (United States); C. Hirata, The Ohio State Univ. (United States); W. Fraser, Queen's Univ. Belfast (United Kingdom); J. Bartlett, Jet Propulsion Lab. (United States); R. Benjamin, Univ. of Wisconsin-Whitewater (United States); J. Brinchmann, Leiden Observatory (Netherlands), Leiden Univ. (Netherlands); R. Chary, Caltech (United States), IPAC (United States); A. Cimatti, Univ. degli Studi di Bologna (Italy); C. Conroy, Harvard-Smithsonian Ctr. for Astrophysics (United States); E. Daddi, CEA-IRFU (France), Univ. Paris Diderot – Paris 7 (France); M. Donahue, Michigan State Univ. (United States); O. Doré, Peter Eisenhardt, Jet Propulsion Lab. (United States); G. Helou, IPAC, Caltech (United States); J.D. Kirkpatrick, Caltech (United States), IPAC (United States); S. Malhotra, NASA Goddard Space Flight Ctr. (United States); L. Moscardini, Univ. degli Studi di Bologna (Italy); M. Ressler, Jet Propulsion Lab. (United States); J. Rhoads, NASA/GSFC (United States); J. Rhodes, Jet Propulsion Lab. (United States); and A. Shapley, Univ. of California, Los Angeles (United States), *"ATLAS probe for the study of galaxy evolution with 300,000,000 galaxy spectra*," Proc. SPIE 10698-17 (2018)

**For additional information, contact Zoran Ninkov:** *ninkov@cis.rit.edu*

# Ultra-Stable Structures: Development and Characterization Using Spatial Dynamic Metrology

Prepared by: Babak N. Saif (PI; NASA/GSFC) and Lee Feinberg (NASA/GSFC)

## Summary

One possible successor to the James Webb Space Telescope (JWST) is an observatory that combines general ultraviolet-optical-infrared (UVOIR) astrophysics with the search for life on habitable Earth-like exoplanets using a large-aperture segmented telescope. Work on this problem began in 2009 as a potential Advanced Technology Large-Aperture Space Telescope (ATLAST) architecture. Early work focused on a scalable 9.2-m segmented telescope that could be launched on a Delta IV Heavy vehicle. More recently, this has progressed to a 16-m segmented telescope architecture. The most significant architectural driver beyond the aperture size is the $10^{-10}$ contrast required to block out the bright stars sufficiently to detect dim Earth-like planets orbiting stars within their habitable zones. Achieving this requires a combination of a high-throughput coronagraph with sufficient bandpass and wavelength range to perform spectroscopic surveys, and an ultra-stable telescope that maintains better-than-10-picometer stability for most observations. Achieving few-picometers stability, given thermal and dynamic disturbances, requires both passive and active means in a system with multi-level hierarchies.

## Background

### *Picometer Interferometry of Reflective Surfaces*

An important first step to achieve this level of stability is achieving picometer-level metrology that can characterize the thermal and dynamic behavior of an optical system, starting from the smallest components, through subsystems, up to the system as a whole. This requires a metrology system capable of measuring thermal and dynamic changes of both diffuse and reflective surfaces of system elements to picometer accuracy. One cannot assume that system stability scales linearly with levels of stimulus over orders of magnitude. More precisely, the transfer function of a system is not constant over orders of magnitude in stimulus level.

At what level of accuracy can one measure dynamics components? Our principal approach is to compare the amplitude of measured Zernike terms when the structure is stimulated mechanically to measurements without stimulus. Different Zernike terms have different phases and their contribution to surface variance vary over a stimulus cycle. However, since these are orthogonal functions, the time-averaged total surface variance is the sum of individual-surface Zernike variances. The relative contributions of each term can be illustrated by showing how the residual root mean square (rms) varies with the Zernike term, by successively removing Zernike components from the net dynamic figure as a function of Zernike term, and computing the resulting rms.

## Objectives and Milestones

Our objective is to develop picometer surface metrology of mirrors and structures. To this end, we work with a vendor to develop a dynamical digital speckle-pattern interferometer with picometer precision. In parallel, we develop an isolated tabletop setup to measure dynamics and drift of material and small structures, including a stimuli system able to exert picometer-level excitations.

We then develop structures and mirrors with dynamics controlled at picometer levels. Finally, we redesign and model the dynamics of the measured material/structures.

## Progress and Accomplishments

The two major components of our picometer-metrology test bed are picometer-level dynamics measurements and a thermal-vacuum chamber capable of fraction-of-a-milliKelvin stability over many hours. Interferometry to picometer levels of diffuse light, such as that reflected by non-specular surfaces, is challenging but required to enable design and fabrication systems with picometer stability. To achieve this, we purchased a high-speed speckle interferometer.

### *High-Speed Speckle Interferometer*

At the end of 2017, the team completed testing on the Mad City actively controlled piezo actuator using a 4D HSI system on a small reflective test mirror. This was done by attaching a convex mirror to the actuator and measuring the mirror motion at its center of curvature. The actuator motion per Mad City was about 12-picometer-amplitude sine wave, and our measurement showed a 13-picometer-amplitude sine motion. This gave us the confidence needed to move on to repeating the test with a composite test article, using our new high-speed speckle interferometer.

The high-speed speckle interferometer was delivered by 4D Technology to GSFC in February of 2018. Extensive testing uncovered some issues. High-frequency noise appeared on the camera, along with aberrations due to phase shifting and low-power coupling in the reference arm of the interferometer. These problems were discussed with 4D Technology and solutions were identified. The interferometer was sent back for repair.

Of three problems identified, the high spatial noise on the camera needed immediate attention as it prevented us from doing our picometer-level measurements. This was isolated to the camera cabling and was resolved. Phase-shifting aberrations is being addressed by ordering new Wollaston prism, while low-power coupling in the reference arm is being addressed by ordering a new fiber coupler, with both parts expected to be delivered in two months. With the cabling repair completed, the interferometer returned to GSFC, allowing us to begin our speckle measurements.

For this measurement we measured a diffuse surface, a piece of carbon fiber attached to the front face of the mirror using super glue, using the speckle mode of the new interferometer. A 20-picometer-amplitude sine wave was applied to the actuator as was done for the reflective measurements last year. The measurement (Fig. 1) showed a 16-picometer-amplitude sine wave. These data show that our measurements do not suffer biases and systematics, and that we can achieve adequate resolution. The large signal to noise ratio (SNR) shows that the amplitude can easily be reduced by a factor of two and still be detectable with good SNR.

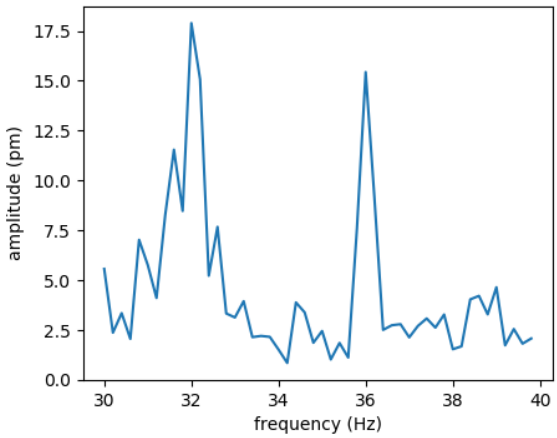


***Fig.1.*** *Carbon Fiber motion*

***Temperature Stability to MilliKelvins***

The Smithsonian Astrophysical Observatory (SAO) Large UVOIR (LUVOIR) ultra-stable aluminum thermal-vacuum chamber system (Fig. 2) is 30" in diameter and 30" in length. The assembly includes two bolt-on aluminum doors (35" outer diameter, OD) with Viton O-ring seals and handles to facilitate door mounting. One door includes a 10"-diameter fused-silica viewport, and the other door has provision for mounting a second 10" viewport. Three heater zones maintain high stability for the test article within the chamber. The heater pads are adhered to the external surfaces of the cylinder. Thermal and acoustical barrier foam panels surround the chamber to dampen local ambient acoustical noise and ambient temperature. The thermal control electronics rack (Fig. 2) includes a control laptop with SAO's nested-heater control-loop-logic software, a heater-power drive module, a high-precision thermometry system, and a power supply.

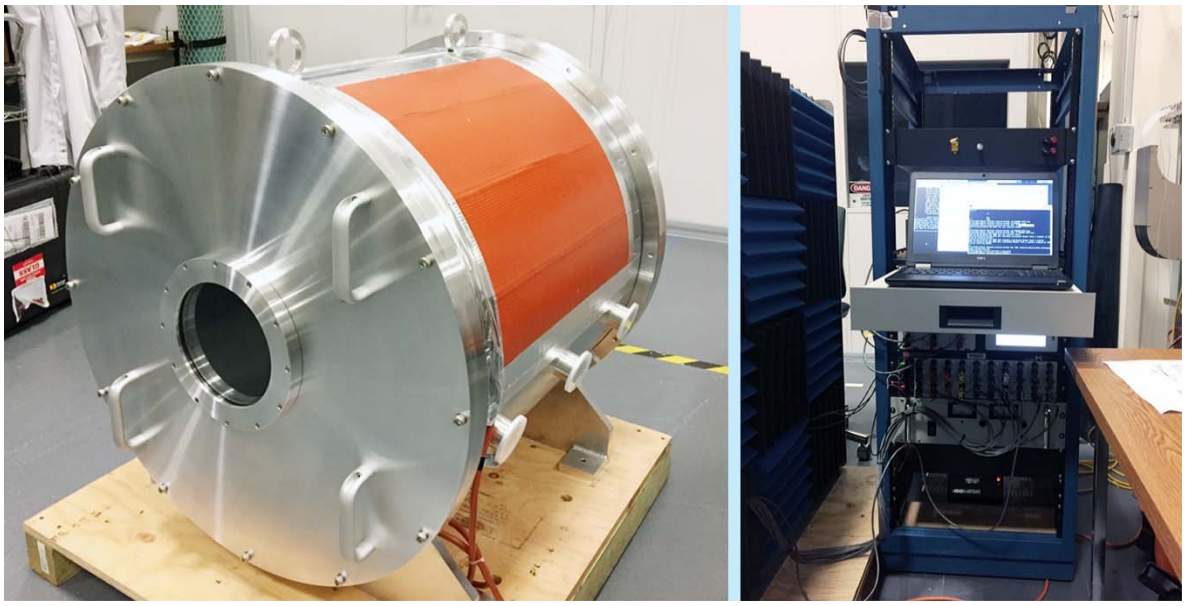

***Fig. 2.*** Left: *Thermal-vacuum chamber.* Right: *Ultra-Stable thermometry sense and control system electronics control rack for the chamber, currently located in the AIM lab in Building 5 GSFC.*

Functional testing with a nominal set-point of 23.5°C showed an average test-article thermal stability of +0.4/-0.2 milliKelvin (23.5 +0.0004/-0.0002°C) over 80 hours (Fig. 3).

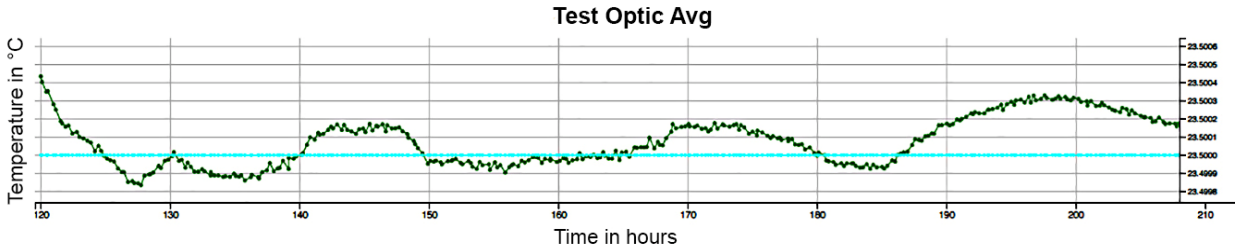


***Fig. 3.*** *Test results: 23.5 +0.0004/-0.0002°C thermal stability achieved for over 80 hours.*

### *Ultra-Stable Picometer-Scale Mirror Assembly*

Preparations for optical tests using a thermally controlled ultra-stable ULE mirror assembly inside the SAO chamber are underway for picometer-scale speckle interferometry characterizations in fiscal year (FY) 2019. To support these activities, an Ultra-Stable Picometer-Scale Mirror Assembly (USPS-MA) optical test article was developed for integration inside the SAO chamber (Fig. 4). The chamber is currently located at the GSFC AIM Lab in Building 5. As of this writing, the USPS-MA is fully assembled and undergoing functional testing for a planned delivery on 18 July 2018.

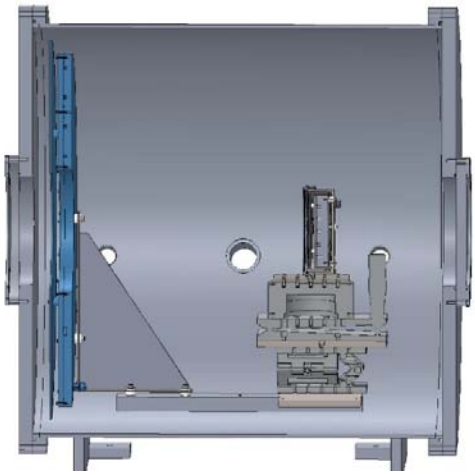

***Fig. 4*** *Cross-sectional view of the USPS-MA test configuration in the SAO ultra-stable thermal-vacuum chamber with 6-dof (degree of freedom) optical stages for proper orientation with respect to the optical window.*

The USPS-MA will be used in three configurations: (1) with a 100-mm-diameter ULE test substrate with a 1-µm rms diffuse surface (Fig. 5), (2) with a 150-mm ULE test substrate with a 1-µm rms diffuse surface (Fig. 6), and (3) with a surrogate mirror assembly using a 150-mm fused-Si substrate. The third configuration is for characterizing the thermal control behavior, helping us understand any thermal gradients within the mirror substrate, and as a reference for control-temperature-sensor locations. Due to the limited number of channels in the current thermometry system, only one sensor per substrate is planned as a control sensor on the ULE substrates. The surrogate fused-Si substrate was 'instrumented' with five high-precision thermistors, allowing us to characterize it and provide the necessary information for the two ULE substrates.

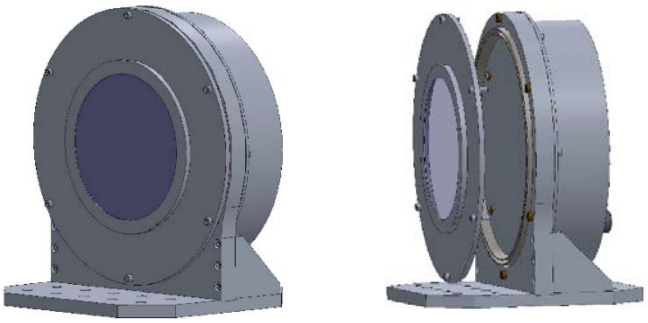

***Fig. 5.*** Left: *USPS-MA with 100-mm-diameter assembly.* Right: *Exploded view for clarity of assembly.*

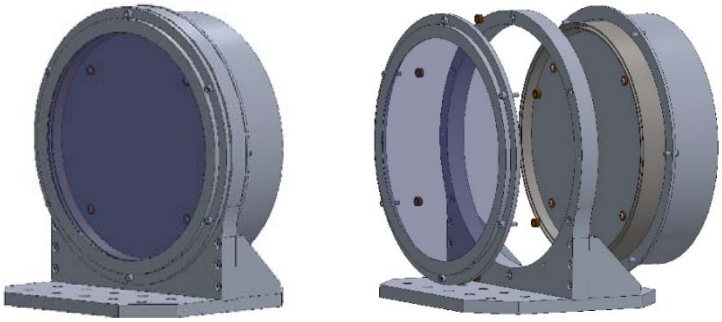

***Fig. 6.*** Left: *USPS-MA with 150-mm-diameter assembly.* Right: *Exploded view for clarity of assembly.*

The USPS-MA consists of thermal control hardware as shown in Fig. 7 below. The thermal control hardware includes, from left to right:

1. A thermal diffuser plate to 'blend' possible thermal gradients that could be 'seen' by the test article substrate.
2. A heater plate with four circular Kapton heaters.
3. A cold plate in conjunction with a re-circulating chiller to provide a cold-bias environment for the heater plate.
4. Two (2×) insulating thermal baffles to prevent thermal instabilities to the thermal-vac chamber thermal control and its performance.
5. An outer cover to 'house' the internal thermal components.

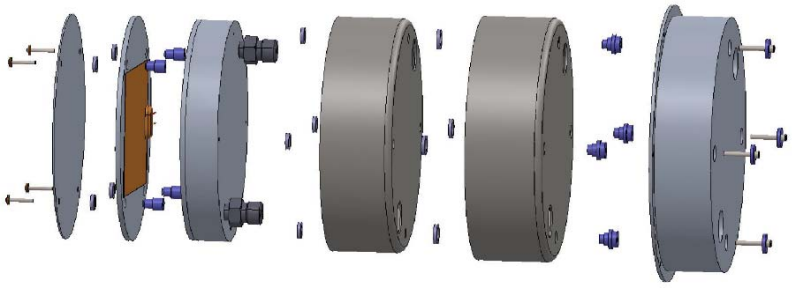

***Fig. 7.*** *Exploded view of the thermal hardware associated with the thermal control system that will maintain the mirror substrates at the milli-Kelvin stability required for picometer-scale metrology.*

The ULE substrates were bonded to holding frames using an SAO-developed miniature flexure design similar to that shown in Figs. 8 and 9. This substrate edge-bonding technique minimizes epoxy-induced surface figure errors (SFE). Also, bonding the substrate to a metal frame minimizes the likelihood of potential micro-lurching associated with 'dry' mirror interfaces such as knife-edge tripod stands.

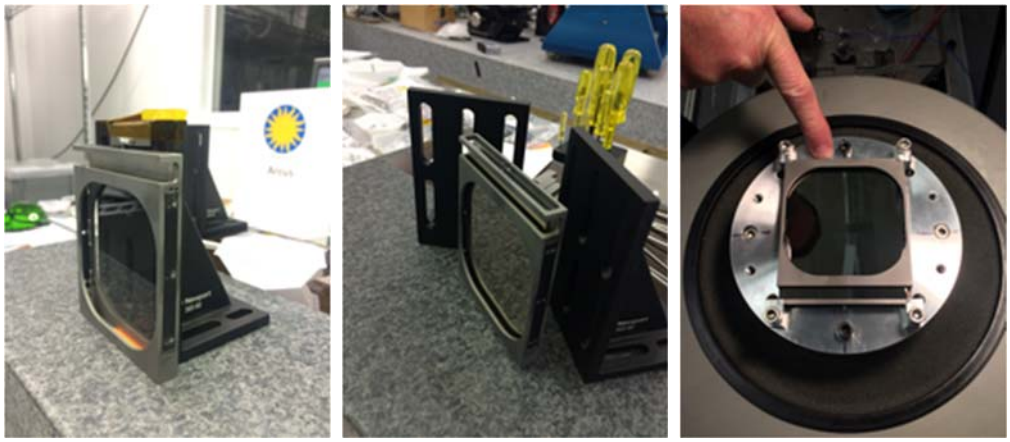

***Fig. 8.*** *Mirror substrate mounting implemented to secure a circular ULE flat to demonstrate the picometer-level metrology system along with the milli-Kelvin thermal control system. A fused-Si square flat substrate is mounted in a titanium frame using micro-flexures bonded between the thin mirror substrate and the housing frame. The assembly was vibrated to verify its structural integrity.*

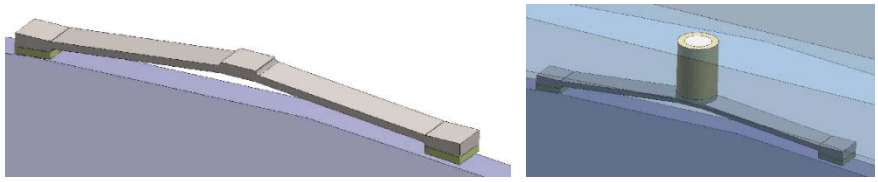

***Fig. 9.*** *Close-up illustration of the micro-flexure design. The edge shown is the 1-mm-thick ULE substrate.*

## Path Forward

The ULE-substrate USPS-MA articles have been fully manufactured and assembled and are thermally controlled using the same high-precision thermometry sense and control system (Fig. 2, right) developed for the ultra-stable chamber. Functional testing is underway at the time of this writing (Fig. 10). The test article assembly will then be placed in the ultra-stable thermal-vacuum chamber for further testing of the picometer-class metrology system.

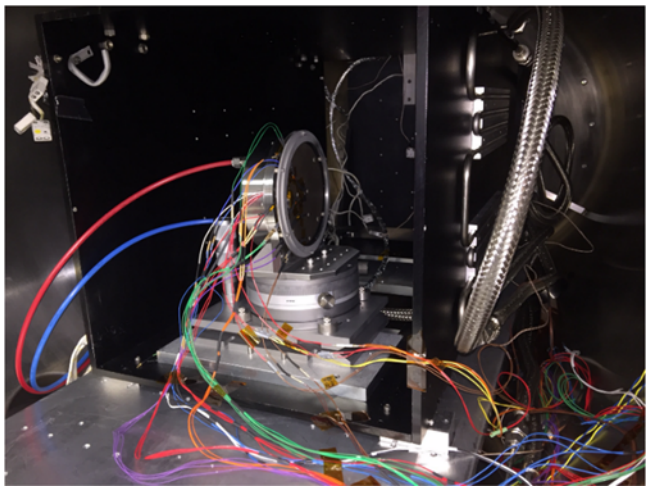

***Fig. 10.*** *USPS-MA functional testing with surrogate fused-Si substrate inside the SAO SES chamber prior to delivery to GSFC.*

**For additional information, contact Babak N. Saif:** babak.n.saif@nasa.gov

# Building a Better ALD - use of Plasma Enhanced ALD to Construct Efficient Interference Filters for the FUV

Prepared by: Paul Scowen (PI; Arizona State University, ASU); Brianna Eller, Daniel Messina, Zheng Ju, Franz Koeck, Robert J. Nemanich, and Hongbin Yu (ASU); Tom Mooney (Materion); and Matt Beasley (Southwest Research Institute, Boulder)

## Summary

The goal of this work is to use plasma-enhanced atomic layer deposition (PEALD) to synthesize mirrors and filters compatible with near-ultraviolet (UV) and far-UV optics. The development of this technology will ultimately provide diagnostic tools to access a range of topics for study, including protostellar and protoplanetary systems, intergalactic-medium (IGM) gas from galactic star formation, and the most distant of objects in the early universe. Since the beginning of the year, our team, from the School of Earth and Science Exploration and the Physics Department at ASU, Materion, and Planetary Resources, has been working to initiate this research. Our most significant progress to date has been the design, development, and the partial assembly of the equipment necessary to complete this research. In this period, the assembly of the PEALD has advanced with demonstration of the plasma system and near completion of the gas delivery and control system.

## 1.1 Background

Atomic layer deposition (ALD) is a layer-by-layer deposition technique that synthesizes ultra-thin, uniform, and conformal films as shown in Fig. 1. The high quality of these films has consequently resulted in augmented coatings and optical elements. At the same time, major advances have been made in optical designs and detector technologies. As a result, measurement of far-UV and near-UV bands has improved dramatically. The development of this technology ultimately allows access to emission and absorption lines in the UV, which are emitted from a range of targets, including protostellar and protoplanetary systems, IGM gas from galactic star formation, and the most distant of objects in the early universe. These diagnostic tools require the implementation of stable optical layers, including high-UV-reflectivity coatings and UV-transparent films [1].

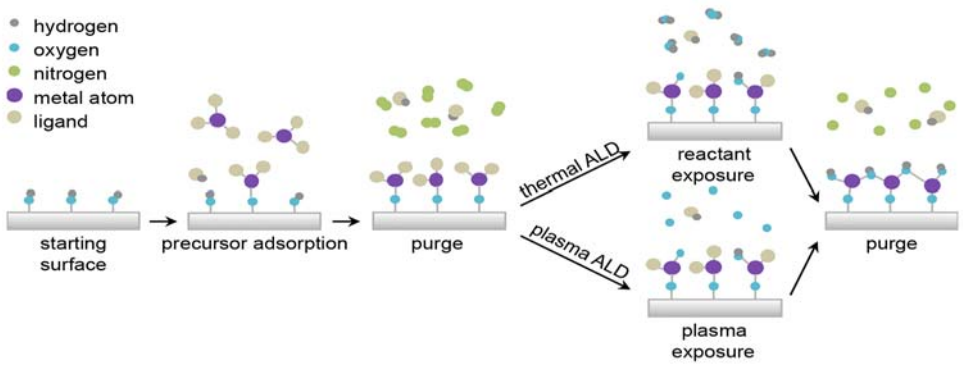


***Fig. 1.*** *Schematic representation of the layer-by-layer deposition process of the thermal and plasma-enhanced ALD. During the reactant or plasma exposure, the surface is exposed to a reactant gas or plasma.*

In this work, we will use a range of materials to implement stable protective overcoats with high UV reflectivity and unprecedented uniformity and use that capability to leverage innovative UV/optical filter construction to enable the science mentioned above. The materials we will use include aluminum

oxide and silicon oxide (as an intermediary step for development only) and a range of fluoride-based compounds (for production). These materials will be deposited in a multilayer format over a metal base to produce a stable construct. Specifically, we will use PEALD for deposition and construction of reflective layers that protect bare aluminum for mirror use in the UV. Our designs indicate that by using PEALD we can reduce adsorption and scattering in the optical films because of the lower concentration of impurities and increased control over the stoichiometry, yielding vastly superior quality and performance over comparable traditional thermal ALD techniques [2-17] currently being developed by other NASA-funded groups [18]. These capabilities will allow us to push the blue edge in usable UV reflectivity for magnesium-fluoride-protected aluminum below the current 115-nm limit.

This work will demonstrate for the first time whether loss-free oxides of materials such as Al, Hf, and Si can be deposited using ALD to lower cutoff reflectivities in the UV to as low as 92 nm. We will also demonstrate the use of PEALD to deposit low-loss thin films of fluoride-based materials, and aluminum metal. Using these techniques, we will then demonstrate our proof-of-concept of using these techniques together to construct thin-film, multilayer metal-dielectric cavities with a reflective surface as the foundation, that can be tuned to isolate specific emission lines of astronomical importance. The resulting optical technologies will advance the coating stability, thickness, and performance of thin films in the far-UV sought by NASA, to match recent UV detector advances. Such improvement will enable next-generation space-based far-UV missions, opening access to the wealth of diagnostic information the far-UV offers for exoplanet, star formation, and cosmological/IGM science.

## 1.2 Objectives and Milestones

Our research seeks to demonstrate several objectives:

- Films of material can be deposited to demonstrate the approach using PEALD techniques to produce loss-free films of e.g. silicon, hafnium, and aluminum oxide; the resulting coatings will be of a thickness and a purity far higher than can be delivered by current techniques that involve sputtering deposition;
- Using the same deposition techniques, PEALD can deposit thin (tens of nm) low-loss films of fluorides of aluminum and magnesium as well as e.g. lithium, lanthanum-calcium, and beryllium, that can serve as protective overcoats for materials which would otherwise be easily oxidized by exposure to air;
- Aluminum deposition, protective-layer deposition, and characterization can be completed in-situ in a controlled environment that minimizes contamination, improving the reflectivity of the resulting films and their interfaces by reducing scattering and adsorption;
- Deposition of such protective overcoats over aluminum metal can be achieved with PEALD to provide a sufficiently crystalline, uniform, and stable structure, pushing blueward the currently observed 115-nm cutoff in efficient reflectivity from atomic sputtering deposition of magnesium fluoride, thereby extending the range of diagnostic emission and absorption lines available for science;
- Extend the metal-dielectric overcoat process to concave mirrors to demonstrate the performance of the reflective surfaces in an optical test bed environment;
- Use our PEALD approach to apply alternating layers of metals and dielectrics, producing multi-cavity structures exhibiting very high performance; this goal is currently limited by the inability to deposit very thin layers with great accuracy, while demonstrating film toughness and 'bulk' thin-film material losses;
- Apply the multilayer approach to the construction of multi-layer dielectric mirrors to act as reflection filters or high reflectors in narrow band systems; and
- Similarly construct multi-layer broadband mirrors, thought to exhibit higher performance than metal-based mirrors (using a short-wave extension to prototype dichroics our group is already developing for space applications).

Table 1 summarizes the timeline to achieve these objectives, modified to accommodate fabrication of equipment.

| Activity Name | Start Date | Finish Date |
|---|---|---|
| Upgrade in-situ reflectivity to 120 nm | | Completed |
| PEALD of oxides on evaporated aluminum | | Completed |
| PEALD of $Al_2O_3$ and $SiO_2$ on aluminum | | Completed |
| Upgrade PEALD for aluminum deposition | 1/1/17 | 8/31/18 |
| PEALD of aluminum | 7/1/17 | 8/31/18 |
| Install precursors for PEALD of fluorides | 8/31/17 | 8/31/18 |
| Oxides on PEALD aluminum | 10/3/17 | 9/30/19 |
| Upgrade in-situ reflectivity to 90 nm | 8/2/17 | 9/30/19 |
| PEALD of aluminum fluoride on aluminum | 10/23/17 | 10/31/18 |
| PEALD of magnesium fluoride on aluminum | 10/23/17 | 10/31/18 |
| PEALD of aluminum and magnesium fluoride | 12/2/17 | 10/31/18 |
| Magnesium fluoride/aluminum filters | 2/1/18 | 11/30/18 |
| Oxide-fluoride multilayers and protective layers | 4/1/18 | 11/30/18 |
| Multi-layer broadband mirrors | 4/1/18 | 11/30/18 |

***Table 1.*** *Timeline for objectives and milestones.*

## 1.3 Progress and Accomplishments

The initial state of this research has largely focused on developing the equipment necessary to synthesize and characterize the oxygen-free structures required to achieve the aforementioned objectives. Assembly of the systems is underway, where the chambers added to the ultra-high vacuum system are highlighted in Fig. 2. Specifically, two systems have been added to the setup:

- A fluoride PEALD system for both the aluminum metal and metal fluorides needed for this work; and
- A visible and UV (VUV) optical system, which will be used to characterize reflectance of the films deposited without atmospheric contamination.

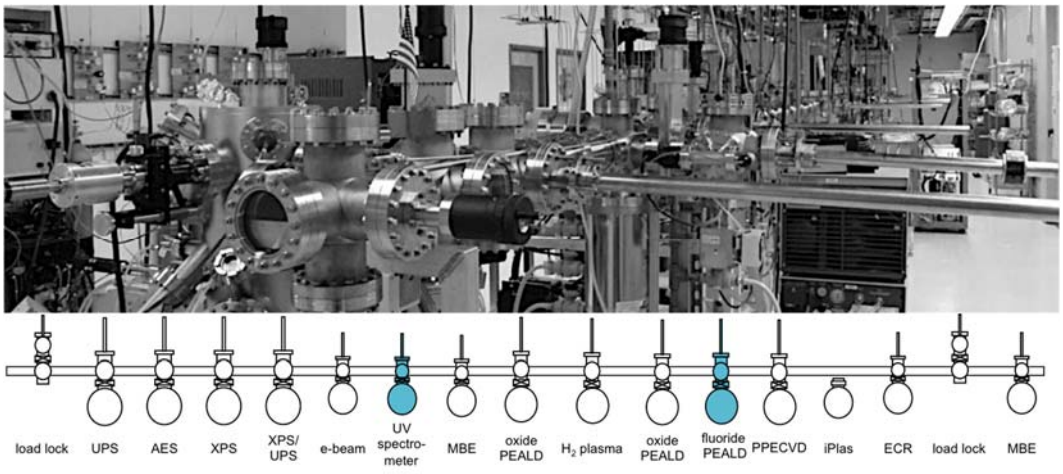


***Fig. 2.*** *Photo (top) and schematic (bottom) of ASU in-situ ultra-high vacuum system; blue shows new systems in progress (UPS, UV Photoelectron Spectroscopy; AES, Auger electron Spectroscopy; XPS, X-ray Photoelectron*

*Spectroscopy; MBE, Molecular Beam Epitaxy; iPlas, Innovative Plasma Chemical Vapor Deposition; ECR, Electron Cyclotron Resonance).*

A key component of this work is related to the in-situ nature of the deposition and characterization soon to be enabled. Since oxidation of aluminum has presented a significant challenge in previous research [18], this work will allow for the deposition of aluminum and metal fluorides without exposure to atmosphere.

### 1.3.1 1. Plasma-Enhanced Atomic Layer Deposition

The new PEALD system is in the initial stages of assembly and based on the previous oxide system available in the lab, with only a few alterations. Specifically, the plasma was designed with a remote configuration, helping reduce ion bombardment of the sample, mitigating potential ion damage. Plasma will be ignited with 13.56-MHz RF-excitation applied at ~200 W to a helical copper coil wrapped around a 32-mm-diameter quartz tube and maintained at a pressure of ~100 mTorr with a flow rate of ~35 sccm (standard cubic centimeters per minute). This system must achieve a background pressure of $< 5\times10^{-8}$ Torr and processing pressures of ~10 mTorr. The pumping requirements, therefore, vary during transfer and deposition. To assist with transfer, the system is equipped with a Pfeiffer turbo with pumping speed of 300 liters/sec and a dry backing pump, enabling lower pressures; however, the chemicals used during deposition are often too harsh, reducing the lifetime of the turbo pumps. Therefore, when operating, the turbo is isolated with a gate valve, and an Ebara two-stage dry pump with a pumping speed of ~7000 liters/sec is used. The pumping stage is vented with nitrogen gas during operation to further ensure system longevity. In addition, the gas-flow mechanisms are designed to deliver the precursors to the chamber with the correct timing sequence using mass flow controllers (MFCs), pneumatically actuated valves, and a custom LabView program. Metering valves were also added to the gas lines to further control the amount of precursor released into the chamber. Lastly, a butterfly valve before the two-stage dry pump is used to maintain the required pressures during processing.

The system is in the final stages of completion, as shown in Fig 3. To facilitate assembly, the fabrication has been completed in stages where the first stages are as follows:

***Fig. 3.*** Left*: Front view of PEALD system. This rack houses all control equipment.* Center: *Side view of system. Mounted on the frame is the chamber and equipment essential for the gas delivery system. The stainless-steel canister is for trapping larger reactor biproducts while the white canister is for HF abatement. The pump in the back is the two-stage dry pump.* Right: *Sample holder mounted on a rotary flange inside the chamber.*

- ☑ **Stage 1.** ***Vacuum and Transfer Mechanisms***. This includes the design of the system and chamber as well as the installation of the equipment needed to achieve and maintain vacuum, as well as transfer the samples from the in-situ vacuum system.
- ☐ **Stage 2.** ***Plasma generation and gas delivery***. The plasma generating system has been added and successfully tested with argon at 35 sccm and 400 mTorr. A similar test will be carried out once the butterfly valve and two-stage dry pump are operational, in order to obtain the desired 100 mTorr operating pressure. The rack to support the equipment has been fabricated and mounted. In addition, the plumbing for the argon and hydrogen lines is in progress.
- ☐ **Stage 3.** ***Aluminum PEALD process and gas delivery***. Fortunately, there has been some work done on PEALD of aluminum, using trimethylaluminum and hydrogen plasma [19]; therefore, this process will be used. The remaining sub-systems are: installation and welding of gas lines, filling and mounting precursor containers, and creating a custom LabView program for system operation.
- ☐ **Stage 4*. Modification for fluorides***. Unfortunately, the corrosiveness and toxicity of HF raise safety concerns that must be carefully considered for this process. To address these concerns, the following precautions will be implemented:
  - ☐ Storing the HF in a bubbler as an HF-pyridine mixture, which is less volatile than HF;
  - ☐ Electroplating the bubbler with gold to prevent corrosion;
  - ☐ Replacing the quartz tube with sapphire to prevent etching;
  - ☑ Introducing an acid dry bed abatement system following the two-stage dry pump to remove waste by-products;
  - ☑ Adding a toxic gas analyzer to ensure all residual HF is within acceptable limits; and
  - ☐ Coating the chamber with a thick aluminum layer, prior to using HF, to prevent etching of the chamber.
- ☐ **Stage 5.** ***Fluoride precursors***. Fluoride processes have not been developed extensively. In fact, to date, there are no published processes for fluoride PEALD. However, there has been some work on thermal ALD processes, which use HF [20, 21], $TiF_4$ [22-25], and $TaF_4$ [26] as the fluorine source. While $TiF_4$ and $TaF_4$ come with significantly less safety hazards, the films deposited with these materials are typically characterized by some metal contamination, which will likely cause absorption in the desired wavelengths. A fluoride-based plasma was also considered for this work but dismissed due to concerns that it might lead to etching rather than deposition. Therefore, an HF-pyridine mixture seems to be the best option at this point. To take advantage of the desirable properties of PEALD, the HF step will be coupled with a hydrogen plasma step to ensure film purity. For aluminum and magnesium fluoride, trimethylaluminum and bis-ethylcyclopentadienylmagnesium have been chosen as the respective metal precursors.

### 1.3.2 2. Visible and Ultraviolet Optical System

We have also established in-situ reflectivity to 120 nm to characterize PEALD oxides and aluminum. In addition, the VUV optical system will need to be upgraded for lower wavelengths (> 90 nm) in the future, which will be accomplished by replacing the deuterium lamp with a windowless hollow cathode lamp using inert gases or mixtures. This system (Fig. 4) has also been designed and fabricated, and is undergoing calibration.

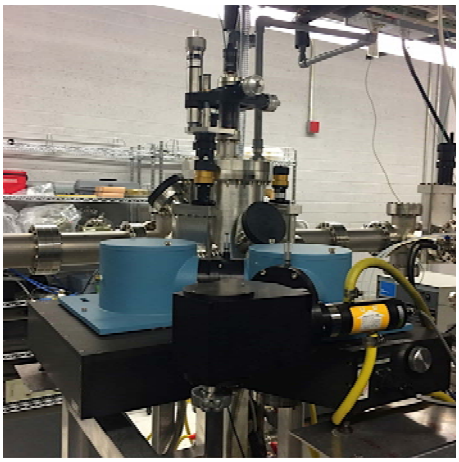

***Fig. 4.*** *Images of the custom-designed UV spectrometer unit, which currently can deliver reflectivity measurements from 254 to 120 nm.*

***2.1 Thermally evaporated aluminum coated in PEALD oxides***. Some testing of PEALD $Al_2O_3$ has been explored as well as a means to test and establish protocols for the system. This testing will continue while the aluminum and fluoride PEALD system is in progress. Some initial results show, as expected, that the thickness of the $Al_2O_3$ layers influences the reflectivity at lower wavelengths as shown in Fig. 5.

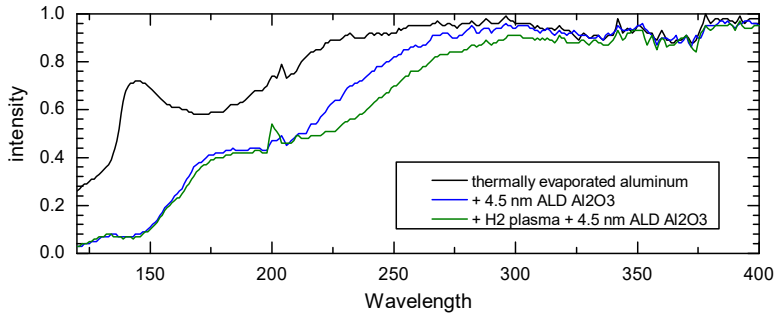


***Fig. 5.*** *UV reflectance of PEALD $Al_2O_3$ on thermally evaporated Al. Some additional work is needed to ensure consistency.*

***2.2 UV reflectance of additional mirrors***. Additional mirrors have been purchased, including gold, silver, aluminum, UV aluminum, and $MgF_2$-coated aluminum; to test, develop, and implement rigorous protocols to ensure reliable and consistent measurements in this system. In particular, small fluctuations in position and pressure influence the measured intensity. Therefore, additional work is needed to ensure the system provides reliable measurements. Using samples with known reflectance is helping to isolate these issues.

## *1.4 3. Filter Design – the Key Contributions of Tom Mooney and Matthew Beasley*

Matthew Beasley inspected the facilities in progress and made specific suggestions as to which materials should be prioritized for ALD deposition.

The chamber would be capable of Al, $AlF_3$ by default and Dr. Beasley suggested $MgF_2$ and $LaF_3$.

Tom Mooney created a trial run of a filter using constants in the literature and analyzed the tolerance to varying film thickness. This provided the direction that measuring the optical constants of the as-deposited films is the next key step. That way a filter with desired performance can be designed for fabrication and testing.

Tom Mooney retired and we now have Dr. Robert Sprague (also of Materion) taking his place.

### *1.5 4. Accomplishments this past year*

The following are some of our team's accomplishments this past year.

- Our filter design and fabrication technology was included in a suborbital rocket proposal submitted in response to ROSES APRA 2018 by co-I Matthew Beasley as PI;
- We developed alternative funding for diamond high-temperature electronics on Venus with NASA's The Venus Exploration Analysis Group (VEXAG);
- We expect additional funding through ARPA-E for atomic-layer etching of GaN, enabled by HF technology similar to that of this SAT project; and
- We leveraged our expertise to begin developing ultra-wide bandgap semiconductors, where fluorides will likely play a central role.

## 1.6 Path Forward

The plan of work is structured around the goals and milestones stated above. In general, the plan is to focus on assembling the PEALD as soon as possible while continuing the calibration of the UV spectrometer. This will enable the fabrication and use of bandpass filters. More specifically, the following will be necessary:

1. Demonstrate the use of PEALD to deposit loss-free oxides of silicon and aluminum on evaporated and e-beam-deposited aluminum surfaces. These oxides were selected based on their promise for stable, high-performance oxides. This is motivated because current methods produce lossy films, which are not usable below 190 nm.
2. Establish the capability for PEALD aluminum films and characterize the UV reflectivity of the films and the surface contamination using in-situ characterization tools. These aluminum surfaces will be the basis of the structures pursued in this program.
3. Demonstrate the feasibility of using PEALD to deposit low-loss films of fluoride compounds on ALD aluminum. The fluorides of interest include most significantly aluminum and magnesium fluoride, but others will be considered as well. We will need to demonstrate stability, uniformity, and performance before advancing.
4. Extend the reflectivity characterization to 90 nm and characterize the fluoride-aluminum structures. This is a critical step, as the aluminum-oxide/fluoride layer will serve as the foundation not only for simple reflective surfaces. For filters, we intend to show proof-of-concept in the next segment. The quality of aluminum and interface will define the required performance, which will be verified before advancing to the next stages.

In this system development phase, work will be conducted by Dr. Nemanich and his team, focusing on developing processes that result in optimized films. A number of complexities in the system design and construction have delayed the development phase, which is now anticipated to be completed in late 2018.

Before moving on to the next sequence, the optics design team of Drs. Scowen, Mooney, and Beasley will revisit the demonstrated performance of the three classes of product (above) and compare them to the models that initiated the work. Stability will be measured using vacuum exposure and spectral retest, and similarly humidity exposure followed by spectral retest. If there are differences in stability and reflectivity, we need to understand their origins before we can build prototype filters, since these parameters are critical for tuning an individual filter for a particular bandpass. Once this has been done, we will implement the techniques used above for the deposition of multilayer constructions.

The next phase will then address the following goals:

5. Optimize far-UV reflectivity of fluorides on aluminum, to deliver a wide-bandpass far-UV-optimized mirror. The optimization will focus on minimizing interface contamination and

optimizing material-growth parameters and film thickness for far-UV reflectivity. We will demonstrate performance as far as possible into the far-UV with our new VUV system.

6. Construct metal-dielectric Fabry-Perot band-pass filters using aluminum and magnesium fluoride, leading to multi-cavity structures that will exhibit very high performance—based on our models. This design approach is currently limited by the ability to deposit very thin layers with great accuracy, film toughness, and 'bulk' thin-film material losses. We believe only two to five layers will be needed to demonstrate proof-of-concept, with each layer ~10 nm thick.
7. Fine-tune approach and models to produce designs for multi-layer dielectric (narrow-band) mirrors to act as reflection filters or high reflectors in narrow-band systems. We will demonstrate construction and performance.
8. Demonstrate the construction of multi-layer broad-band mirrors, which we believe—based on models—will exhibit higher performance than metal-based mirrors.
9. We expect this design and construction phase to occupy most of the remainder of 2018. To achieve all this work, we will demonstrate our approach, designs, and methodologies deliver the necessary improvements in thickness control, lower 'bulk' losses, absence of color centers, smoother films (lower scatter), ability to deposit very thin films (with bulk-like optical properties), durability, and lower stress. The above plan, executed in this manner, will demonstrate all these goals.

## 1.7 References


[1] J.M. Shull and C.W. Danforth, "*Identifying the Baryons in a Multiphase Intergalactic Medium*," arXiv1208.3249S (2012)

[2] O.K. Kwon, S.H. Kwon, H.S. Park, and S.W. Kang, "*PEALD of a ruthenium adhesion layer for copper interconnects*," J. Electrochem. Soc. **151**, C753 (2004)

[3] O.K. Kwon, S.H. Kwon, H.S. Park, and S.W. Kang, "*Plasma-enhanced atomic layer deposition of ruthenium thin films*," Electrochem. Solid-State Lett. **7**, C46 (2004)

[4] J.W. Lim, S.J. Yun, and J.H. Lee, "*Low temperature growth of $SiO_2$ films by plasma-enhanced atomic layer deposition*," ETRI J. **27**, 118 (2005)

[5] W.J. Maeng, S.J. Park, and H. Kim, "*Atomic layer deposition of Ta-based thin films: Reactions of alkylamide precursor with various reactants*," J. Vac. Sci. Technol. B **24**, 2276 (2006)

[6] M.K. Song and S.W. Rhee, "*Phase formation in the tantalum carbo-nitride film deposited with atomic layer deposition using ammonia*," J. Electrochem. Soc. **155**, H823 (2008)

[7] J.S. Park, M.J. Lee, C.S. Lee, and S.W. Kang, "*Plasma-enhanced atomic layer deposition of tantalum nitrides using hydrogen radicals as a reducing agent*," Electrochem. Solid-State Lett. **4**, C17 (2001)

[8] J.S. Park, H.S. Park, and S.W. Kang, "*Plasma-enhanced atomic layer deposition of Ta-N thin films*," J. Electrochem. Soc. **149**, C28 (2002)

[9] J.Y. Kim, K.W. Lee, H.O. Park, Y.D. Kim, H. Jeon, and Y. Kim, "*Barrier Characteristics of TaN Films Deposited by Using the Remote Plasma Enhanced Atomic Layer Deposition Method*," J. Korean Phys. Soc. **45**, 1069 (2004)

[10] J.Y. Kim, Y. Kim, and H. Jeon, "*Characteristics of TiN Films Deposited by Remote Plasma-Enhanced Atomic Layer Deposition Method*," Jpn. J. Appl. Phys., **42** Part 2, No. 4B, L414 (2003)

[11] Y. Kim, J. Koo, J. W. Han, S. Choi, H. Jeon, and C.G. Park, "*Characteristics of $ZrO_2$ gate dielectric deposited using Zr t–butoxide and $Zr(NEt_2)_4$ precursors by plasma enhanced atomic layer deposition method*," J. Appl. Phys. **92**, 5443 (2002)

[12] J. Koo, Y. Kim, and H. Jeon, "*$ZrO_2$ Gate Dielectric Deposited by Plasma-Enhanced Atomic Layer Deposition Method*," Jpn. J. Appl. Phys., **41** Part 1, No. 5A, 3043 (2002)

[13] B. Hoex, J. Schmidt, P. Pohl, M.C.M. van de Sanden, and W.M.M. Kessels, "*Silicon surface passivation by atomic layer deposited $Al_2O_3$*," J. Appl. Phys. **104**, 044903 (2008)

[14] J. Koo, S. Kim, S. Jeon, H. Jeon, Y. Kim, and Y. Won, "*Characteristics of $Al_2O_3$ Thin Films Deposited Using Dimethylaluminum Isopropoxide and Trimethylaluminum Precursors by the Plasma-Enhanced Atomic-Layer Deposition Method*," J. Korean Phys. Soc. **48**, 131 (2006)

[15] P.K. Park and S.W. Kang, "*Enhancement of dielectric constant in $HfO_2$ thin films by the addition of $Al_2O_3$*," Appl. Phys. Lett. **89**, 192905 (2006)

[16] P.K. Park, E.S. Cha, and S.W. Kang, "*Interface effect on dielectric constant of $HfO_2$ /$Al_2O_3$ nanolaminate films deposited by plasma-enhanced atomic layer deposition*," Appl. Phys. Lett. **90**, 232906 (2007)

[17] P.K. Park, J.S. Roh, B.H. Choi, and S.W. Kang, "*Interfacial Layer Properties of $HfO_2$ Films Formed by Plasma-Enhanced Atomic Layer Deposition on Silicon*," Electrochem. Solid-State Lett. **9**, F34 (2006)

[18] J. Hennessy, A.D. Jewell, F. Greer, M.C. Lee, and S. Nikzad, "*Atomic layer deposition of magnesium fluoride via bis(ethylcyclopentadienyl)magnesium and anhydrous hydrogen fluoride*," J. Vac. Sci. Technol. A **33**, 01A125 (2015)

[19] J.-H. Park, D.-S. Han, Y.-J. Kang, S.-R. Shin, and J.-W. Park, "*Self-forming Al oxide barrier for nanoscale Cu interconnects created by hybrid atomic layer deposition of Cu–Al alloy*," J. Vac. Sci. Technol. A **32**, 01A131 (2014)

[20] Y. Lee and S.M. George, "*Atomic Layer Deposition of Metal Fluorides using Various Precursors and Hydrogen Fluorides*," ALD conference (2015)

[21] J. Hennessey, B.K. Balasubramanian, A. Jewell, S. Nikzad, C.S. Morre, and K. France, "*Thin ALD fluoride films to protect and enhance Al mirrors in Far UV*," ALD conference (2015)

[22] T. Pilvi, T. Hatanpää, E. Puukilainen, K. Arstila, M. Bischoff, U. Kaiser, N. Kaiser, M. Leskelä, and M. Ritala, "*Study of novel ALD process for depositing $MgF_2$ thin films*," J. Mater. Chem. **17**, 5077 (2007)

[23] M. Mäntymäki, J. Hämäläinen, E. Puukilainen, F. Munnik, M. Ritala, and M. Leskelä, "*Atomic Layer Deposition of LiF Thin Films from Lithd and $TiF_4$ Precursors*," Chem. Vap. Dep. **19**, 111 (2013)

[24] M. Mäntymäki, M. J. Heikkilä, E. Puukilainen, K. Mizohata, B. Marchand, J. Räisänen, M. Ritala, and M. Leskelä, "*Atomic Layer Deposition of $AlF_3$ Thin Films Using Halide Precursors*," Chem. Mater. **27**, 604 (2015)

[25] T. Pilvi, K. Arstila, M. Leskelä, and M. Ritala, "*Novel ALD process for depositing $CaF_2$ thin films*," Chem. Mater. **19**, 3387 (2007)

[26] T. Pilvi, E. Puukilainen, U. Kreissig, M. Leskelä, and M. Ritala, "*Atomic Layer Deposition of $MgF_2$ Thin Films Using $TaF_5$ as a Novel Fluorine Source*," Chem. Mater. **20**, 5023 (2008)

**For additional information, contact Paul Scowen:** paul.scowen@asu.edu

# High-Performance Sealed-Tube Cross-Strip Photon-Counting Sensors for UV-Vis Astrophysics Instruments

Prepared by: Oswald Siegmund (Space Sciences Laboratory, UC Berkeley)

## Summary

Microchannel-plate (MCP) detectors have been the detector of choice for many ultraviolet (UV) astronomy missions and instruments operated successfully over the last two decades, such as EUVE, FUSE, GALEX, HST-STIS and HST-COS [1-4]. They are also implemented on the soon to be launched NASA ICON Small Explorer [5], GOLD Mission of Opportunity [6], and are widely used on NASA UV sub-orbital sounding rocket investigations. MCP detectors have the potential to combine high spatial resolution (<20 μm full width at half maximum, FWHM), photon-counting (noiseless) imaging in a robust, radiation-hard package that is scalable to very large formats (>10 cm and > 5k×5k resels) and even curved focal planes (JUNO-UVS [7]). They operate at ambient temperatures with very low dark count rate and new readout technologies allow operation at MCP gains factors of ~20 lower than before. The objective of this Strategic Astrophysics Technology (SAT) program is to exploit the developments in atomic-layer-deposited (ALD) MCPs, photocathodes and cross-strip (XS) readout techniques to provide a new generation of enhanced-performance, sealed-tube, photon-counting sensors that span the 115-nm to 400-nm regime. Efforts in subcomponent areas have achieved considerable technical advancement, but putting them into a robust, integrated package and advancing the Technology Readiness Level (TRL) from 4 to 6 for the next UV-Vis Astrophysics instruments has yet to be attempted. In this SAT program, we are employing these recent advances in MCP detector technology to gain performance improvements in spatial resolution, quantum efficiency (QE), long-term stability, environmental stability, noise reduction and large-area formats economically by increasing the TRL by:

1. Implementing sealed-tube, XS-readout, 5-cm format MCP detectors based on redesign of a commercial sealed-tube package (Planacon) by incorporating a ceramic XS anode, ALD MCPs, and photocathodes and windows to accommodate the UV regime.
2. Incorporating ALD MCPs with large-area formats (5-cm × 5-cm active area with 10-μm pores) into the tubes, and showing that they can undergo the processing steps while maintaining their performance and stability characteristics.
3. Integrating ceramic XS anodes into the tubes and showing that ultra-high vacuum (UHV) processing can be established so that the longevity of the final tube is maximized while providing the performance characteristics of the XS scheme.
4. Establishing UV-Vis photocathodes in the sealed tube by adapting the design to accommodate opaque photocathodes onto the MCPs, and incorporating semitransparent UV photocathodes on $MgF_2$ input windows.
5. Showing that the sealed tube can operate in, and withstand, full flight-like environmental tests; and that it can be integrated with electronics systems being developed in parallel for spaceflight-compatible, low-power-mass-volume, ASIC-readout electronics.

We began this project in early 2018 and have made progress on initiating the major development tasks. The first semitransparent cathode tests are about to commence after commissioning the UHV facility and loading $MgF_2$ windows. ALD sample MCPs have been tested and an opaque alkali-halide cathode has been deposited and is ready to be evaluated. A meeting with the MCP vendor has allowed us to establish the required fabrication specifications and the initial MCP order for the sealed tube

MCPs is in place. The XS anode design was reviewed and discussed with the sealed-tube vendor. Subsequently a first batch of anodes was ordered and received, and is in test. A meeting with the sealed-tube vendor facilitated a design review that refined the mechanical design and processing steps. The initial tube fabrication order is now in place. Meanwhile, we have commissioned an XS/MCP test facility (detector/electronics) and tested it with sample 50-mm-format 20-µm-pore ALD MCPs and were able to resolve the pores across the entire detector.

## Background

The 2010 Astrophysics Decadal Survey recommended that NASA prepare for a UV mission to be considered by the forthcoming 2020 Astrophysics Decadal Survey. In response to this recommendation, the Astrophysics Visionary Roadmap of 2015 identified a large UV/Optical/IR (LUVOIR) Surveyor observatory with improvements in sensitivity, spectroscopy, high-contrast imaging, astrometry, angular resolution, and/or wavelength coverage as a prime mission candidate. Additionally, the Cosmic Origins (COR) Program Annual Technology Report (PATR; NASA 440-RPT-0017) listed as a Priority 1 technology requirement the need to routinely produce large-format UV-sensitive detector arrays that can be used in a variety of Explorer, medium, and strategic missions such as a LUVOIR telescope. In response, the Study on Applications of Large Space Optics (SALSO) workshop highlighted [8] possible future (large-aperture) UV astronomy missions such as (i) LUVOIR [9], (ii) the Habitable Exoplanet Observatory (HabEx) [10] and (iii) Cosmic Evolution Through UV Spectroscopy (CETUS) [11]. These on-orbit UV facilities would be able to probe the very limits of the universe as outlined in the science investigations of strategic goal 3.4 of the NASA Science Mission Directorate plan for 2007–2016. Future UV detectors must possess larger formats with higher spatial resolution to take advantage of this increased capability of the large photon-collecting area as well as low inherent read-noise / or dark rate in order to fully exploit the very low sky background at far-UV wavelengths, thus enabling the observation of very faint objects.

In this project, we aim to demonstrate that XS sealed tubes with ALD MCPs can be implemented as robust, high-performance detectors for 115 nm to 400 nm, addressing needs described in the LUVOIR/HABEX/CETUS study requirements, and for potential application to many future NASA missions. In addition, we aim raise the TRL by minimizing the mass/volume and qualifying the detector for space use.

MCPs with imaging readouts in sealed tubes are not recent inventions. However, readouts, electronics, MCPs, photocathodes, and sealed-tube techniques have advanced considerably in the last few years and can now be implemented in a high TRL (5-6) XS sealed-tube sensor with superior performance characteristics. A cross-strip-sensor anode scheme (Fig. 1) derives photon-event centroid positions from the charge distribution an event produces across a set of strips in an MCP-amplified detector. The incoming photon produces a primary electron from a photocathode on the MCP input, or from a photocathode on the input window. The photoelectron is then multiplied within the pores of a microchannel-plate pair and the resulting electron cloud is collected on two orthogonal sets of metal strips that form the XS anode. To ensure an accurate event centroid position is achieved, the size of the electron cloud is optimized so the charge impinges on several neighboring strips.

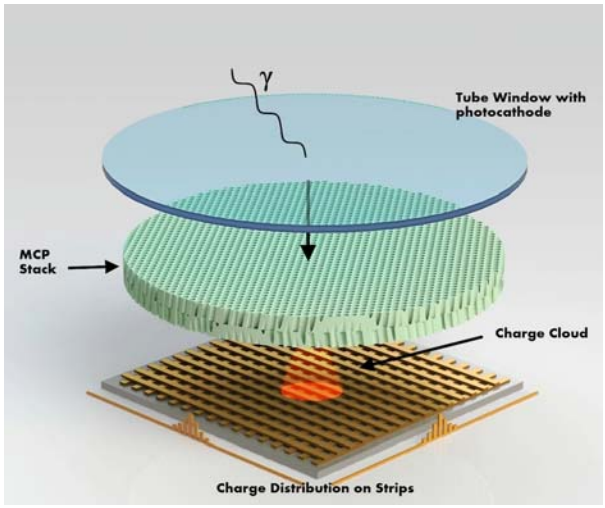


***Fig. 1.*** *An XS-readout MCP sealed-tube imaging-sensor scheme. A photocathode is deposited on a window facing a pair of MCPs. Emitted photoelectrons are detected by the MCPs, multiplied, and collected by several strips in each axis of the anode to enable event centroid positions to be calculated.*

Recent work on the subcomponents of this device through Astrophysics Research and Analysis (APRA) funding has resulted in significant advances [12]. ALD MCPs with large-area formats (12 cm × 12 cm with 10-μm pores, up to 20 cm × 20 cm with 20-μm pores), very low background rates (<0.05 events/cm$^2$/sec), extended lifetimes (> 4×10$^{13}$ events cm$^{-2}$) without degradation. XS anodes and electronics with spatial resolutions of <20μm FWHM over formats of 100 mm × 100mm and event handling rates of 5 MHz at <15% dead time. Photocathodes in the UV-Vis provide 50% QE at ~115 nm to 180 nm and range cutoffs in the range 300 nm to 400 nm (solar blindness).

Combining these developments has a significant impact on potential future NASA sub-orbital and satellite instruments. An effective way to do this is by adoption of a commercial device, the Planacon (Fig. 2), and developing/integrating all the necessary elements ($MgF_2$ window, UV photocathodes, ALD MCPs, and XS readout). The smaller pore sizes (~10 μm) and high-resolution XS readouts will facilitate higher spatial resolutions over the large formats. At the same time, the reduced (÷3) detection efficiency for high-energy background events demonstrated by use of ALD MCPs will also improve observational sensitivities. The chemical compatibility of the new MCP borosilicate glass and the ALD materials has the potential to provide further improvements in the stability and lifetime of these detectors, due to the rigorous pre-conditioning steps for sealed tubes. In addition, improvements in fabrication processes provide the opportunity to reduce the imaging fixed pattern modulation. XS readouts integrated into sealed-tube packages can also take full advantage of the efforts currently taking place [13] to establish high-performance, spaceflight-compatible, low-power-mass-volume ASIC readout electronics. Together, these developments will provide a significant step in realizing high-performance, robust MCP detectors for all classes of astrophysics instruments from sub-orbital to major facility instruments.

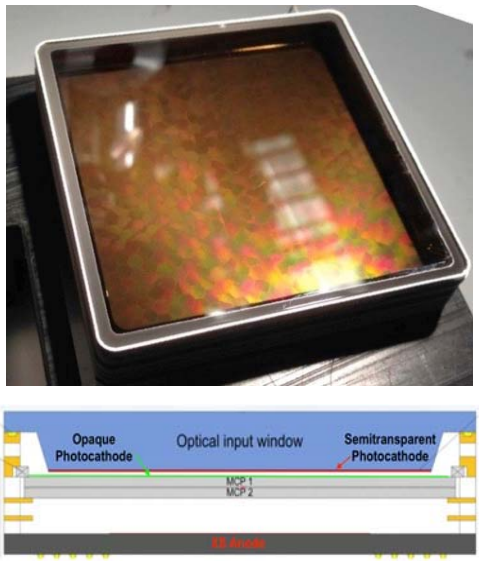


***Fig. 2**:* Top: *Sealed-tube 50-mm Planacon with a 10-µm-pore ALD MCP pair and a 32×32 pad anode readout.* Bottom: *Cross-section of proposed Planacon sensor scheme. $MgF_2$ is used for input window, with a UV/Vis semitransparent multialkali cathode. A pair of ALD MCPs coated with an opaque photo-cathode provides enhanced UV detection and signal amplification, and a XS anode accomplishes photon-counting imaging readout.*

## Objectives and Milestones

The "commercial" Planacon (Fig. 2) [14] has a 50-mm format that uses a square sealed-tube configuration. The photocathode is a semitransparent multialkali on a standard glass window with a proximity gap to a pair of 10-µm pore standard MCPs. The readout is an array of either 8 × 8 or 32 × 32 pads. Our objective to implement a Planacon scheme (Fig. 2) with a UV $MgF_2$ entrance window and a UV-optimized bialkali semitransparent photocathode with a narrow (~200-µm) proximity gap. Two ALD MCPs replace the standard MCPs, while an opaque UV photocathode would be deposited onto the surface of the input MCP. The pad array anode would also be replaced with a XS anode readout. Specific areas of development required are:

1. Obtaining high-performance ALD MCPS in 10-µm pore size compatible with introduction into Planacon devices. This entails establishment of gain value ($10^6$), uniformity, and stability as described in the background information above; along with demonstration of spatial resolution at ~20-µm FWHM.
2. Implementing high-resolution XS anodes in a refractory ceramic compatible with Planacon integration. This includes fabricating anodes capable of withstanding Planacon-tube integration and processing. In addition, demonstrating the high spatial-resolution and imaging performance at ~20-µm FWHM.
3. Optimizing and incorporating UV photocathodes into the Planacon, both semitransparent on $MgF_2$ entrance windows and opaque photocathodes on the ALD MCPS. Initial milestones are demonstration of semitransparent multialkali photocathodes on $MgF_2$ windows and opaque alkali halides on ALD MCPs with high efficiency and sharp long-wavelength cutoffs (350nm). These must then be implemented into the Planacon devices.
4. Demonstrating the fully implemented Planacon XS-detector scheme with existing electronics to show subcomponent performance characteristics; then testing them in appropriate flight-like environments (thermal and vibration), along with eventual radiation testing.

## Progress and Accomplishments

### *Sealed-Tube Planacon Implementation*

Initial work in the design and testing of the photocathodes, MCPs, and XS readouts is being undertaken by UCB-SSL. Meanwhile we are working with Photonis (the Planacon vendor) in a step-wise manner to include all of these into final sealed-tube test articles. We held a kickoff meeting with Photonis and

reviewed the design, processing steps, and packaging to incorporate all the new hardware. The dimensions for the anodes have been established and we are procuring ceramic anode blanks for making test seals of ceramic anode substrates to Planacon bodies and then verifying the high-vacuum seal. The distance between the anode and the MCP stack in the design is set at 2.5 mm and is optimized for the charge cloud spread of the MCP configuration. Then an initial tube construction effort will incorporate a ceramic XS anode into a Planacon with a 10-μm MCP pair and a bialkali photocathode with a sapphire planar UV window. The objective is to get an initial process run that establishes the ALD MCP environmental (UHV) processing regime including a high-temperature bakeout and a subsequent "burn-in" before the photocathode is deposited. Secondly, we aim to show leak-tight sealing of the tube so that we can confirm photocathode performance, as well as XS and ALD MCP operation, in support of the second iteration of sealed tubes. We established an order for the initial setup tests at Photonis and for processing the first tube iteration that is expected to be accomplished by the end of 2018.

***UV-Vis Photocathodes for 115 nm to ≥ 400 nm***

The photocathode and photoelectron detection by the MCP determine the MCP's QE [15]. The photocathode can be deposited on a window directly in front of the MCP (a proximity-focused semitransparent cathode, Fig. 2) or directly onto the MCP (opaque mode) [16-19]. Opaque alkali halide photocathodes are widely used for extreme-UV (EUV)/UV sensors, as are semitransparent multialkali photocathodes for visible detectors. New materials exemplified by GaN [12] are also candidates for far-UV/near-UV photocathodes.

Alkali halide (CsI, KBr) opaque photocathodes on MCPs obtain high QE (50% @ ~110 nm) and have broad band sensitivity from 10 nm to 160 nm [20]. We have previously used these photocathodes in sealed tubes and achieved good performance on early ALD MCPs. To establish the process for using them as opaque cathodes in the Planacon tubes, we obtained sample ALD MCPs for trial depositions and began by depositing a CsI photocathode (Fig. 3), soon to be tested for efficiency and uniformity.

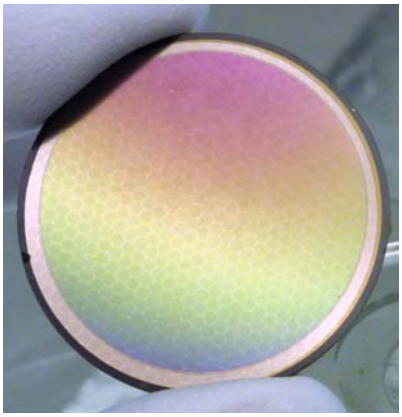

***Fig. 3.*** *CsI opaque photocathode deposited onto a 20-μm pore 33-mm, 60:1 L/d, ALD MCP with MgO and 13° pore bias.*

Photonis is continuously producing multialkali and bialkali photocathodes for their existing Planacon devices, so are fully equipped to implement them. However, to meet LUVOIR goals for example, we wish to optimize for UV response and long-wavelength cutoff, and minimize the intrinsic dark rate. Traditional visible-sensitive photocathodes like bialkali ($Na_2KSb$) have a 30% peak at 350 nm but also show high QE in the UV [21] that has not been previously accessed for UV sensors. In our existing UCB facilities, we have produced many semitransparent bialkali photocathodes [22] up to 20-cm format with peak QEs of 25% at 350 nm. We just completed setting up a process tank for bialkali-photocathode ($Na_2KSb$) deposition onto $MgF_2$ substrates, to set the process and thickness that optimizes the QE below 300 nm while obtaining a sharp cutoff above 400 nm. The general practice is to make the cathodes thin, because the high attenuation coefficient for blue light produces photoelectrons close to the surface where they can escape, but allows red light to pass through without interaction. Initial tests are shown

in Fig. 4 for thin bialkali photocathodes made on $MgF_2$ windows. Although the peak QE is not optimized yet, we demonstrated a good cutoff at 350 nm with the most recent deposition.

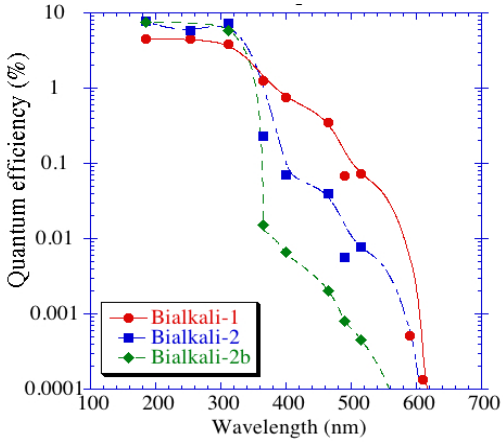


***Fig. 4.*** *QE for blue-optimized semitransparent bialkali photo-cathodes on a $MgF_2$ window.*

We subsequently prepared a new set of three $MgF_2$ windows and installed them into the process tank to permit a further iteration of the process, intending to optimize the "in-band" QE. The system has been successfully preconditioned (high-vacuum bake) and is ready for photocathode depositions. Following the establishment of a baseline, we would work with Photonis to adjust their photocathode deposition process to suit.

### *ALD Microchannel Plates*

A new type of MCP (Fig. 5) constructed by ALD on borosilicate microcapillary arrays, using inexpensive hollow borosilicate tubes, has recently been developed. The fabrication method is somewhat similar to that of conventional MCPs [23], but without the need to remove a core glass inside the tubes. Resistive layers and secondary emissive layers are deposited using ALD, replacing the hydrogen reduction used for conventional MCP activation. Borosilicate microcapillary substrates are very robust compared with standard MCP glass. MCPs are regularly made with 20-µm-pore borosilicate up to 20 cm, and 10-µm pore, 10-cm and 5-cm square formats with 60:1 L/d ratio. The gain uniformity is good even over the largest areas [24]. The background event image distribution of ALD MCPs is uniform and is very low-rate, 0.03 events/cm$^2$/sec$^1$ [25] (> 5x lower than standard MCPs). Detection efficiency for MeV gamma rays is a potentially important factor in reducing instrumental background rates in high-radiation environments. For ALD MCPs, the efficiency is ~0.7% [25] as compared with ~2% for conventional lead-glass MCPs.

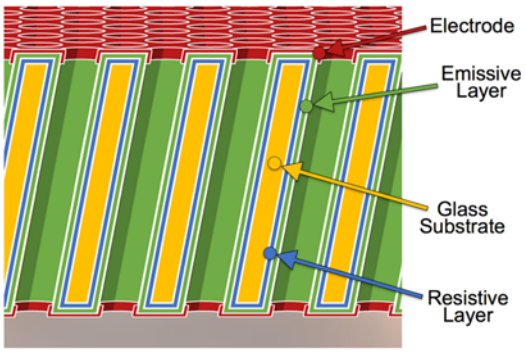


***Fig. 5****. Borosilicate glass microcapillary substrates are functionalized with ALD. Separate sets of ALD depositions set the resistances and secondary emission ($Al_2O_3$ and MgO) layers to create a working MCP.*

We met with the MCP vendor, Incom Inc., to establish MCP specifications and processing. The ALD MCPs will be 53.5 mm square using 10-µm pores, 60:1 L/d, 13° pore bias and MgO secondary emissive layers, which is a standard MCP configuration for the Photonis Planacon. borosilicate ALD MCPs from Incom also come standard with 10-µm pore substrates. They can be made in a variety of

sizes, however the most convenient scheme for the Planacon MCPs is to use the standard-size block material and then dice into the final 53-mm format. The nominal open area for the substrates is ~75%, which maximizes photoelectron detection efficiency for semitransparent photocathode photoelectron detection. The goal for MCP resistance is in the range 20 -30 MΩ, in keeping with models for acceptable power dissipation, as well as high local event rate handling. We also just tested some 10-µm pore sample MCPs to establish expectations for MCPs for the Planacon trials. The results (Fig. 6) show good gain characteristics, allowing Incom to proceed with construction of full-size MCPs. We placed an order for the first sets of 10-µm pore MCPs for the first Planacon build.

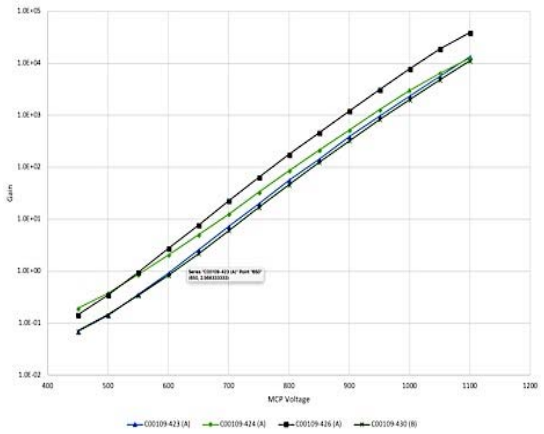


***Fig. 6.*** *Gain is high and repeatable for 33-mm-diameter borosilicate ALD MCPs with 10 µm pore, 74% open area, 60:1 L/D with a MgO emissive layer.*

### *XS Readouts for Sealed Tubes*

The XS anode itself is made with layers of metals and insulators on an insulating substrate, producing two sets of strips in orthogonal directions. The top and bottom layers have equal exposed areas, and thus collect the charge from the MCPs with equal charge sharing (Fig. 1). Each anode strip is connected to the back side of the anode using hermetically sealed vias, allowing mounting of all the detector electronics outside the vacuum. In this case, we employed ceramics for the substrates and insulating layers using standard thick-film technologies. Ceramic XS anodes are low-outgassing, refractory, and accommodate being put into sealed-tube ultra-high-vacuum devices. We adopted a 47-mm XS, 72×72 strip-anode (Fig. 7) design that is capable of high resolution [26] with good image linearity. The upper and lower orthogonal fingers occupy approximately 50% of the area respectively (Fig. 8) and are separated by insulating glass layers. The first batch of anodes has already been procured and was recently delivered. These are currently undergoing tests, but initial bench measurements show that the finger isolation and the inter-capacitances (< 10 pF) are all within expectations. In parallel, we are obtaining ceramic blanks so that Photonis can seal these anode blanks to the current production bodies before using the actual XS anodes.

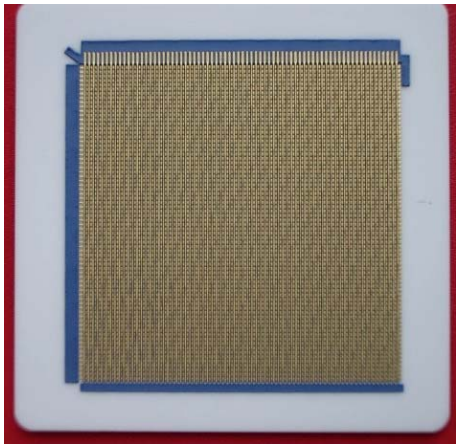

***Fig. 7.*** *Cross-strip anode with 47-mm active area on ceramic substrate for inclusion in a high-vacuum Planacon sealed-tube package*.

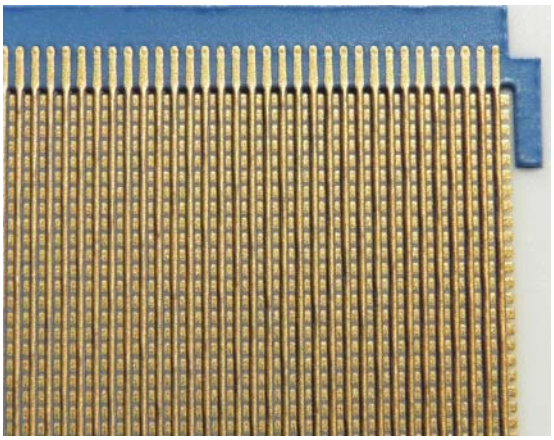

***Fig. 8.*** *Section on one corner of the 47-mm XS anode showing the upper and lower fingers of the cross strips that are exposed for event charge collection.*

### *Component Testing*

We have established cross-delay-line and cross-strip (Fig. 9) readout anode detectors in 50-mm format, and readout electronics for photon-counting tests of MCPs and XS anodes. The current PXS-II (Fig. 10) encoding electronics has also been commissioned for evaluation and testing of XS anodes, and to provide the high-resolution imaging for ALD MCP testing. We installed sample 53-mm ALD MCPs with 20-µm pores into the detector to verify the system is ready to test the final 10-µm MCPs when they are delivered to us. The results are shown in Figs. 11 and 12. The imaging is sufficient to resolve every MCP pore, and the gain for these MCPs is very uniform across the field of view. The performance of this test-bed is sufficient for all our evaluations of the sealed-tube sub-components as we accumulate them and proceed to integrate the final devices.

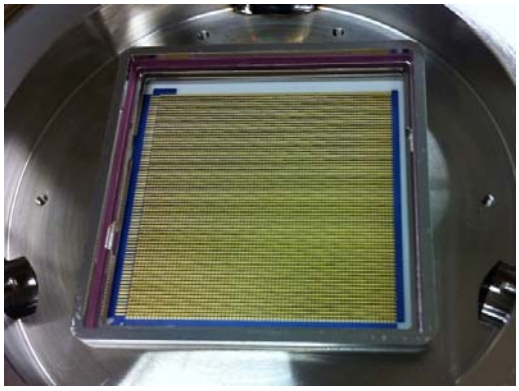

***Fig. 9.*** *50-mm active area, cross-strip-anode imaging detector for 50-mm MCP and XS anode tests. Planacon style detector body.*

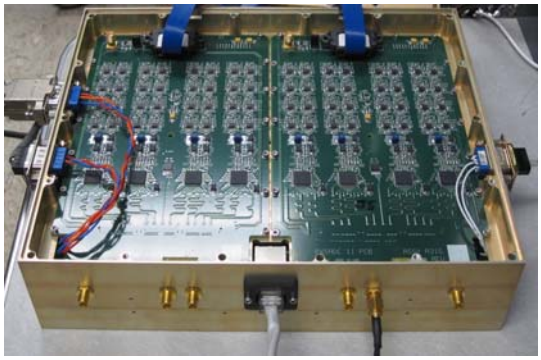

***Fig. 10.*** *PXS-II main electronics system; providing photon position to 16k×16k accuracy (achieved < 20-µm FWHM spatial resolution with XS detectors at MCP gains of ~2×10$^6$ at MHz rates.*

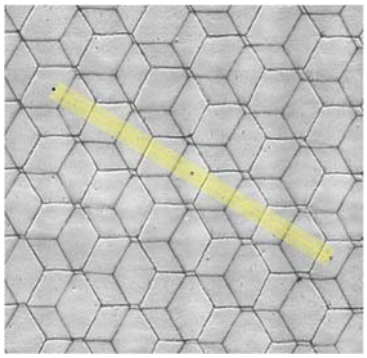

***Fig. 11.*** *Image with cross-strip anode detector for a 50×50 mm$^2$ cross-strip readout detector at ~2×10$^6$ gain (pair of 20-µm-pore MCPs).*

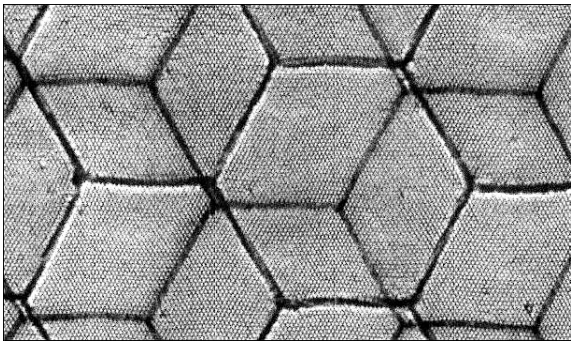

***Fig. 12.*** *Magnified area of Fig. 11 shows it is capable of very high resolution (~5 µm/pixel) with the cross-strip detector. Individual 20-µm pores are clearly visible.*

## Path Forward

The next steps include receipt and dispatch of the anode blanks to Photonis for vacuum-sealing-process verification. Meanwhile, we will complete the verification tests, both functional and physical, of the 47-mm XS anodes we received, and make any adjustments needed to ensure they are compatible with the Planacon structure. This paves the way to subsequently send them to Photonis for sealing to Planacon tube bodies. ALD MCPs in 10-µm pore, 13°-bias material with MgO emissive layers are on order, but will not arrive before fall 2018. In the meantime, we will be testing all the ALD MCP performance characteristics of 33-mm sample MCPs to verify ALD processing conditions and make recommendations for the final processing sequence for the MCPs to be incorporated into the sealed Planacon tubes. When the full-size, 10-µm MCPs do arrive, we will test them and then dice them to the required size. Then, we will test the performance of the 53-mm MCPs in pairs, including,

gain, pulse-height distribution (PHD), background, uniformity, etc. in our high-resolution open-face XS detector system, and dispatch to Photonis for Planacon tube integration. In concert with these efforts, we are poised to test both opaque-alkali-halide and semitransparent-photocathode processes. These will take the form of a number of process iterations where we measure the QE and background, as well as the effect on MCP imaging characteristics. It is not anticipated that the first Planacon device will use the modified photocathode process. Rather, the initial Planacon sealed tube will be directed at including the XS anode element and ALD MCPs, for measuring its performance compared to standard devices. A significant milestone is to complete the first Planacon device and carry out the basic functional tests (gain, QE, background, imaging, etc.).

## References


[1] O.H.W. Siegmund, M.A. Gummin, J.M. Stock, G. Naletto, G.A. Gaines, R. Raffanti, J. Hull, R. Abiad, T. Rodriguez-Bell, T. Magoncelli, P.N. Jelinsky, W. Donakowski, and K.E. Kromer, "*Performance of the double delay line microchannel plate detectors for the Far-Ultraviolet Spectroscopic Explorer*," Proc. SPIE, **vol. 3114**, pp. 283–294 (Oct. 1997)

[2] J. Vallerga, J.B. McPhate, A.P. Martin, G.A. Gaines, O.H.W. Siegmund, E. Wilkinson, S. Penton, and S. Beland, "*HST-COS far-ultraviolet detector: final ground calibration*," Proc. SPIE, **vol. 4498**, pp. 141–151 (Dec. 2001)

[3] P.N. Jelinsky, P.F. Morrissey, J.M. Malloy, S.R. Jelinsky, O.H.W. Siegmund, C. Martin, D. Schiminovich, K. Forster, T. Wyder, and P.G. Friedman, "*Performance results of the GALEX cross delay line detectors*," Proc. SPIE, **vol. 4854**, pp. 233–240 (Feb. 2003)

[4] J. Green, J. Bally, R. Brown, D. Ebbets, W. Freedman, J. Grunsfeld, J. Huchra, S. Kilston, R. Kimble, J. Morse, R. O'Connell, K. Sembach, K. Shull, O.H.W. Siegmund, and E. Wilkinson, "*Scientific Rationale for a 10 meter UV-Optical Telescope*," presented at the Astronomical Society of the Pacific Conference Series, **vol. 348**, p. 559 (2006)

[5] T.J. Immel, S.B. Mende, R.A. Heelis, C.R. Englert, J. Edelstein, J.M. Forbes, S. England, A.I. Maute, J.J. Makela, F. Kamalabadi, G. Crowley, A.W. Stephan, J.D. Huba, J. Harlander, G.R. Swenson, H.U. Frey, G.S. Bust, J.M. Gerard, B.A. Hubert, D.E. Rowland, D.L. Hysell, A. Saito, S. Frey, M. Bester, and C.E. Valladares, "*ICON: The Ionospheric Connection Explorer - NASA's Next Space Physics and Aeronomy Mission*," AGU, **vol. 42**, p. 03 (Dec. 2013)

[6] R. Eastes, M. Codrescu, W. McClintock, A. Aksnes, D. Anderson, L. Andersson, A. Burns, S. Budzien, R. Daniell, K. Dymond, F. Eparvier, J. Harvey, T. Immel, A. Krywonos, M. Lankton, J. Lumpe, G. Prolss, A. Richmond, D. Rusch, O.H.W. Siegmund, S. Solomon, D. Strickland, and T. Woods, "*Global-scale Observations of the Limb and Disk (GOLD) - New Observing Capabilities for Space Weather Specification and Forecasting,*" AGU, **vol. 13**, p. 1085 (Dec. 2007)

[7] R. Gladstone, M. Versteeg, T.K. Greathouse, V. Hue, M. Davis, J.-C. Gerard, D. Grodent, and B. Bonfond, "Ju*no Ultraviolet Spectrograph (Juno-UVS) Observations of Jupiter during Approach*," AAS, **vol. 48**, p. #402.02 (Oct. 2016)

[8] P.A. Scowen, T. Tripp, M. Beasley, D. Ardila, B.G. Andersson, J.M. Apellániz, M. Barstow, L. Bianchi, D. Calzetti et al., "F*inding the UV–Visible Path Forward: Proceedings of the Community Workshop to Plan the Future of UV/Visible Space Astrophysics*," PASP **129**(977), 076001, IOP Publishing (2017)

[9] K. France, B. Fleming, G. West, S.R. McCandliss, M.R. Bolcar, W. Harris, L. Moustakas, J.M. O'Meara, I. Pascucci et al., "*The LUVOIR Ultraviolet Multi-Object Spectrograph (LUMOS): instrument definition and design*," Proc. SPIE **10397**, 1039713, (2017)

[10] P.A. Scowen, D. Stern, R. Somerville, M. Rud, S. Martin, and M. Beasley, "*Science and architecture drivers for the HabEx Ultraviolet Spectrograph (UVS)*," Proc. SPIE **0398**, 1039807 (2017)

[11] S. Heap and the CETUS Team, "*The UV Survey Mission Concept, CETUS*," American Astronomical Society, AAS Meeting #231, id.#355.30 (2018)

[12] C. Ertley, O.H.W. Siegmund, A. Tremsin, and J. Hull, "*Microchannel Plate Imaging Detectors for High Dynamic Range Applications*," IEEE Trans. Nucl. Sci., **vol. PP**, no. 99, pp. 1–1 (2017)

[13] J. Vallerga, R. Raffanti, M. Cooney, H. Cumming, G. Varner, and A. Seljak, "C*ross strip anode readouts for large format, photon counting microchannel plate detectors: developing flight qualified prototypes of the detector and electronics*," TWEPP, pp. 91443J–91443J–12 (Jul. 2014)
[14] Photonis online catalog, "Planacon"
[15] O.H.W. Siegmund, J. B. McPhate, J. Vallerga, A. Tremsin, S.R. Jelinsky, and H.J. Frisch, "*Novel large format sealed tube microchannel plate detectors for Cherenkov timing and imaging*," **vol. 639**, no. 1, pp. 165–168 (May 2011)
[16] S.R. Jelinsky, O.H.W. Siegmund, and J.A. Mir, "*Progress in soft x-ray and UV photocathodes*," Proc. SPIE, **vol. 2808**, pp. 617–625 (Oct. 1996)
[17] A. Tremsin and O.H.W. Siegmund, "*UV radiation resistance and solar blindness of CsI and KBr photocathodes*," IEEE Trans. Nucl. Sci., **vol. 48**, no. 3, pp. 421–425 (2001)
[18] J.I. Larruquert, J.A. Méndez, J.A. Aznárez, A. Tremsin, and O.H.W. Siegmund, "*Optical properties and quantum efficiency of thin-film alkali halides in the far ultraviolet*," Appl. Opt., **vol. 41**, no. 13, pp. 2532–2540 (May 2002)
[19] A. Tremsin and O.H.W. Siegmund, "T*he quantum efficiency and stability of UV and soft X-ray photocathodes*," Proc. SPIE, **vol. 5920**, pp. I–13, Aug. 2005.
[20] O.H.W. Siegmund, J. Vallerga, and A. Tremsin, "C*haracterizations of microchannel plate quantum efficiency*," Proc. SPIE, **vol. 5898**, pp. 113–123 (Aug. 2005)
[21] P. Dorenbos, J.T.M. de Haas, R. Visser, C.W.E. van Eijk, and R.W. Hollander, "Qu*antum efficiencies of several VUV-sensitive photomultiplier tubes*," Nucl. Instr. Meth. Phys. Res. A, **vol. 325**, no. 1, pp. 367–369 (Feb. 1993)
[22] O.H.W. Siegmund, J.B. McPhate, S.R. Jelinsky, J. Vallerga, A. Tremsin, R. Hemphill, H.J. Frisch, R.G. Wagner, J. Elam, and A. Mane, "*Large Area Microchannel Plate Imaging Event Counting Detectors with Sub-Nanosecond Timing*," IEEE Trans. Nucl. Sci., **V 60**(2), pp. 923–931 (Apr. 2013)
[23] M. Lampton, "*The Microchannel Image Intensifier*," Scientific American, **vol. 245**(5), pp. 62 (1981)
[24] O.H.W. Siegmund, J. Vallerga, A. Tremsin, J. McPhate, H. Frisch, J. Elam, A. Mane, R. Wagner, and G. Varner, "*Large Area and High Efficiency Photon Counting Imaging Detectors with High Time and Spatial Resolution for Night Time Sensing and Astronomy*," AMOS Conf. p. 92 (2012)
[25] O.H.W. Siegmund, C. Ertley, C.A. Craven, J. Vallerga, M. Popecki, A. O'Mahony, and M.J. Minot, "*High Speed Large Format Photon Counting Microchannel Plate Imaging Sensors*," Proc AMOS, **vol. 1**, p. 94 (2015)
[26] O.H.W. Siegmund, A. Tremsin, and J. Vallerga, "*Development of cross strip MCP detectors for UV and optical instruments*," Proc. SPIE, **vol. 7435**, pp. 74350L–74350L–10 (Aug. 2009)

**For additional information, contact Oswald Siegmund: ossy@berkeley.edu**

# Advanced UVOIR Mirror Technology Development for Very Large Space Telescopes

Prepared by: H. Philip Stahl (NASA MSFC)

## Summary

The Advanced Mirror Technology Development (AMTD) project is in Phase 2 of a multiyear effort initiated in Fiscal Year (FY) 2012, to mature the Technology Readiness Level (TRL) of critical technologies required to enable 4-m-or-larger monolithic or segmented ultraviolet, optical, and infrared (UVOIR) space telescope primary-mirror assemblies for general astrophysics, ultra-high-contrast observations of exoplanets and National Interest missions. AMTD-2 is jointly funded by NASA and the Air Force.

In 2012, AMTD-2 defined three major milestones. During 2016/17 AMTD-2 successfully accomplished half of these:

- ✓ Harris Corp fabricated a ~150 Hz 1.5-meter Ultra-Low Expansion (ULE®) mirror (1/3rd scale of a 4-m mirror) substrate using stacked core method, demonstrating lateral scalability of the stacked core technology.
- o NASA MSFC characterized the mechanical and thermal performance of the Schott owned 1.2-meter Zerodur® mirror (polished and integrated into an assembly by Arizona Optical Systems).
- o NASA MSFC validated by test its integrated STOP model prediction of the 1.2m Zerodur® mirror's mechanical and thermal performance; including verification of CTE homogeneity.

The balance is scheduled for completion in the fourth quarter of FY17:

- o Characterizing the mechanical and thermal performance of the Harris 1.5-m ULR® mirror.
- o Validating by test MSFC's integrated STOP model prediction of the 1.5-m ULE® mirror's mechanical and thermal performance; this testing also includes verification of CTE homogeneity.

Additionally, lessons learned about low-temperature-slumping (LTS) of large stiff mirror substrates from fabricating the 1.5m ULE® mirror are being incorporated into various current and planned NASA and National Interest missions. An AMTD-3 proposal to resolve the issues was submitted to the ROSES 2016 SAT. Finally, NASA MSFC is using integrated design tools developed on AMTD-2 to design candidate optical telescope assemblies for the potential Habitable Exoplanet Imager mission.

The foundation of AMTD's success continues to be its integrated team of Government/Industry scientists, systems engineers, and technologists executing a science-driven systems engineering approach to technology development. Additionally, AMTD continues mentoring the next generation of scientists and engineers via interns, co-ops, and volunteers. In this cycle AMTD hosted two undergraduate student interns: Samantha Hansen of Rutgers University and Mary Elizabeth Cobb of University of Alabama in Huntsville.

AMTD results were presented at Mirror Tech Days 2016 and published in proceedings of the 2016 SPIE Astronomy Conference[1] and 2017 SPIE Optics and Photonics Conference[2,3] (see list at report end).

## Background

"Are we alone in the Universe?" is probably the most compelling science question of our generation.

Per the 2010 *New Worlds, New Horizons* Decadal Report[4]: "One of the fastest growing and most exciting fields in astrophysics is the study of planets beyond our solar system. The ultimate goal is to image rocky

planets that lie in the habitable zone of nearby stars." The Survey recommended, as its highest priority, medium-scale activity such as a "New Worlds Technology Development (NWTD) Program" to "lay the technical and scientific foundations for a future space imaging and spectroscopy mission." The National Research Council (NRC) report, *NASA Space Technology Roadmaps & Prioroties*[5], states that the second highest technical challenge for NASA regarding expanding our understanding of Earth and the universe in which we live is to "Develop a new generation of astronomical telescopes that enable discovery of habitable planets, facilitate advances in solar physics, and enable the study of faint structures around bright objects by developing high-contrast imaging and spectroscopic technologies to provide unprecedented sensitivity, field of view, and spectroscopy of faint objects." NASA's *Enduring Quests Daring Visions*[6] called for a LUVOIR surveyor mission to "enable ultra-high-contrast spectroscopic studies to directly measure oxygen, water vapor, and other molecules in the atmospheres of exoEarths," and "decode the galaxy assembly histories through detailed archeology of their present structure." As a result, NASA will study in detail a LUVOIR surveyor and a HabEx Imager concept for the 2020 Decadal Survey.[7,8] Additionally, AURA's *From Cosmic Birth to Living Earths*[9] details the potential revolutionary science that could be accomplished from "directly finding habitable planets showing signs of life."

Directly imaging and characterizing habitable planets requires a large-aperture telescope with extreme wavefront stability. For an internal coronagraph, this requires correcting wavefront errors (WFEs) and keeping that correction stable to a few picometers rms for the duration of the science observation. This places severe specification constraints upon the performance of the observatory, telescope, and primary mirror. One important problem is dynamic WFE. For either large monolithic mirrors (for HabEx) or smaller mirror segments (for LUVOIR), mechanical disturbances create rigid-body motion of the mirror on its mount. These inertial motions introduce dynamic WFE when the mirror distorts (or bends) as it reacts against its mount. Achieving wavefront stability is a systems engineering trade between mirror stiffness and vibration isolation. Per Lake,[10] WFE is proportional to rms magnitude of the applied inertial acceleration divided by the square of the structure's first mode frequency. Therefore, to achieve <10 pm rms requires either a very stiff system or very low acceleration loads. It is easier to improve performance by increasing stiffness rather than increasing isolation. For a given stiffness mirror, a 10× reduction in acceleration results in a 10× WFE reduction. For a given acceleration level, a 10× increase in stiffness results in a 100× WFE reduction. While systems engineering analysis is still preliminary, the HabEx program estimates that it needs a 4-m monolithic primary mirror with a first mode frequency greater than 100 Hz and maybe as high as 200 Hz. The LUVOIR program estimates that it needs 1.5-m segments with a first mode frequency greater than 220 Hz (JWST) and maybe as high as 500 Hz.

Before AMTD, the state of art for lightweight stiff glass mirror substrates was defined by AMSD and ATT. For their sizes (AMSD 1.5m × 50mm; ATT 2.5m × 150mm) both mirrors have >150 Hz first mode required for stable on-orbit mechanical performance. But neither has sufficient structural depth for >100 Hz at 4m. The easiest way to increase stiffness is to increase thickness. AMTD-1 advanced TRL by successfully demonstrating a new process (stacked-core low-temperature fusion) that extended the previous state of art (SOA) for deep-core substrates from <300 mm to >400 mm. This was done by making a 43-cm diameter full-scale 'cut-out' of a 4-m mirror. AMTD-2 continued this advance by making a 450 Hz, 1.5-m x 165-mm mirror.

## Objectives and Milestone:

AMTD's objective is to mature towards TRL6 technologies to enable large monolithic or segmented UVOIR space telescopes. Phase 1 advanced technology readiness of six key technologies required to make an integrated primary mirror assembly (PMA) for a large aperture UVOIR space telescope.

- *Large-Aperture, Low-Areal Density, High-Stiffness Mirror Substrates*
- *Support System*
- *Mid/High-Spatial Frequency Figure Error*
- *Segment Edges*

- *Segment-to-Segment Gap Phasing*
- *Integrated Model Validation*

Phase 2 is continuing the efforts in High-Stiffness Substrates, Support Systems, Segment-to-Segment Gap Phasing and Integrated Model Validation with three clearly defined milestones:

- *Fabricate a ⅓-scale model of 4-m class 400-mm thick deep-core ULE® mirror substrate* to demonstrate lateral scaling of the deep-core process. (Successfully Completed in 2016.)
- *Characterize two candidate primary mirrors* (the ⅓-scale mirror and a 1.2-m Extreme Lightweight Zerodur® Mirror owned by Schott) by measuring their modal performance and optical performance from 250 K to ambient. (Schott 1.2-m Zerodur® mirror successfully characterized in 2016; 1.5-m ULE® Harris mirror is schedule for characterization in 2017.)
- *Add capabilities and validate integrated design and modeling tools* to predict the mechanical and thermal behavior of the candidate mirrors, validate models, generate Pre-Phase-A point designs, and predict on-orbit optical performance. (Schott 1.2-m Zerodur® mirror mechanical and thermal performance models were successfully validated by test in 2016; 1.5-m ULE® Harris mirror models are schedule for validation by test in 2017; Additionally, NASA MSFC is using integrated design and modeling tools on the potential Habitable Exoplanet Imager mission.).

## Progress and Accomplishments:

***Large-Aperture, Low-Areal-Density, High-Stiffness Mirror Substrates***

**Need:** To achieve ultra-stable mechanical and thermal performance required for high-contrast imaging, either (4-m to 8-m) monolithic or (8-m to 16-m) segmented mirrors require thicker, stiffer mirrors.

**Milestone #1:** Fabricate a ⅓-scale model of 4-m class 400-mm thick deep-core ULE® mirror substrate to demonstrate lateral scaling of the deep-core process.

**Accomplishment:** During FY 2016/17, AMTD-2 progressed this technical area by fabricating a 450Hz 1.5m substrate to accomplish its defined milestone and learning lessons from turning that substrate into a mirror.

High-Stiffness Mirror Substrates: Previously, AMTD-1 advanced TRL by successfully demonstrating the ability to make a 40-cm thick subscale mirror substrate via the stacked-core low-temperature fusion (LTF) process. This extended the previous SOA for deep-core substrates from <300 mm to >400 mm. This was done by making a 43-cm diameter 40-cm thick full-scale 'cut-out' of a 4-m mirror. In 2016, AMTD-2 achieved its major milestone for this technology when Harris Corp successfully LTF'ed a 1.5-m diameter by 165 mm thick 5-layer ULE® mirror substrate with a 450 Hz first mode frequency. In 2016/17 Harris Corp low-temperature-slumped (LTS) the mirror substrate to a 3.5 meter radius of curvature then ground, polished, coated it with protective aluminum and integrated it into a flight-like mount (Figure 1). In 2017 the mechanical and thermal performance of this mirror assembly will be characterized at NASA MSFC.

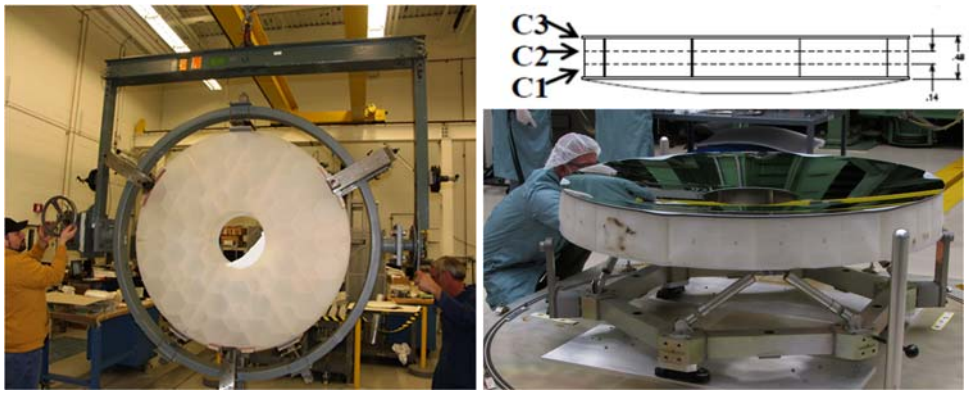

***Figure 1:*** *(left) Low-Temperature-Fused Mirror Substrate; (top right) 5-layer design; (bottom right) completed mirror assembly.*

During AMTD-1 when the 43-cm deep-core mirror was slumped from 5.0 to 2.5-meter radius of curvature, there was noticeable deformation in the core walls. To quantify the magnitude of this bending MSFC imaged the mirror's internal structure via x-ray tomography. A small amount of bending was expected because slumping places the concave surface in compression and stretches the convex surface; this places the core elements in shear stress. The measured deformation exceeded that expectation. Fortunately, analysis indicated that such core-wall bending had a limited effect on the mirror's strength.

In designing the 1.5-meter 1/3rd scale model of a 4-meter mirror, Harris Corp used proprietary modeling tools to predict the visco-elastic performance of the mirror (Figure 2). The spacing between the wedge-shaped core elements was specifically increased to prevent adjacent core-walls from touching. While the core walls never touched, they did get within <0.25 mm at four locations. (Figure 2). In 2017 MSFC plans to image the internal structure of the mirror via X-Ray computed tomography, use that data to create an as-built 3D model of the mirror to predict its mechanical and thermal performance, and characterize its performance.

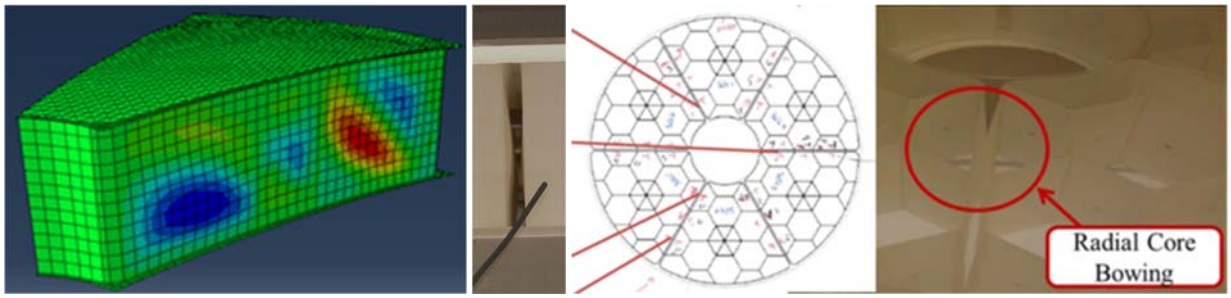


***Figure 2:*** *(left) predicted visco-elastic deformation used to design mirror substrate; (right 3 images) actual visco-elastic deformation; 4-locations had gaps of less than 0.25 mm.*

Explaining core-wall bending is complicated. Previous to AMTD, the only mirrors fabricated via LTS replication were AMSD/MMSD. Neither of these mirrors exhibited core-wall bending. Preliminary analysis indicates that the effect depends upon the shear stress in the radial core-walls. The greater the amount of shear stress, the greater the amount of viscous flow of the glass during LTS replication and the greater the core-wall bending. Preliminary analysis indicates that this shear stress is proportional to the unsupported radial core wall length divided by the radius of curvature (independent of core thickness and independent of whether the core is composed of a single layer or multiple layers). The AMTD-1 2.5-m ROC 0.43-m diameter x 400-mm thick mirror had significantly larger core cells than the AMTD-2 3.5-m ROC 1.5-m diameter x 165-mm thick mirror; and thus, less bending. An AMTD-3 proposal to resolve this issue was submitted to the ROSES 2016 SAT.

Arnold Mirror Modeler: the Arnold Mirror Modeler was developed under AMTD to rapidly create and analyze detailed mirror designs. The AMM creates a complete analysis stream, including model, loads [static and dynamic], plots and a summary file of input variables and results suitable for optimization or trade studies. Values of all settings can be archived and recalled to continue or redo any configuration. In FY16/17 an updated AMM was released and is being used to perform point design trade studies for HabEx closed-back ULE® and open-back Zerodur® mirror systems.

***Support System***

**Need:** Large-aperture mirrors require large support systems to ensure they survive launch and deploy on-orbit, stress-free, and undistorted. Additionally, segmented mirrors require large structure systems that establish and maintain the mirror's shape.

**Accomplishment:** During FY 2016/17, AMTD-2 progressed this technical area by continuing to develop mount capabilities in the Arnold Mirror Modeler and use it to perform trade studies of candidate mirror mount systems for HabEx. The emphasis of these trade studies has been on understanding and specifying dynamic primary mirror wavefront error.

Dynamic WFE is produced when a mirror is placed in inertial acceleration by a mechanical disturbance, causing it to react (i.e. bend) against its mounts. A 'static' example is gravity sag. The acceleration of gravity causes a mirror to bend on its mount. Assuming that no resonant mode is excited, a mirror's dynamic WFE has the same shape as its gravity sag with an amplitude proportional to the disturbance's 'G-acceleration'. Assuming that the mirror substrate's first mode stiffness is higher than the mechanical disturbance frequencies, the biggest accelerations occur when the mechanical disturbance excites a mount resonance mode. AMTD-2 has studies dynamic WFE for various mirror substrates on both 3-point and 6-point mounts attached to the substrate at the edge, 80% and 50% radial points (Figure 3).

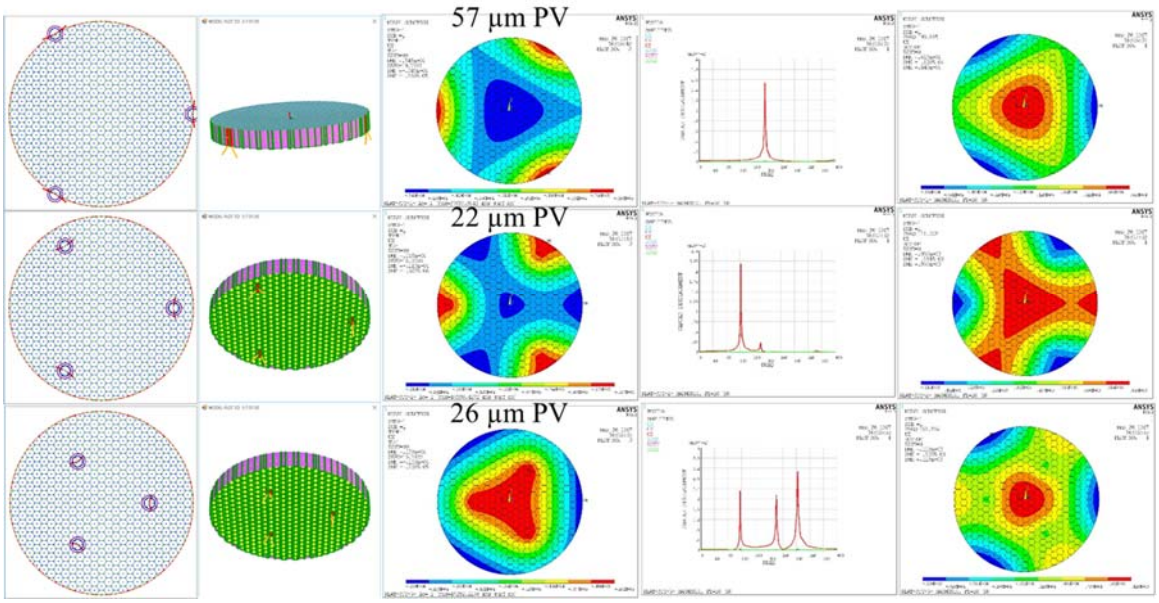


***Figure 3*** *Static gravity sag and dynamic deformation of 180-Hz 4-m diameter closed-back mirror on 3-point mount attached at edge, 80% and 50% radial locations.*

***Mid/High-Spatial Frequency Error:***

**Need:** High-contrast imaging requires mirrors with very smooth surfaces (< 10 nm rms). While deformable mirrors can correct low-order errors, they cannot correct mid and high-spatial frequency errors. Such errors can arise from the fabrication process or CTE inhomogeneity and can introduce artifacts into the dark hole.

**Milestone #2:** Characterize thermal induced surface figure error of two candidate primary mirrors (1.5-m ULE® mirror and 1.2-m Zerodur® mirror owned by Schott) from 250 K to ambient.

**Accomplishment:** During FY 2016/17, AMTD-2 progressed this technical area by characterizing the thermal performance of the 1.2-m Extreme Lightweighted Zerodur® Mirror (ELZM) owned by Schott. This test accomplishes half of this major milestone. Anticipated testing of the 1.5-m ULE® mirror in 2017 will complete this milestone. Previously, AMTD-1 had demonstrated the ability of the Harris Corp's ion polishing process to produce a 5.4-nm rms surface.

Thermal Characterization: In 2016/17 NASA MSFC enhanced its 23m x 7m thermal vacuum test chamber by adding a pressure tight enclosure that allows test equipment to be placed at the center of curvature of short radius of curvature mirrors (Figure 4). This new capability enabled testing of the

Schott 1.2-m ELZM mirror from ambient to 250K. No thermal deformation induced high-spatial quilting associated with the lightweight was measured. The test did measure 9.4 nm rms of mid-spatial error associated with coefficient of thermal expansion (CTE) inhomogeneity (Figure 4).

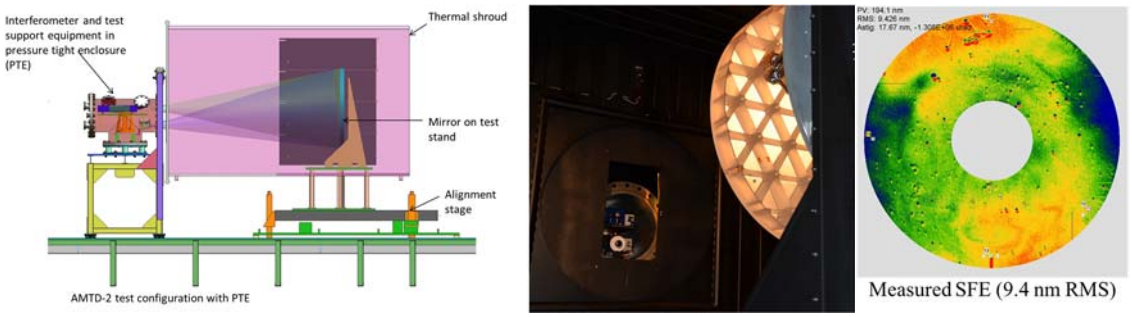


***Figure 4:*** *(left) Short radius of curvature mirror test setup with pressure tight enclosure. (center) Schott ELZM Mirror in test setup. (right) Measured thermal surface figure error from 250K to ambient.*

***Segment-to-Segment Gap Phasing***

**Need:** To avoid speckle noise which can interfere with exoplanet observation, internal coronagraphs require an ultra-stable wavefront.

**Accomplishment:** During FY 2015/16, AMTD Phase 2 progressed this technical area by continuing the systems engineering effort to understand the interaction between optical telescope wavefront stability and coronagraph contrast leakage.

Contrast Leakage WFE Tolerances: In our previous studies, we evaluated the contrast leakage over specific regions of interest (ROI). These studies showed a correlation between numbers of segment rings and noise in a dark-hole ROI. These studies also provided preliminary tolerance values for the allowed amounts of different wavefront errors. Because of the asymmetric nature of the ROI, the tolerance results were misleading. Therefore, in FY2016/17 we implemented a new method that decomposes contrast leakage into average radial (photometric noise) and azimuthal (systematic noise) components as defined by Shaklan[11]. The new method confirms our previous conclusions that segment-to-segment co-phasing (piston and tip/tilt) errors must be stable in the 10 to 20 picometer PV range. The new method was used to evaluate the contrast leakage in annular ROI for 50 random trials global Seidel and Zernike aberration produced by rigid body motion of the primary and/or secondary mirror assemblies. The maximum allowance for static aberration and contrast leakage for aberration exhibiting sinusoidal variation was also studied. Table 1 lists the maximum amount of random WFE that a 4$^{th}$ order radial coronagraph can tolerate while keeping the photometric noise less than $10^{-10}$ and the systematic noise less then $5x10^{-11}$ over an annular ROI from 1.5 to 2.5 λ/D.

**Table 1:** PV Aberration Amplitude Tolerance for Contrast Leakage over an annular ROI from 1.5 to 2.5 λ/D

| Aberration (Random) | WFE (pm) for $1x10^{-10}$ of Photometric Noise | WFE (pm) for $5x10^{-11}$ of Systematic Noise |
|---|---|---|
| Tip/Tilt | 9,600 | 35,000 |
| Seidel Power | 1,100 | 22,000 |
| Zernike Astigmatism | 6,800 | 49,000 |
| Zernike Trefoil | 6,800 | 44,000 |
| Zernike Hexafoil | 9,600 | 78,000 |
| Seidel Spherical | 300 | 11,000 |
| Seidel Coma | 6,800 | 840 |

Clearly, photometric noise (radial average) is more sensitive to Seidel spherical than Seidel power. It is equally apparent that systematic noise is more sensitive to rotationally asymmetric aberrations, such as Seidel coma, than to rotationally symmetric aberrations like Zernike astigmatism.

***Integrated Model Validation***

**Need:** On-orbit performance is driven by mechanical stability (both thermal and dynamic). As future systems become larger, compliance cannot be fully tested; performance verification will rely on results from a combination of sub-scale tests and high-fidelity models. It is necessary to generate and validate as-built models of representative prototype components to predict on-orbit performance for transmitted wavefront, point spread function (PSF), pointing stability, jitter, thermal stability, vibro-acoustic, and launch loads.

**Milestone #3A:** Add capabilities to integrated design and modeling tools to predict the mechanical and thermal behavior of the candidate mirrors; use these tools to generate Pre-Phase-A point designs and predict on-orbit optical performance.

**Milestone #3B:** Validate by test integrated design and modeling tools to predict the mechanical and thermal behavior of the candidate mirrors.

**Accomplishment:** During FY 2016/17, AMTD Phase 2 accomplished Milestone 3A by continuing to develop its integrated design and modeling tools and by using these tools to conduct point design trade studies for the HabEx primary mirror, including on-orbit performance predictions. Additionally during FY2016/17, AMTD-2 accomplished half of major Milestone 3B by using its integrated modeling tools to predict the mechanical and thermal behavior of the Schott 1.2-m ELZM mirror assembly then validating those predictions by test. AMTD-2 expects to complete major Milestone B in 2017 by validating by test its performance predictions for the 1.5-m ULE® mirror assembly.

Mechanical and thermal models were made of the Schott 1.2-m ELZM mirror. The mechanical model predicted a gravity sag deformation of 125 nm rms and a first free-free resonant bending mode of 207 Hz. The thermal model predicted a 21 nm rms total surface figure error (SFE) consisting of contributions from its athermal mount, through thickness thermal gradient and bulk CTE homogeneity. The largest contributor of this error is from an assumed CTE homogeneity of 10 ppb (based on Schott catalog data). (Figure 5)

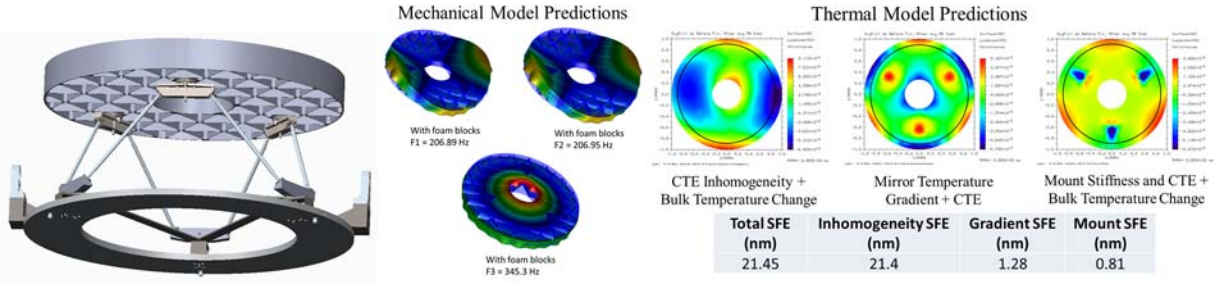


***Figure 5:*** *(left) Schott 1.2-m ELZM assembly. (center) Predicted first mode frequency. (right) Predicted thermal surface figure error.*

The models were validated by test in the MSFC XRCF. First mode frequency was measured via tap test on foam blocks to be 196 Hz (5% agreement). Gravity sag was measured by rotation test to be 142 nm rms; with a 31 nm rms difference between predicted and measured. (Figure 6) This difference could be caused by a 2-mm error between the model and the 'as-built' mount pad locations.

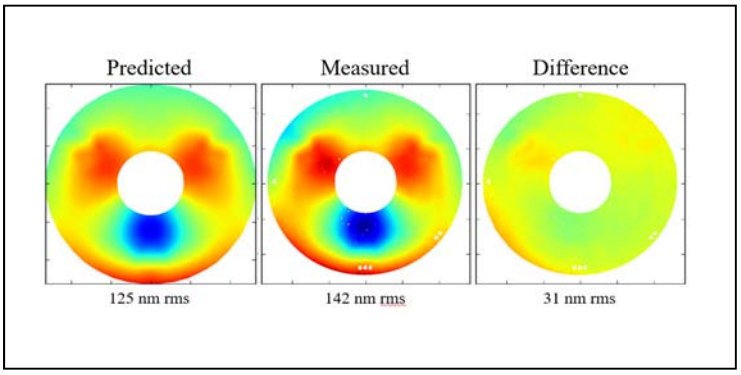


Thermal model predictions are validated by measuring how the mirror shape deforms from 294K to 250K. For input into the thermal model, the mirror assembly is fully instrumented with thermal sensors to measure its bulk temperature and thermal gradients. Using the Schott catalog specification of 10 ppb CTE homogeneity the predicted thermal SFE is 21 nm rms. But, the measured SFE is 9.4 nm rms. After consulting with Schott, we were informed that the 1.2-m ELZM mirror has a CTE homogeneity of 5 ppb. With this new CTE specification, the predicted SFE is 9.55 nm rms. (Figure 7)

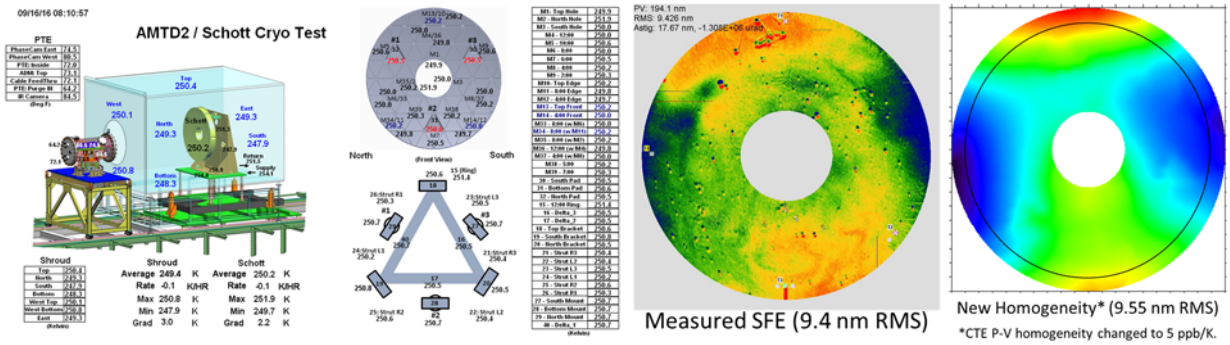


***Figure 7:*** *(left) Instrumented Thermal Test. (center) Measured Thermal SFE. (right) Predicted Thermal SFE with corrected CTE Homogeneity.*

**Milestone Schedule and Future Plans**

AMTD has quantifiable milestones for each technology. Figure 8 shows the Phase 2 schedule. The primary tasks for FY 2017 are to predict the mechanical and thermal performance of the 1.5-m ULE® mirror and validate those predictions by test at the MSFC XRCF.

Figure 8. AMTD Phase 2 schedule.

## AMTD Publications


1. Stahl, H. Philip, "Advanced mirror technology development (AMTD) project: year five status," Proc. SPIE 10401, 2017.
2. Brooks, Thomas, Tony Hull, Ron Eng and H. Philip Stahl, "Modeling the extremely lightweight Zerodur mirror (ELZM) thermal soak test", Proc. SPIE 10374, 2017.
3. Stahl, H. Philip, "Advanced mirror technology development (AMTD) project: overview and year four accomplishments," Proc. SPIE 9912, Advances in Optical and Mechanical Technology for Telescopes and Instrumentation II, (22 July 2016); doi:10.1117/12.2234082.
4. Committee for a Decadal Survey of Astronomy and Astrophysics; National Research Council, New Worlds, New Horizons in Astronomy and Astrophysics, The National Academies Press, Washington, D.C., 2010.
5. NASA Space Technology Roadmaps and Priorities: Restoring NASA's Technological Edge and Paving the Way for a New Era in Space, NRC Report, 2012.
6. Kouveliotou, Centrella, Peterson, et al, Enduring Quests, Daring Visions: NASA Astrophysics in the Next Three Decades, 2014, arXiv:1401.3741, 2014.
7. Hertz, Paul, "Planning for the 2020 Decadal Survey: An Astrophysics Division White Paper", January 4, 2015, available at science.nasa.gov/astrophysics/documents/.
8. NASA Town Hall, AAS Winter Meeting, Kissimmee, FL, 2016.
9. Dalcanton, Seager, et al, From Cosmic Birth to Living Earths: The Future of UVOIR Space Astronomy, Association of Universities for Research in Astronomy, 2015, www.hdstvision.org/report/.
10. Lake, Peterson, and Levine, Rationale for defining Structural Requirements for Large Space Telescopes, AIAA Journal of Spacecraft and Rockets, Vol. 39, No. 5, 2002.
11. Stuart B. Shaklan, Luis Marchen, John Krist and Mayer Rud, "Stability error budget for an aggressive coronagraph on a 3.8m telescope", SPIE Proceedings 8151, 2011.



**For additional information, contact H. Philip Stahl:** h.philip.stahl@nasa.gov


# Predictive Thermal Control (PTC) Technology to Enable Thermally Stable Telescopes

Prepared by: H. Philip Stahl (NASA/MSFC)

## Summary

The Predictive Thermal Control (PTC) technology development project is a multiyear effort initiated in Fiscal Year (FY) 2017, to mature the Technology Readiness Level (TRL) of critical technologies required to enable ultra-thermally stable telescopes for exoplanet science.

During 2017/2018, PTC has successfully progressed its three defined objectives:

1. Validate thermal optical performance models.
2. Derive thermal-system stability specifications.
3. Demonstrate Predictive Thermal Control.

by accomplishing or advancing three of its five quantifiable milestones:

- ✓ **Milestone #1 (Complete):** Created a high-fidelity STOP model of the1.5-m ULE® Advanced Mirror Technology Development (AMTD-2) mirror, including 3D coefficient of thermal expansion (CTE) distribution and reflective coating, that predicts its optical performance response to steady-state and dynamic thermal gradients. Structural model was created using 3D X-Ray Computed Tomography;
- ✓ **Milestone #2 (Complete):** Derived specifications for thermal control system as a function of wavefront stability for a Vector Vortex Coronagraph;
- **Milestone #3 (In Process):** Designed and started fabricating a predictive Thermal Control System for the AMTD-2 1.5-m ULE® mirror that senses temperature changes and actively controls the mirror's thermal environment;
- **Milestone #4 (In Process):** Performed preliminary Structural-Thermal-Optical-Performance (STOP) model validation tests of the 1.5-m ULE® mirror in a relevant thermal vacuum environment at the MSFC X-ray and Cryogenic Facility (XRCF) test facility; and
- o **Milestone #5:** Use validated model to perform trade studies to determine how thermo-optical performance can be optimized as a function of mirror design, material selection, mass, etc.

The foundation of MSFC's technology development success is our approach of using science-driven systems engineering and teaming with the best scientists, engineers, and technologists in industry, academia, and government. PTC is a joint effort between NASA MSFC and Harris Corporation. Additionally, MSFC continues mentoring the next generation of scientists and engineers as interns, co-ops, and volunteers. In this cycle, MSFC hosted three undergraduate student interns: Jonathan McCready, North Carolina State University (Summer 2018); Hao Tang, University of Michigan (Spring 2018); and Jonathan Gaskins, University of North Carolina Charlotte (Fall 2017, Summer 2018).

PTC results were published in SPIE proceedings and presented at Mirror Technology Days in the Government Workshop [1-4].

## Background

"*Are we alone in the universe?*" is probably the most compelling science question of our generation.

Per the 2010 *New Worlds, New Horizons* Decadal Report [5]: "*One of the fastest growing and most exciting fields in astrophysics is the study of planets beyond our solar system. The ultimate goal is to image rocky planets that lie in the habitable zone of nearby stars*." The Survey recommended as its highest priority medium-scale activity such as a "New Worlds Technology Development (NWTD) Program" to "*lay the technical and scientific foundations for a future space imaging and spectroscopy mission*." The National Research Council (NRC) report, "*NASA Space Technology Roadmaps and Priorities*" [6], states that the second-highest technical challenge for NASA regarding expanding our understanding of Earth and the universe in which we live is to "*develop a new generation of astronomical telescopes that enable discovery of habitable planets, facilitate advances in solar physics, and enable the study of faint structures around bright objects by developing high-contrast imaging and spectroscopic technologies to provide unprecedented sensitivity, field of view, and spectroscopy of faint objects*." NASA's "*Enduring Quests, Daring Visions*" [7] called for a Large Ultraviolet/Optical/Infrared (LUVOIR) Surveyor mission to "*enable ultra-high-contrast spectroscopic studies to directly measure oxygen, water vapor, and other molecules in the atmospheres of exoEarths*," and "*decode the galaxy assembly histories through detailed archeology of their present structure*." As a result, NASA is studying in detail the LUVOIR and HabEx concepts for the 2020 Decadal Survey [8, 9]. Additionally, the Association of Universities for Research in Astronomy (AURA) report "*From Cosmic Birth to Living Earths*" [10] details the potential revolutionary science that could be accomplished from "*directly finding habitable planets showing signs of life*."

Directly imaging and characterizing habitable planets requires a large-aperture telescope with extreme wavefront stability. For an internal coronagraph, this requires correcting wavefront errors (WFEs) and keeping that correction stable to a few picometers root mean square (rms) for the duration of the science observation. This places severe specification constraints on the performance of the observatory, telescope, and primary mirror. Per the 2015 Cosmic Origins Program Annual Technology Report (PATR) [11], a "Thermally Stable Telescope" is critical, highly desirable technology for a strategic mission. "*Wavefront stability is the most important technical capability that enables $10^{-10}$ contrast exoplanet science with an internal coronagraph. State of art for internal coronagraphy requires that the telescope must provide a wavefront that is stable at levels less than 10 pm for 10 minutes (stability period ranges from a few minutes to 10s of minutes depending on the brightness of the star being observed and the wavefront-sensing technology being used).*"

Thermal wavefront error occurs because of coefficient of thermal expansion (CTE); slewing the telescope relative to the sun causes its structure or mirrors to change temperature. Changes in thermal heat load cause the structure holding the mirrors to expand/contract and the mirrors themselves to change shape. Fortunately, thermal drift tends to be slow, i.e., many minutes to hours. No previous mission has ever required a telescope with a wavefront that is stable at levels of less than 10 pm per 10 minutes. State-of-the-art (SOTA) for ambient temperature space telescopes are 'cold-biased' with heaters. The telescope is insulated from solar load such that, for all orientations relative to the sun, it is always at a 'cold' temperature (for example, 250 K). The telescope is then warmed to an ambient temperature via heater panels on the forward stray-light baffle tube as well as behind and beside the mirror. SOTA thermal control systems have demonstrated ~1-K stability for a 1-m class telescope using a 'bang/bang' controller. Analysis indicates that ~100 mK should be possible with a proportional integral differential (PID) controller.

PTC plans to advance the SOTA in thermal control by demonstrating a control logic called Model Predictive Control (MPC) [12, 13]. MPC places a physics-based model into the control loop to determine control variables (heater power levels) based on state variables (temperature measurements). MPC

determines heater power levels using a completely different logic than proportional control. Proportional control adjusts heater power in proportion to the difference between measured and desired temperatures at one location. MPC uses multiple control zones and takes into account the interdependency between all control zones' temperatures and heater power. Preliminary analysis indicates that (assuming that thermal performance is linear) it is possible to achieve pm wavefront stability by either controlling the shroud to a small temperature (10 mK) or by rapidly correcting the temperature. Given that mirrors and telescope have a thermal response time, the best way to achieve pm-level stability is to sense and correct for changes in the thermal environment faster than the telescope can respond. Additional stability can be achieved by increasing the system's thermal mass. Based on this analysis, we currently assess such a system's TRL at 3. PTC will advance this TRL by test using the 1.5-m Ultra Low Expansion (ULE®) mirror fabricated by AMTD-2.

## Objectives and Milestone

PTC has defined three objectives to mature the technology needed for an exoplanet science thermally stable telescope by developing "thermal-design techniques validated by traceable characterization testing of components."

1. Validating models that predict thermal-optical performance of real mirrors and structure based on their structural designs and constituent material properties, i.e., CTE distribution, thermal conductivity, thermal mass, etc.
2. Deriving thermal system stability specifications from wavefront-stability requirement.
3. Demonstrating utility of a Predictive Control thermal system for achieving thermal stability.

To achieve our objectives, we defined a detailed technical plan with five quantifiable milestones:

**Milestone #1:** Develop a high-fidelity traceable model of the 1.5-m ULE® AMTD-2 mirror, including 3D CTE distribution and reflective coating, that predicts its optical performance response to steady-state and dynamic thermal gradients.

**Milestone #2:** Derive specifications for thermal control system as a function of wavefront stability.

**Milestone #3:** Design and build a predictive Thermal Control System for a 1.5-m ULE® mirror that senses temperature changes and actively controls the mirror's thermal environment.

**Milestone #4:** Validate model by testing the 1.5-m ULE® mirror in a relevant thermal-vacuum environment at the XRCF test facility.

**Milestone #5:** Use validated model to perform trade studies to determine how thermo-optical performance can be optimized as a function of mirror design, material selection, mass, etc.

## Progress and Accomplishments

### *Objective #1: Validated High-Fidelity STOP Model*

**Need:** Designing a telescope to have 10-pm-per-10-minutes WFE stability using model predictive control requires a validated high-fidelity STOP model.

**Milestone #1:** Develop a high-fidelity STOP model of the 1.5-m ULE® AMTD-2 mirror, including 3D CTE distribution and reflective coating, that predicts its optical performance response to steady-state and dynamic thermal gradients.

**Milestone #4:** Validate high-fidelity STOP model by testing the 1.5-m ULE® mirror in a relevant thermal-vacuum environment at the XRCF test facility.

**Accomplishment:** During FY 2018, PTC completed Milestone #1 and advanced Milestone #4. A high-fidelity model of 1.5-m ULE® AMTD-2 mirror was developed and used to correlate a 231-K static

thermal soak deformation of approximately 20 nm rms to an uncertainty of 13.4 nm rms. Additionally, it was used to correlate a deformation of approximately 80-nm rms for a 115-K lateral thermal gradient.

To accomplish Milestone #1, the PTC Team created a high-fidelity model of the AMTD-2 1.5-m ULE® mirror in NASTRAN that accurately models its 'as-built' mechanical dimensions and 3D CTE distribution. The 'as-built' mechanical dimensions were accurately modeled using 3D X-ray computed tomography to measure the internal structure of the mirror (Fig. 1). These measurements were then ported into a mechanical model (Fig. 2). To add a 3D mapping of CTE distribution, Harris Corporation provided MSFC with Corning CTE data maps for each of the 18 core elements and the location of each element in the core (Fig. 3).

***Fig. 1.*** *1.5-m AMTD-2 mirror being X-Ray CT scanned.*

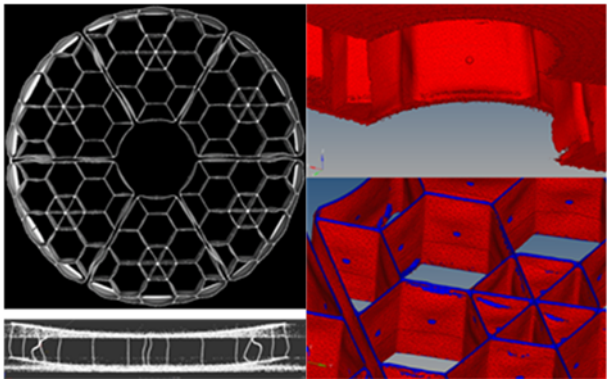

***Fig. 2.*** *X-Ray CT data was converted into Mechanical model.*

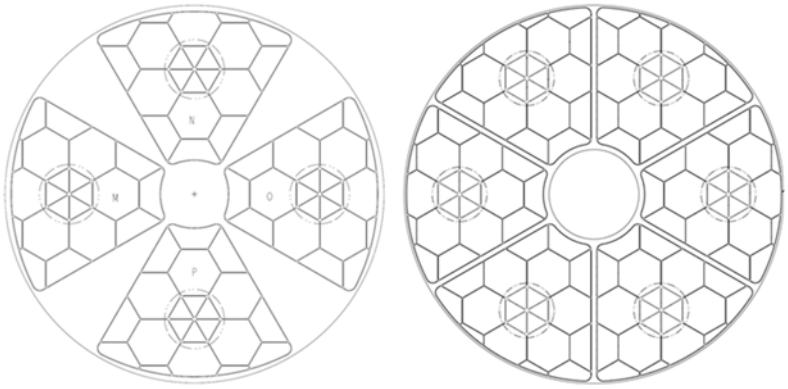

***Fig. 3.*** *Harris Corp provided Corning CTE data for from where each core element was cut from its boule (left) and the location of that core element in the AMTD-2 mirror (right).*

The process by which the AMTD-2 mirror was fabricated resulted in bowing of the core walls. The effect was discovered because the ATMD-2 mirror was deliberately fabricated to a very fast F/# which placed the mirror in an unusually high stress state during fabrication. Such a stress state would not be imposed on an actual flight mirror. The 3D X-ray CT scan produced a 3D mapping of the core wall bowing. A custom algorithm was written to convert the X-ray CT 3D mapping into a finite element model.

To advance Milestone #4, the 1.5-m ULE® AMTD-2 mirror's response to static thermal loads and lateral thermal gradients was tested in the XRCF. This test was conducted jointly with the AMTD-2 static thermal soak test. This test was a bare-mirror-only test, i.e. mirror only with no thermal control system.

First, the high-fidelity model was correlated to cryo-deformation of the AMTD-2 mirror measured during the static thermal load test. This deformation consists of two components: the opto-mechanical-thermal deformation of the mirror mount system and the mirror substrate's CTE distribution. Critical

to model correlation is understanding the temperature distribution on the mirror and its mount system. To achieve this distribution, the mirror is fully instrumented in the test setup (Fig. 4).

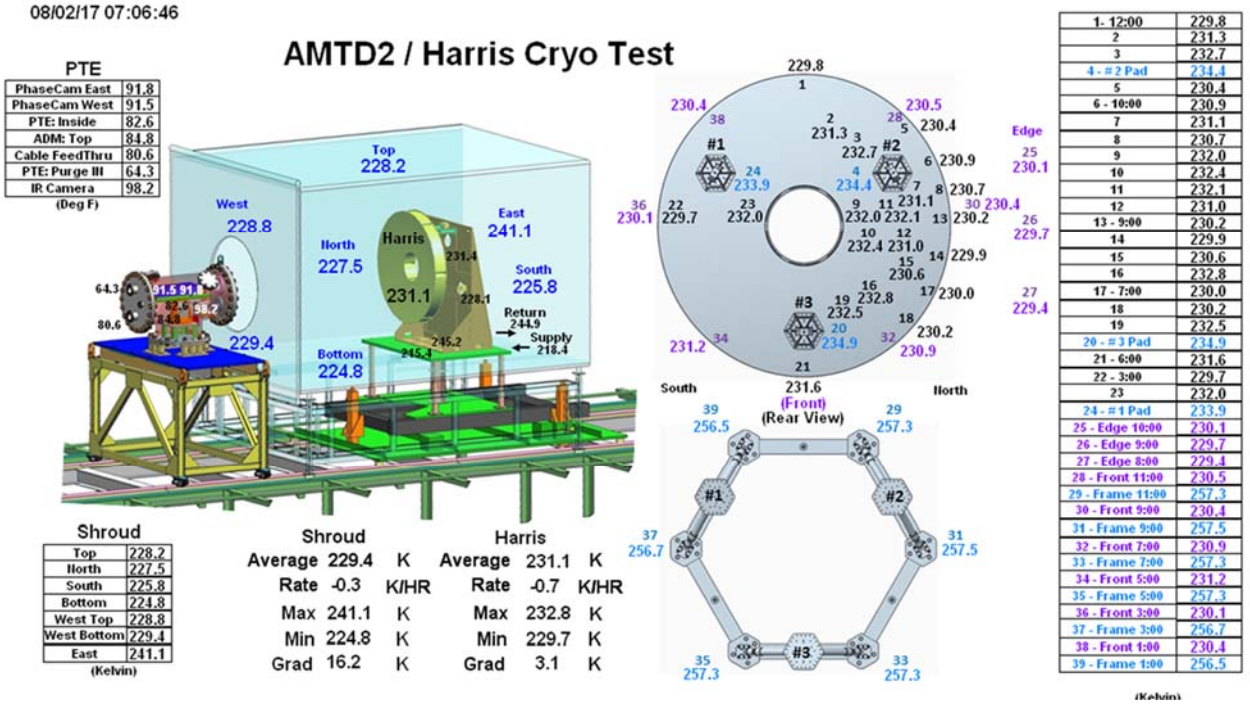


***Fig. 4.*** *PTC Test Setup with Thermal Sensors*

As the temperature of the mirror and mount changes from 293 to 231K, the aluminum backplane expands, and the mount struts apply a prying force to the mirror. The prying signature is not symmetric even though the design is symmetric, which means that the as-built mount has unintended asymmetries. The model applies prying forces directly to the bond pad and the combination of forces that most closely matches the test data was found. Figure 5 shows an 18.9-nm rms surface shape that best fits the test data produced entirely by applying forces onto the bond pads. CTE inhomogeneity also produce cryo-deformation. Figure 6 shows a 16.6-nm rms surface shape that best fits the test data produced entirely by the mirror's 3D CTE distribution.

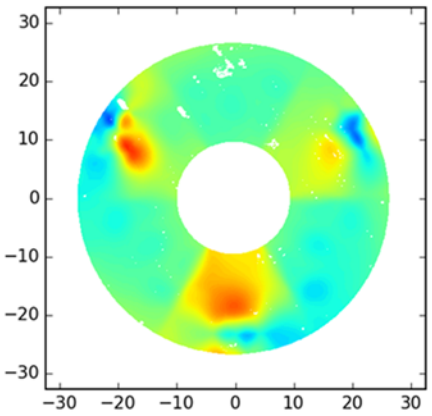


***Fig. 5.*** *Predicted AMTD-2 18.9-nm rms Mount Cryo-Deformation.*

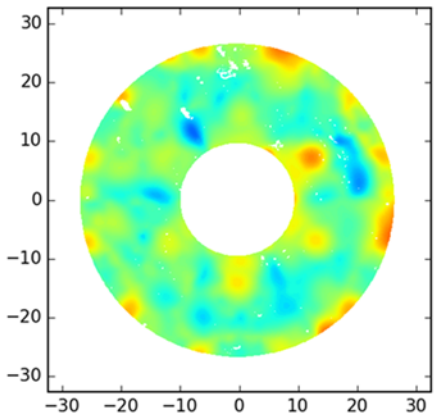


**Fig. 6.** Predicted AMTD-2 16.6-nm rms CTE Cryo-Deformation.

Combining mount and CTE effects, the PTC high-fidelity model of the AMTD-2 mirror predicts 24.7-nm rms of the measured 28.8-nm rms with a 13.4-nm rms uncertainty (Fig. 7).

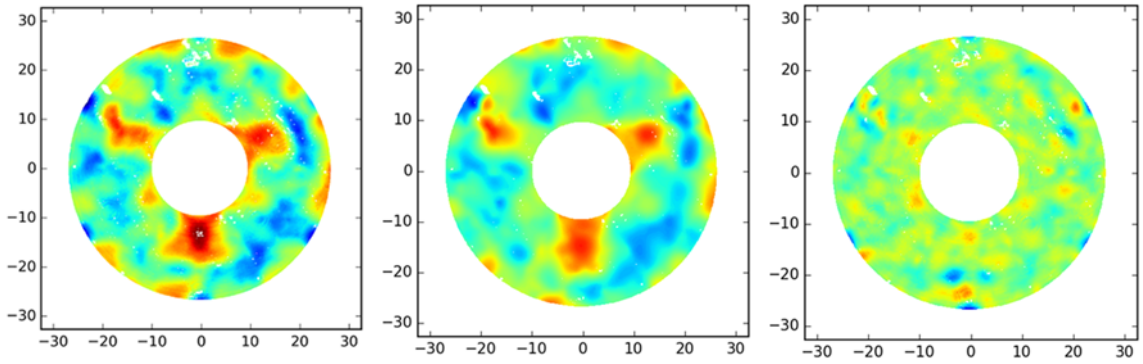

***Fig. 7.*** Left: *Thermal soak of the mirror and mount going from 293 to 231 K resulted in a measured cryo-deformation of 28.8-nm rms.* Center: *High-fidelity AMTD-2 model predicts 24.7-nm rms of deformation from mount effects and CTE inhomogeneity.* Right: *Difference between measured deformation and predicted deformation is 13.4-nm rms.*

To further advance Milestone #4, the 1.5-m ULE® AMTD-2 mirror's response to a lateral thermal gradient was tested in the XRCF. Again, this test was conducted jointly with the AMTD-2 static thermal soak test and was a bare-mirror-only test.

PTC has modified MSFC's XRCF facility to introduce thermal gradients into mirror systems using solar lamps (Fig. 8). This capability has been tested on the1.5-m AMTD ULE® mirror using a single lamp array. A thermal gradient of 115 K was introduced into the mirror causing a 78.7-nm rms surface deformation (Fig. 9). Our next step is to add an active thermal control system to this mirror.

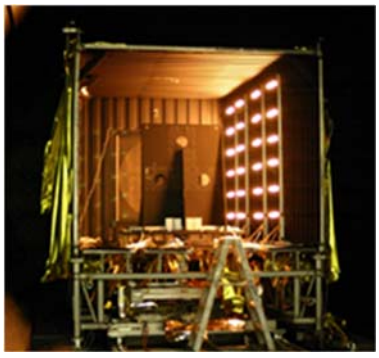

***Fig. 8.*** *Solar Lamp Array added to MSFC XRCF.*

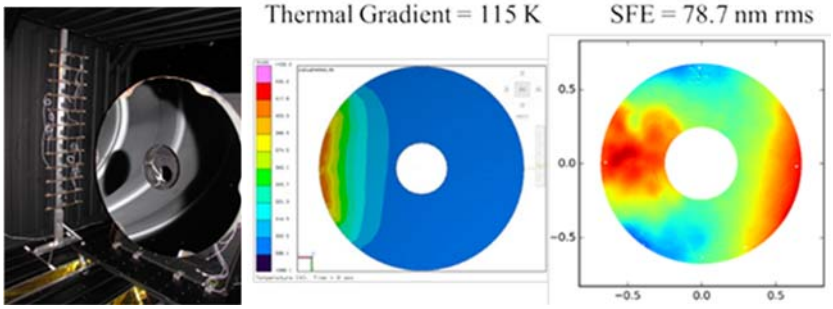


***Fig. 9.*** *AMTD-2 mirror tested with one Lamp Array Element; Thermal Gradient produced; and measured Surface Figure Error.*

### *Objective #2: Traceable Specifications for an Active Thermal Control System*

**Need:** Designing a telescope to have 10-pm-per-10-minutes WFE stability via active thermal control requires a validated STOP model. Such a model is required to derive the active thermal control system's

performance specifications, such as: sensing resolution (1 mK or 10 mK), control accuracy (10 mK or 50 mK), control period (1 min or 5 min), number and distribution of sense and control zones, etc.

**Milestone #2:** Derive specifications for thermal control system as a function of wavefront stability.

**Milestone #5:** Use validated model to perform trade studies to determine how thermo-optical performance can be optimized as a function of mirror design, material selection, material properties (i.e., CTE), mass, etc.

**Accomplishment:** During FY 2018, in collaboration with the HabEx engineering team, PTC completed Milestone #2. The HabEx engineering team has defined and provided to PTC a sensitivity analysis of Zernike polynomial terms for the Vector Vortex 6 coronagraph and flowed these sensitivities in an error budget down to thermal stability for the primary mirror. PTC measured the Schott Zerodur mirror, showing 11.3-nm rms of surface deformation per 62 K of bulk temperature change. Decomposing this error into Zernike polynomials indicates that if this mirror's bulk temperature has a thermal stability of approximately 1 mK, it will meet the HabEx VVC-6 wavefront stability requirement (Fig. 10). Milestone #5 is not scheduled for completion until the end of PTC.

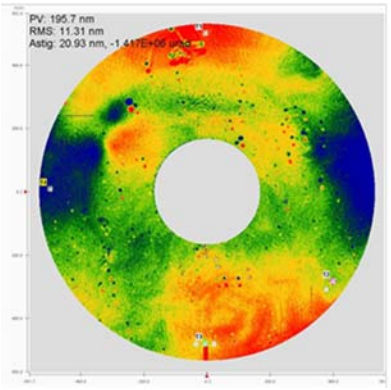


| | | | OUTPUT | INPUT |
|---|---|---|---|---|
| | | | 1mK | Zernikes |
| | | | RMS Wavefront | Deformation |
| Aberration | Tolerance [pm rms] | MARGIN | (pm rms) | (pm) |
| Bias | | | 0.008 | 237 |
| Tilt | | | 0.002 | 95 |
| Power (Defocus) | 150 | 19360.7 | 0.008 | 416 |
| Pri Astigmatism | 120 | 435.2 | 0.276 | 20940 |
| Pri Coma | 105 | 3624.6 | 0.029 | 2540 |
| Pri Spherical | 120 | 13886.8 | 0.009 | 599 |
| Pri Trefoil | 1.56 | 29.5 | 0.053 | 4630 |
| Sec Astigmatism | 0.21 | 9.0 | 0.023 | 2280 |
| Sec Coma | 0.21 | 8.7 | 0.024 | 2590 |
| Sec Spherical | 0.21 | 16.1 | 0.013 | 1067 |
| Pri Tetrafoil | 0.21 | 5.1 | 0.041 | 4060 |
| Sec Trefoil | 0.21 | 4.7 | 0.045 | 4800 |
| Ter Astigmatism | 0.06 | 2.0 | 0.030 | 3460 |
| Ter Coma | 0.06 | 2.4 | 0.025 | 3070 |
| Ter Spherical | 0.06 | 7.7 | 0.008 | 729 |
| Pri Pentafoil | 0.21 | 12.3 | 0.017 | 1840 |
| Sec Tetrafoil | 0.06 | 6.4 | 0.009 | 1090 |
| Ter Trefoil | 0.06 | 1.1 | 0.055 | 6860 |
| Qua Astigmatism | 0.06 | 53.7 | 0.001 | 147 |
| Qua Coma | 0.06 | 2.3 | 0.026 | 3660 |
| Qua Spherical | 0.06 | 3.3 | 0.018 | 1883 |
| Qin Spherical | 0.06 | 2.5 | 0.024 | 2635 |

***Fig. 10.*** *1.2-m Schott Zerodur Mirror Thermal Soak Deformation will meet the HabEx VVC-6 Thermal Stability Requirement if its temperature is stable to ~1 mK.*

***Objective #3: Demonstrate utility of a predictive-control thermal system for achieving thermal stability.***

**Need:** A telescope with 10-pm-per-10-minutes WFE stability requires an active thermal control system that is beyond the current state of art (i.e., bang-bang or proportional control).

**Milestone #3:** Design, build, and test a predictive thermal control system for the 1.5-m ULE® AMTD-2 mirror that demonstrates the utility of a physics-based model in the control loop to determine control variables (heater power levels) based on state variables (temperature measurements).

Milestone #3 has two goals. First, provide data needed by **Milestone #4** to validate **Milestone #1's** thermal model. Second, demonstrate Predictive Thermal Control. PTC will be considered demonstrated if it can correct for externally imposed thermal gradients (i.e., radial, lateral, and axial gradients). Other goals of Milestone #3 include: self-tuning of less well-known thermal parameters in the thermal model to improve the PTC's veracity, informing the design of hardware like heated bathtubs and thermal shrouds to enable controllability, and directly imposing measurable thermally induced WFE into the mirror.

**Accomplishment:** During FY 2018, PTC progressed technology for Objective #3 by modifying the XRCF to be able to impose into mirror systems axial and lateral thermal gradients (Fig. 8). Additionally, MSFC and Harris Corp designed and started fabrication of a thermal control system for the Harris 1.5-m ULE® mirror (Fig. 11). The thermal-control hardware has 26 control zones that will be used to actively

correct surface figure error or mitigate the effect of an external thermal disturbance (Fig. 12). Thermal, stress, and optical analysis of this design has been done to evaluate the design's utility.

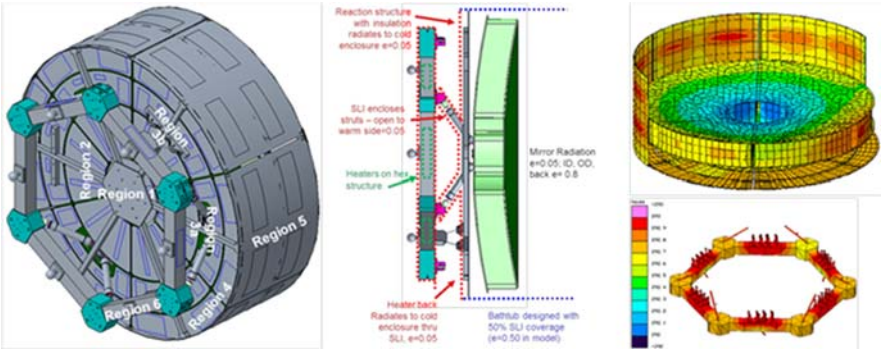


***Fig. 11.*** *Thermal Control System with a 26-zone control for AMTD-2's 1.5-m ULE® mirror*

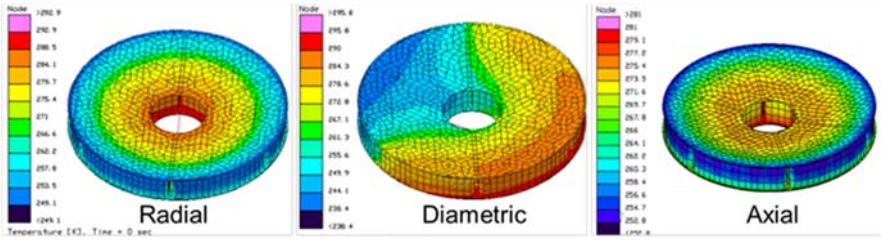


***Fig. 12.*** *Thermal Control System can introduce Radial, Lateral, and Axial thermal gradients.*

STOP analysis was done to estimate how much the surface might change and how well the thermal control system can correct the surface when heat lamps are turned on. Without thermal control, the mirror's surface figure error is estimated to be 7.5-nm rms (Fig. 13). With thermal control, this error is expected to be reduced to 1.5-nm rms (Fig. 14). Because the estimated error is so small, PTC is investigating fabricating a 1-m aluminum test mirror in FY 2019.

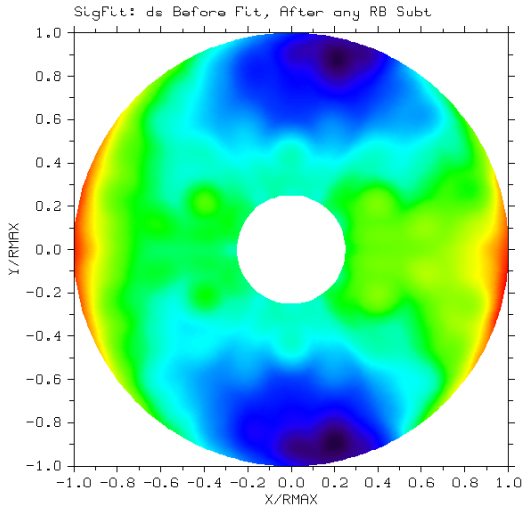


***Fig. 13.*** *Estimated surface figure error without active thermal control.*

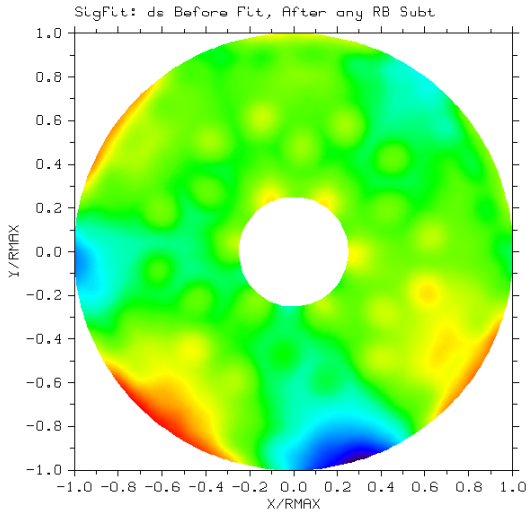


***Fig. 14.*** *Estimated surface figure error with active thermal control correction.*

## Path Forward

PTC has quantifiable milestones for each technology. Figure 15 shows PTC's five quantifiable milestones for each technology on the 'new' baseline schedule. PTC was originally proposed as a three-year project, but due to lack of funding was stretched to four years.

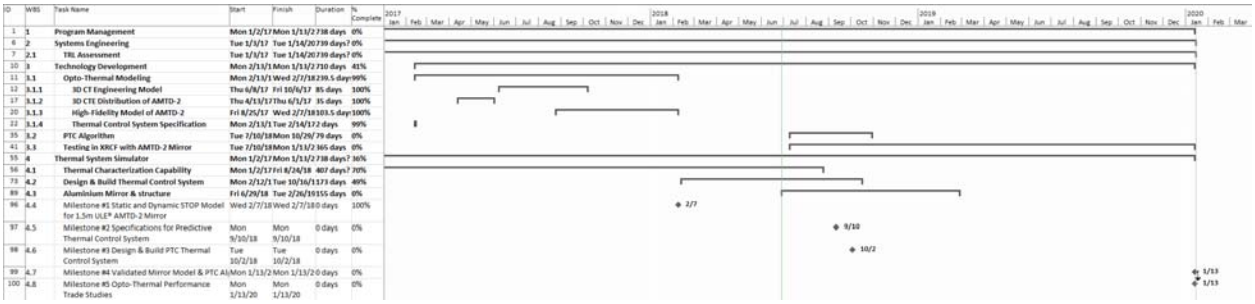

| ID | WBS | Task Name | Start | Finish | Duration | % Complete |
|---|---|---|---|---|---|---|
| 1 | 1 | Program Management | Mon 1/2/17 | Mon 1/11/21 | 738 days | 0% |
| 6 | 2 | Systems Engineering | Tue 1/3/17 | Tue 1/14/20 | 739 days | 0% |
| 7 | 2.1 | TRL Assessment | Tue 1/3/17 | Tue 1/14/20 | 739 days | 0% |
| 10 | 3 | Technology Development | Mon 2/13/17 | Mon 1/11/21 | 710 days | 41% |
| 11 | 3.1 | Opto-Thermal Modeling | Mon 2/13/17 | Wed 2/7/18 | 239.5 days | 99% |
| 12 | 3.1.1 | 3D CT Engineering Model | Thu 6/8/17 | Fri 10/6/17 | 85 days | 100% |
| 17 | 3.1.2 | 3D CTE Distribution of AMTD-2 | Thu 4/13/17 | Thu 6/1/17 | 35 days | 100% |
| 20 | 3.1.3 | High-Fidelity Model of AMTD-2 | Fri 8/25/17 | Wed 2/7/18 | 103.5 days | 100% |
| 22 | 3.1.4 | Thermal Control System Specification | Mon 2/13/17 | Tue 2/14/17 | 2 days | 99% |
| 35 | 3.2 | PTC Algorithm | Tue 7/10/18 | Mon 10/29/18 | 79 days | 0% |
| 41 | 3.3 | Testing in XRCF with AMTD-2 Mirror | Tue 7/10/18 | Mon 1/13/20 | 365 days | 0% |
| 55 | 4 | Thermal System Simulator | Mon 1/2/17 | Mon 1/11/21 | 738 days | 36% |
| 56 | 4.1 | Thermal Characterization Capability | Mon 1/2/17 | Fri 8/24/18 | 407 days | 70% |
| 73 | 4.2 | Design & Build Thermal Control System | Mon 2/12/18 | Tue 10/16/18 | 173 days | 49% |
| 89 | 4.3 | Aluminium Mirror & structure | Fri 6/29/18 | Tue 2/26/19 | 155 days | 0% |
| 96 | 4.4 | Milestone #1 Static and Dynamic STOP Model for 1.5m ULE® AMTD-2 Mirror | Wed 2/7/18 | Wed 2/7/18 | 0 days | 100% |
| 97 | 4.5 | Milestone #2 Specifications for Predictive Thermal Control System | Mon 9/10/18 | Mon 9/10/18 | 0 days | 0% |
| 98 | 4.6 | Milestone #3 Design & Build PTC Thermal Control System | Tue 10/2/18 | Tue 10/2/18 | 0 days | 0% |
| 99 | 4.7 | Milestone #4 Validated Mirror Model & PTC Al | Mon 1/13/20 | Mon 1/13/20 | 0 days | 0% |
| 100 | 4.8 | Milestone #5 Opto-Thermal Performance Trade Studies | Mon 1/13/20 | Mon 1/13/20 | 0 days | 0% |

***Fig. 15.*** *PTC Phase-1 schedule.*

## References


[1] T.E. Brooks, R. Eng, T. Hull, and H.P. Stahl, "*Modeling the Extremely Lightweight Zerodur Mirror (ELZM) thermal soak test*," Proc. SPIE 10374, Optical Modeling and Performance Predictions IX, 103740E (6 September 2017), doi: 10.1117/12.2274084

[2] T.E. Brooks, "*Predictive thermal control applied to HabEx*," Proc. SPIE 10398, UV/Optical/IR Space Telescopes and Instruments: Innovative Technologies and Concepts VIII, 1039814 (5 Sept 2017), doi: 10.1117/12.2274338

[3] T.E. Brooks and R. Eng, "*1.5-m ULE® Cryo & Mechanical Test Results*," Mirror Technology Days in the Government (2017)

[4] T.E. Brooks, "*Computed Tomography and Stiction in a Low Temperature Slumped Mirror*," Mirror Technology Days in the Government (2017)

[5] Committee for a Decadal Survey of Astronomy and Astrophysics; National Research Council, "*New Worlds, New Horizons in Astronomy and Astrophysics*," The National Academies Press, Washington, D.C. (2010)

[6] NRC, "*NASA Space Technology Roadmaps and Priorities: Restoring NASA's Technological Edge and Paving the Way for a New Era in Space*," (2012)

[7] C. Kouveliotou et al., "*Enduring Quests, Daring Visions: NASA Astrophysics in the Next Three Decades*," (2014), arXiv:1401.3741

[8] P. Hertz, "*Planning for the 2020 Decadal Survey: An Astrophysics Division White Paper*," (January 4, 2015), available at science.nasa.gov/astrophysics/documents/

[9] NASA Town Hall, AAS Winter Meeting, Kissimmee, FL (2016)

[10] J. Dalcanton et al., "*From Cosmic Birth to Living Earths: The Future of UVOIR Space Astronomy*," Association of Universities for Research in Astronomy, (2015), www.hdstvision.org/report/.

[11] *"Cosmic Origins Program Annual Technology Report"* (October 2015)

[12] T.E. Brooks, H.P. Stahl and W.R. Arnold, "*Advanced Mirror Technology Development (AMTD) thermal trade studies*," Proc. SPIE 9577, Optical Modeling and Performance Predictions VII, 957703 (23 September 2015); doi: 10.1117/12.2188371

[13] T.E. Brooks, "*Predictive thermal control applied to HabEx*," Proc. SPIE 10398, UV/Optical/IR Space Telescopes and Instruments: Innovative Technologies and Concepts VIII, 1039814 (5 Sept 2017), doi: 10.1117/12.2274338



**For additional information, contact H. Philip Stahl:** h.philip.stahl@nasa.gov


# Development of Large-Area (100 cm$^2$) Photon-Counting UV Detectors

Prepared by: John Vallerga (Space Sciences Laboratory, UC Berkeley)

## Summary

Micro-Channel-Plate (MCP) detectors have been an essential imaging technology in space-based NASA ultraviolet (UV) missions for decades, and have been used in numerous orbital and interplanetary instruments. The Experimental Astrophysics Group (EAG) at the University of California (UC) Berkeley's Space Sciences Laboratory (SSL) was awarded an Astrophysics Research and Analysis (APRA) grant in 2008 to develop massively parallel cross-strip (XS) readout electronics. These laboratory XS electronics have demonstrated spatial resolutions of 15-μm full-width at half-maximum (FWHM), global output count rates of 2 MHz, and local count rates of 100 kHz; all at gains a factor of ~20 lower than existing delay-line readouts [1]. They have even been deployed in biomedical and neutron-imaging labs but are presently too bulky and high-powered for space applications, though a current version was successfully flown on four rocket flight since 2014 [2].

EAG has been awarded two Strategic Astrophysics Technology (SAT) grants to develop XS technology for large, photon-counting UV detectors: the first in 2012 for a 50-mm square detector, and more recently (2016) scaling this technology to a 100-mm square design. The goal of these SAT programs is to raise the Technology Readiness Level (TRL) of this XS technology by:

1. Developing new Application Specific Integrated Circuits (ASICs) that combine optimized faster amplifiers and associated Analog-to-Digital Converters (ADCs) in the same chip(s).
2. Developing a Field-Programmable-Gate-Array (FPGA) circuit that will control and read out groups of these ASICs so that XS anodes of many different formats can be supported.
3. Developing a spaceflight-compatible 100-mm XS detector that can be integrated with these electronics and tested as a system in flight-like environments. This detector design can be used directly in many rocket, satellite, and interplanetary UV instruments, and could be easily adapted to different sizes and shapes to match various mission requirements. New technological developments in photocathodes (e.g., GaN) or MCPs (e.g., low-background, surface-engineered, borosilicate-glass MCPs) could be accommodated into this design as their TRLs advance.

Since the start of our project in April 2012, we have designed and constructed a 50-mm XS detector with a new low-noise anode and have demonstrated its excellent performance using our best laboratory electronics. We have scaled up and fabricated the 50-mm detector design to 100 mm × 100 mm (320 channels), and confirmed its performance before and after a full 3-axis vibration test. The new version of our ASIC design, fabricated in a 130-nm CMOS process that combines the functions of the previous two versions to reduce board complexity, will soon be submitted to a foundry. Upon receipt of the mounted dies in ~4 months, we plan to demonstrate its dynamic performance and incorporate it into a full 100-mm XS readout system.

## Background

XS readouts collect the charge exiting from a stack of MCPs with two sets of coarsely spaced and electrically isolated orthogonal conducting strips (Fig. 1). When the charge collected on each strip is measured, a centroid calculation determines the incident location of the incoming event (photon or particle). This requires many (e.g., 160, 320) identical amplifiers whose individual outputs must all be digitized and analyzed. The advantage of this technique over existing and previous MCP readout techniques (wedge and strip, delay-line, intensifiers) is that the anode capacitance per amplifier is

lower, resulting in lower noise. This allows (factor of ~20) lower MCP gain operation while still achieving better spatial resolution compared to the delay-line MCP readouts of current space missions [3], thereby increasing the dynamic range of MCP detectors by up to two orders of magnitude. This can also be scaled readily to large (> 100 mm × 100 mm) or unique formats (e.g., circular for optical tubes, rectangular for spectrographs, and even curved anodes to match curved MCP focal planes). The XS readout technology is mature enough to be presently used in the field in many laboratory environments producing quality scientific results [4, 5], and is ready for the next step of development – preparing for an orbital or deep-space-mission implementation.

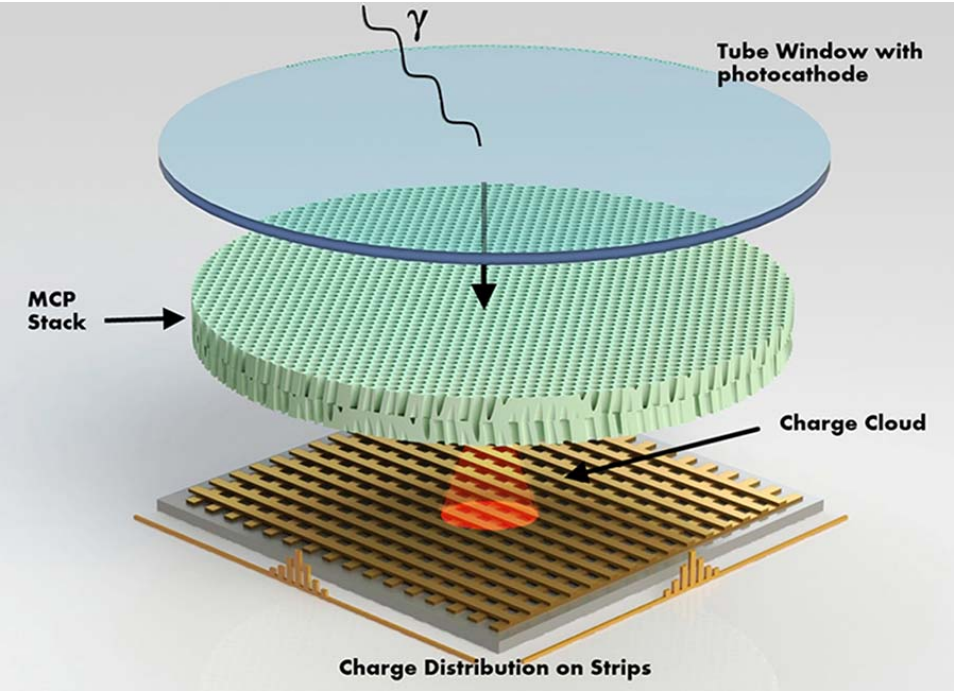


***Fig. 1.*** *Schematic of a XS readout behind an MCP stack.*

Our laboratory XS readout electronics, called the Parallel XS (PXS) electronics, consist of a preamplifier board placed near the MCP anode and a boxed set of electronics containing ADCs and FPGAs. The PXS electronics performance presently meets or exceeds all of the specifications of the previous flight systems mentioned above. However, the PXS laboratory electronics are too bulky and massive, and use relatively high power and therefore are not currently suitable for a long-term space mission. One important goal of the present effort is to replace the PXS electronics with ASICs that combine the functionality of the preamp board and the downstream ADCs into one or two low-power, low-mass chip(s). When a set of these chips is combined with an FPGA and XS anode, we expect the performance to exceed the higher-power PXS electronics due to the noise improvement expected from the smaller-scale components.

In addition to space-flight-appropriate ASIC development, our first SAT program planned to construct a flight prototype 50-mm XS MCP detector with a XS readout using our new ASICs. The new ASICs and FPGA control electronics are being integrated into a compact package so the performance of the whole detector system can be qualified in space-like environments (e.g., thermal and vibration tests). In fact, we expect this detector to be the baseline of many Explorer-class mission proposals in the future. This XS design can also be scaled easily to other useful formats required by specialized instruments. For example, doubling the length of one detector dimension entails adding more strips to the anode and more ASICs to read them out, but not a redesign of the ASIC.

## Objectives and Milestones

### *1. Design and fabricate ASICs to amplify and digitize cross-strip signal charges*

A major thrust of our 50-mm program was developing new ASICs that can overcome the limitations on the front end of our laboratory electronics. We designed and fabricated input ASICs that have the following features:

a. An optimized front-end charge-sensitive amplifier (CSA) matched to the anode-strip load capacitance with fast signal rise and fall times to minimize event "collision."
b. Fast (~GHz) analog sampling to fully characterize both amplitude and arrival time of the intrinsically fast input charge pulse.
c. Digital conversion of the analog samples in the ASIC, avoiding complex, bulky, and high-power discrete ADCs downstream.
d. ASIC self-triggering capabilities to select and transfer only event data across long cables to the FPGA, where the centroiding and timing calculations take place.

After demonstrating two working ASICs (CSAv3 and HalfGRAPH2 described below), integrated into the 50-mm readout electronics, we returned to the original concept of combining the CSA with the fast sampling ADC. As the new digitizer/sampler will now be in the same CMOS process as the CSAv3, we can realize the original "GRAPH" ASIC concept, combining both on a single die. There are many reasons for doing this, but the two most important are a faster digital readout in the 130-nm process, and reduced layout space and power afforded by combining the ASIC designs into a single die. We also have methods to protect the low-noise analog amplifier from induced noise from the digital circuit.

We have also characterized the first two separate ASICs in realistic radiation environments (total ionizing dose, TID) consistent with MIL STD 833 TM1019 for low Earth orbit (~10 krad), interplanetary missions (~30 krad), and the higher doses associated with Jupiter missions (100 krad behind shielding), having placed MCP detectors in all such environments. These successful radiation tests of the CSAv3 and HalfGRAPH2 informed the design of the GRAPH, and we have an opportunity to improve its robustness to radiation dose by using standard industry design techniques for radiation hardness.

### *2. FPGA system to read out HalfGRAPH ASICs*

Our proposed parallel-XS readout system was not simply comprised of the new ASICs. New board assemblies had to be designed, laid out, and constructed to couple these ASICs to our existing XS anodes, minimizing stray-load capacitances. These boards also included control FPGAs that not only have a new input interface, but also a new output interface to couple to the high-bandwidth computer interface required for our ultimate event rates.

### *3. Design of 50-mm and 100-mm XS MCP detectors incorporating new electronics*

Key issues for large-area XS MCP detector implementations include low-mass and robust construction schemes that can accommodate the capability for a high-vacuum sealed-tube configuration. Without incurring excessive costs, a reasonable format to accomplish this first was the 50-mm detector. This detector achieved spatial resolutions of ~20 μm FWHM, background rates < 0.1 events $cm^{-2}$ $sec^{-1}$, low fixed-pattern noise, long lifetime, multi-MHz rate capability with low dead time, and detector mass of a few hundred grams. The design and construction of brazed-body assemblies provides for the best packaging and diversity of applications, so this was one of the core tasks.

In the 100 mm × 100 mm effort, we scaled up the brazed-body assembly, detector backplate, XS anode, and number of channels by a factor of 2 in each dimension (320 electronic channels total), with the goal of maintaining the performance parameters achieved with the 50-mm assembly and to test in appropriate environments, thermal and vibrational.

## Progress and Accomplishments

Work progresses on all three objectives of the 100-mm XS detector objectives: ASIC design, fabrication, and test at the University of Hawaii; FPGA control electronics at UC Berkeley; and 50-mm and 100-mm XS detector design and test, also at UC Berkeley. Two versions each of the ASICs have been fabricated and tested, as has the 100-mm detector (using the PXS readout electronics). The 160-channel FPGA-controlled amplifier and digitizer boards were fabricated along with their electronics boxes, and photon events are now being read out, albeit at a low event rate, but enough to demonstrate high-resolution imaging. Radiation testing of both the CSAv3 and the HalfGRAPH2 has been completed successfully up to 460-kRad TID level. The 100-mm brazed body, anode, and backplate design was completed; and the detector was fabricated and tested in vacuum with UV photons using the PXS electronics. It has been successfully vibrated to the levels specified in the General Environmental Verification Standard (GEVS, GSFC-STD-7000A), 14g rms (root mean square) in three axes.

### *ASIC Design*

We have successfully fabricated and tested two working ASIC designs: the 16-channel CSA called "CSAv3" (Fig. 2) and the 16-channel analog sampling and digitizing HalfGRAPH2. The sections below discuss these designs and their testing to date.

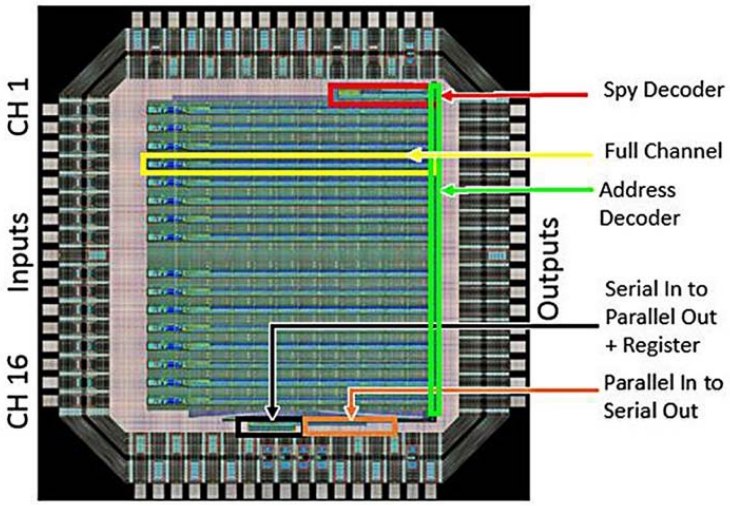


***Fig. 2.*** *CSAv3 die layout showing 16 channels along with regions of control circuitry including Digital-to-Analog Converters (DACs) and registers.*

### *CSAv3*

At an MCP gain of $10^6$ (160 fC), the largest signal expected on a single strip is ~50 fC. The CSAv3 amplifier was designed to drive the input of the HalfGRAPH2, including the short trace between them. We designed the amplifier to have linear output swings of ±600 mV.

The components of a single amplifier stage (Fig. 3) consist of a charge-sensitive preamp followed by a pole-zero cancellation (PZC) network, a shaper, an optional polarity inverter, and a buffer amp to drive the downstream HalfGRAPH2. The preamp is an inverting folded-cascode integrator, with the feedback-circuit time constant controlled by a PMOS (P-type metal-oxide-semiconductor) transistor operating as a voltage-controlled resistor. The PZC circuit cancels the pole of the preamp, removing the long baseline recovery. Additional programmable shaping and buffering circuits allow us to optimize the gain and noise of the amplifier.

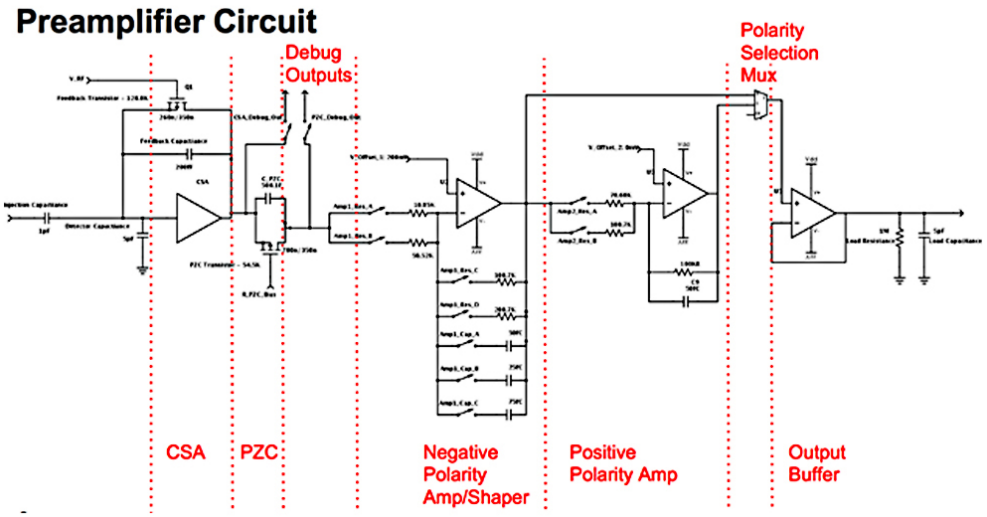


***Fig. 3.*** *A generalized schematic of the new CSAv3.*

Initial performance tests with the amplifier show that it meets the specifications for gain, noise, rise-time, and fall-time [6]. In summary, the overall gain is ~9.5 mV/fC over a range of 0 to 60 fC input charge. Within this range, the gain linearity is within 7%, and the output pulse width is confined within 100 ns. The rms noise was estimated from a fit of noise measurements for different input load capacitances, and results in a noise equivalent of 586 $e^-$ + 96 $e^-$/pF input load. An example of a measured waveform for a charge injection of 50 fC is shown in Fig. 4. Details of the design, simulation, and fabrication of CSAv3 can be found in [6].

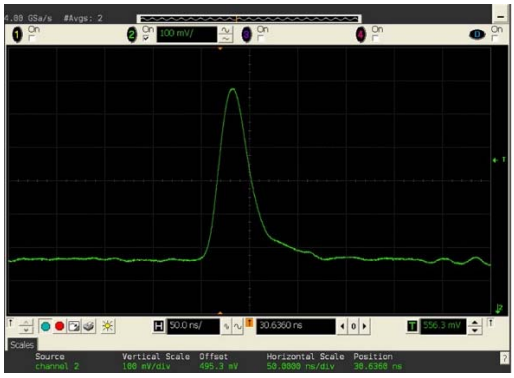

***Fig. 4.*** *Amplifier response to a 50-fC input pulse with a 5-pF load. Note the 20-ns rise time and a return to baseline in 75 ns while retaining a noise value of ~1000 $e^-$ rms.*

### *HalfGRAPH ASIC*

HalfGRAPH2 [7] is a 16-channel, 1 giga-sample-per-second waveform-digitizing chip with 12-bit resolution (Figs. 5 and 6). It was designed in the Taiwan Semiconductor Manufacturing Company (TSMC) 0.25-µm CMOS technology, using Tanner EDA design and simulation tools. The circuit's heritage is the TeV Array Readout with GSa/s sampling and Event Trigger (TARGET) ASIC used for photomultiplier-waveform sampling in the Cherenkov Telescope Array. Each channel of this digitizer chip has a two-stage analog storage mechanism. In the first stage, a short sampling array is subdivided into two sample windows, each with 32 switched-capacitor storage cells. In the second stage, in a ping-pong fashion, as one sample window is filling, the other is transferred into a larger storage array. This storage array has 8192 cells, organized as two banks of 64 rows of 64 samples each (also called a storage window) for every channel. This results in a continuous sample of 8.192-µs length before being overwritten in a circular buffer.

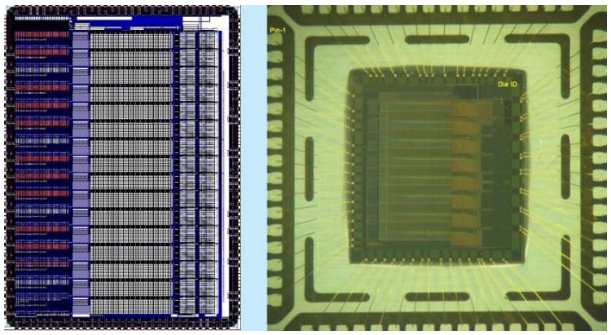

***Fig. 5.*** *HalfGRAPH2 16-channel ASIC layout (left) and die mounted in carrier (right).*

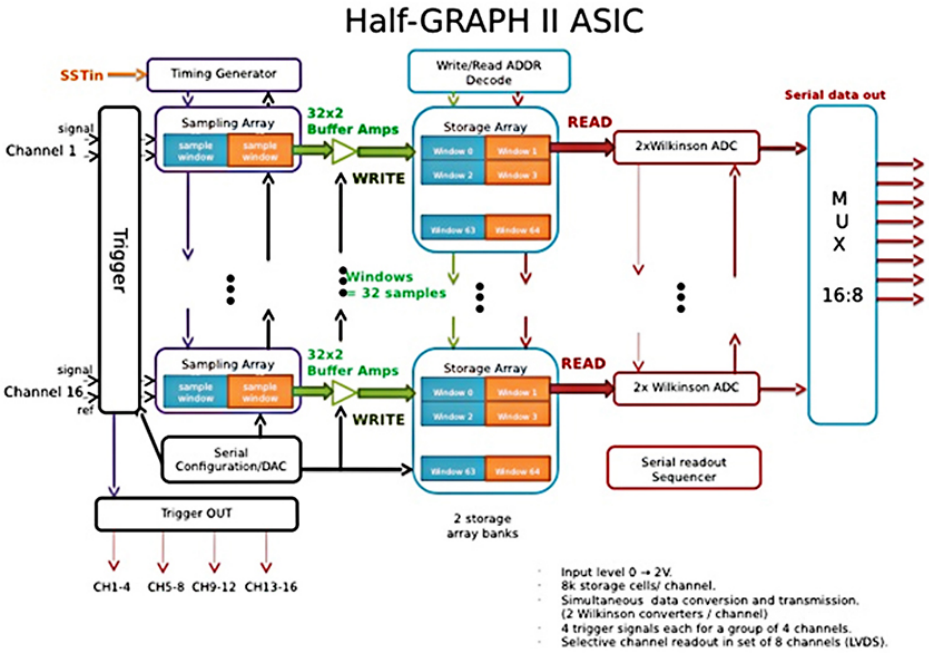


***Fig. 6.*** *Functional schematic of the HalfGRAPH2 ASIC design (described in detail in the text).*

The input analog trigger circuit has four digital output lines that notify a control FPGA of a new event. A trigger pulse is set in place if the measured signal on a channel is higher than a preset threshold. Trigger lines are organized to cover channels 1-4, 5-8, 9-12, and 13-16. This allows finer localization of the strip where the event occurred. The trigger arrival into the FPGA marks the address in the storage array of the samples for that event.

In order to digitize the acquired signal (e.g., Fig. 4), each channel uses two banks of 12-bit Wilkinson ADCs. An FPGA selects the storage window to be digitized. Thirty-two analog samples in parallel on all 16 channels of the storage window are converted concurrently into digital values using comparators, a voltage ramp, and counting (12-bit counter) with a 500-MHz dual-phase clock until the comparator fires when the ramp exceeds the analog value on the cell. It takes 4.1 μs to complete the digitization.

As the FPGA has the address of the events in the storage array, it can prevent the overwriting of those cells. Therefore, the theoretical throughput of the system is limited by the 4.1-μs conversion time of the ADCs. The maximum throughput of one channel is 240 kHz, but there is no dead time at rates below this frequency due to the multiple buffering.

### *FPGA Controller and Integrated Readout Electronics for 50-mm Detector*

In parallel with the ASIC testing described above, we designed the electronics layout for the full 160 channels of the 50 mm × 50 mm anode readout (Fig. 7). The sensitive preamps must be mounted close

to the anode to minimize capacitance loading of the input, and the HalfGRAPH2 digitizing ASICs must be close to the preamp outputs to minimize their output load. Given these constraints, as well as the desire to fit the electronics into a small enclosure mounted directly to the detector backplate (Fig. 8), we decided to construct two printed circuit boards: an amplifier board with 10 CSAv3 chips and a digitizer board with 10 HalfGRAPH2 chips and two FPGAs (ArtixAX200), one for each axis, X and Y. The digitizer board will interface with a downstream FPGA development board (e.g., SP601) via 11 LVDS pairs.

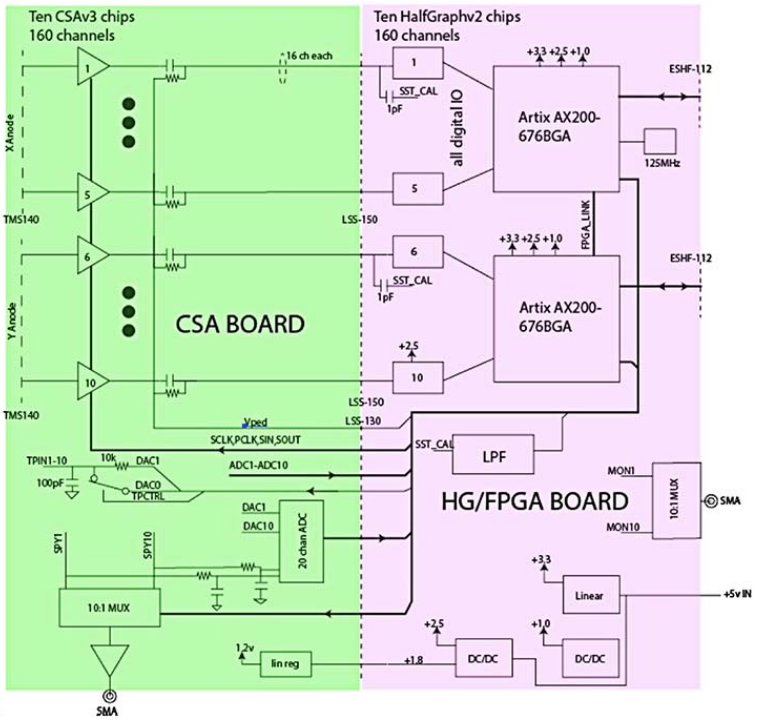


***Fig. 7.*** *High-level schematic of 50-mm detector electronics, including a 160-channel amplifier board (left) and 160-channel digitizer board with two FPGAs to control ASICs and calculate event centroids (right).*

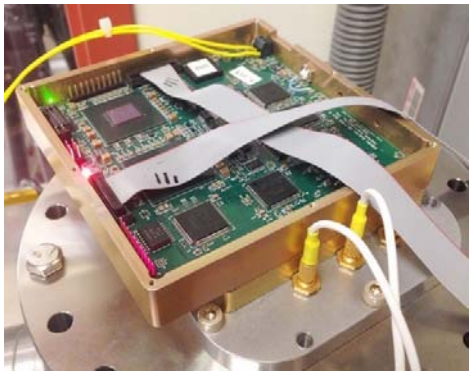

***Fig. 8.*** *Amplifier (bottom) and digitizer (top) boxes mounted to 50-mm detector backplate.*

The 160 total anode channels (80 × 80) are input to a CSAv3 amplifier board using two Samtec TMS-140-01-S-D connectors, and the 160 amplified signals pass through an inter-board connector (Samtec LSS-150-02-F-DV-A) to the 10 HalfGRAPH2 chips on the digitizer board. Additional connectors also exist for inter-board power, control, and command/data out. The main data interface (using 11 LVDS lines running at 100 MHz double data rate, DDR, to the development board) communicates with both FPGAs, X and Y, and is controlled by the downstream host. Initially in raw output mode, we transmit all 160-channel samples of 128-ns duration just for triggered events, achieving 8000 events/s using both X and Y interfaces.

The boards have been fabricated, installed in their boxes, and coupled to the 50-mm detector backplate (Fig. 8). We can test them either with test pulses capacitively coupled into their input or directly with photon events from the 50-mm detector. Learning to control the HalfGRAPH2 chip with the FPGA has been a long and laborious process, as the trigger timing of the analog giga-samples in the ring buffer is very sophisticated while maintaining synchronicity between the X and Y channels. We are now able to read out in full raw-data mode photon events into our computer at 360 Hz (limited by the "ZED" board to Ethernet interface), which allows us to check our event-centroiding algorithms and finite-impulse-response (FIR) filtering techniques.

We discovered four issues with the HalfGRAPH chip which we want to improve/fix in the GRAPH design. The two least significant bits (LSBs) of the Wilkinson ADC do not seem to function, so our pulses are sampled at 10 bits instead of 12. This is due to a race condition in the logic for the pseudo-synchronous counter used in the gray-code count generator, which has been reproduced in simulation. This probably won't affect the spatial resolution, since we will be combining many of the nanosecond samples with a FIR filter, effectively increasing the sample resolution. Second, the combined total power dissipation of the two boards comes to 11.4 W (including the two FPGAs and the voltage regulator inefficiencies). We have not yet designed a method to remove this power in vacuum, so we want to design the GRAPH chip to achieve a lower power level, and the 100-mm enclosure box and boards to extract this power to a better heat sink. We also want to correct the layout issue that causes the pedestal features seen in Fig. 9. The fourth issue with the HalfGRAPH architecture is its actual throughput. The Wilkinson clock was only reliable to 250 MHz. The multiplexing circuit required three reads (rather than two) to read out all channels and the readout clock could only operate up to 100 MHz. At best, the throughput could reach 50 to 100kHz. This is also addressed by the GRAPH chip (below).

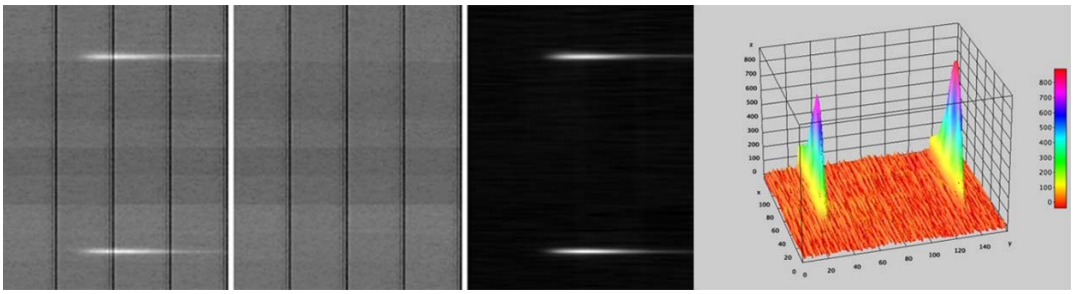

***Fig. 9.*** *Examples of raw mode output from all 160 channels (vertical/spatial axis) of 128 ns of data (horizontal/temporal axis).* Left: *Raw data from a single amplified photon event showing detector X axis in the top set of 80 channels and detector Y axis in the bottom 80 channels.* Left Center: *Pedestal of those memory locations.* Right Center: *Pedestal-subtracted image showing just the photon data.* Right: *3-D representation of the right center image, with charge events occupying ~8 channels in both the X and Y axes.*

### *50-mm XS Detector*

There are two key aspects to our flight-like 50-mm and 100-mm XS detector designs. The first is a photolithographic and laser-cut XS anode design made with polyimide. Polyimide's dielectric constant is lower than that of alumina ceramic by a factor of three, resulting in lower individual strip capacitance and thus lower amplifier noise. The top strip pattern is first etched in the copper, after which a laser ablates the material between the strips. This top layer is then bonded to the bottom strip pattern etched on a much thicker polyimide substrate. The input side of the anode is shown in Fig. 10, installed in the 50-mm XS detector, with measured strip capacitances matching our design model. Outputs from the 80 × 80 strips go through a hermetic seal consisting of 2 × 80-pin connectors sealed with vacuum epoxy (Fig. 11). The other key aspect of our detector is using a Kovar and ceramic brazed body to mount the MCPs over the XS anode. This technique is used in vacuum-image-tube construction to make a strong, robust, and clean detector that can survive launch stress.

Figure 10 shows the brazed body of the 50-mm detector mounted over our XS anode onto a vacuum backplate with three high voltage (HV) feedthroughs (MCPs removed to show the anode below).

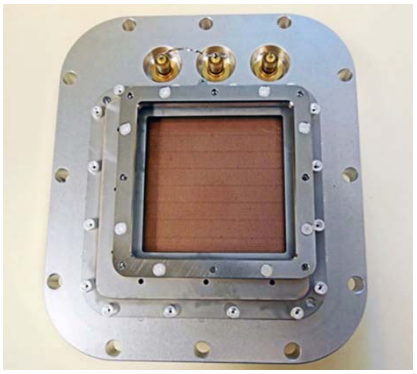

***Fig. 10.*** *View of windowless 50-mm XS detector mounted on a vacuum flange with three HV feed-throughs showing the XS anode (MCPs removed).*

***Fig. 11.*** *External side of detector showing 80-contact feed-throughs (×2) sealed with epoxy and a 64-channel preamp board plugged into one axis.*

### *Imaging Results with 50-mm Detector*

Since the readout firmware is still being developed, we used our existing PXS2 electronics and 64-channel amplifier boards to read out the central 64 × 64 strips of this 80 × 80 XS anode. This corresponds to a central active area of 40 mm × 40 mm. The results below use a stack of two MCPs from Photonis USA with 10-µm pores on 12.5-µm centers, 53.7 mm × 53.7 mm, and 60:1 L/d ratio (600-µm-thick each). We measured the spatial resolution and linearity and acquired flat fields to measure the UV response uniformity to 183-nm light from a Hg pen-ray lamp.

To measure the spatial resolution, we used a pinhole mask grid mounted directly on the input MCP. The pinholes are 10 µm in diameter and spaced 1 mm apart on a square grid (Fig. 12), an excellent method of sampling the Point Spread Function (PSF) across the field of view. To measure the spatial resolution, we had to bin the X, Y event data to 8192 × 8192 (5-µm pixels) to resolve the PSF. The inset of Fig. 13 shows the X dimension PSF (top strips) of a single pinhole. The average spatial resolutions in the X and Y dimensions were 17.5 µm FWHM and 22 µm FWHM, respectively.

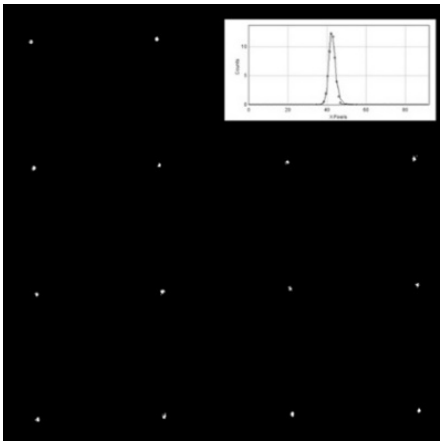

***Fig. 12.*** *UV image of pinhole mask of 10-µm holes on 1-mm square grid. Inset shows the PSF of a single hole with resolution of ~4 pixels FWHM (20 µm).*

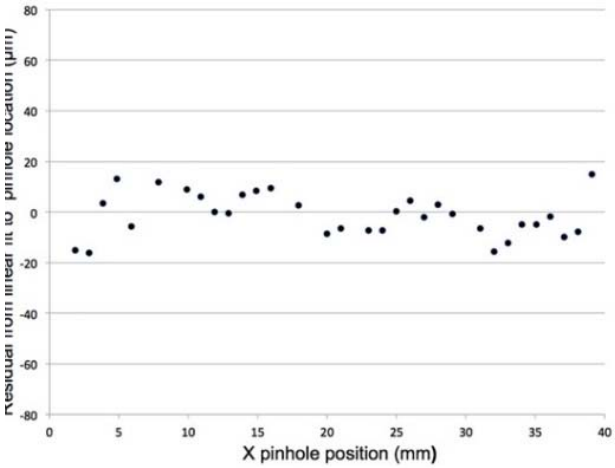


***Fig. 13.*** *Residuals to linear fit of derived pinhole position across central 40 mm of the 50-mm XS detector.*

The detector linearity can also be measured with the pinhole mask data, as the pinholes are uniformly spaced at 1 mm. Figure 13 shows residuals (in μm) to a linear fit to pixel position of the pinhole vs. pinhole number. The ±15-μm deviation from zero is smaller than the detector spatial resolution measured above, and comparable to the hexagonal 12.5-μm pore spacing. This measurement attests to the accuracy of the photolithographic anode strip regularity.

***Environmental Testing of 50-mm and 100 mm Detector***

One of the main goals of this SAT program was to advance the TRL of the 50-mm and 100-mm detector systems. Since the new 50-mm detector on its backplate is a new design, we decided to go beyond testing its performance on the bench, and confirm its performance at temperature extremes, as well as its ability to survive the g-forces of standard rocket launches.

The detector and front-end electronics were mounted onto a vacuum housing inside a thermal chamber and cycled from –30°C to +45°C (Fig. 14). We measured detector performance from –15°C to +45°C, allowing the temperature to equilibrate for about one hour at each test level before taking a deep-UV flat-field image. In all measures – resolution, background rate, and dynamic range – the detector worked flawlessly.

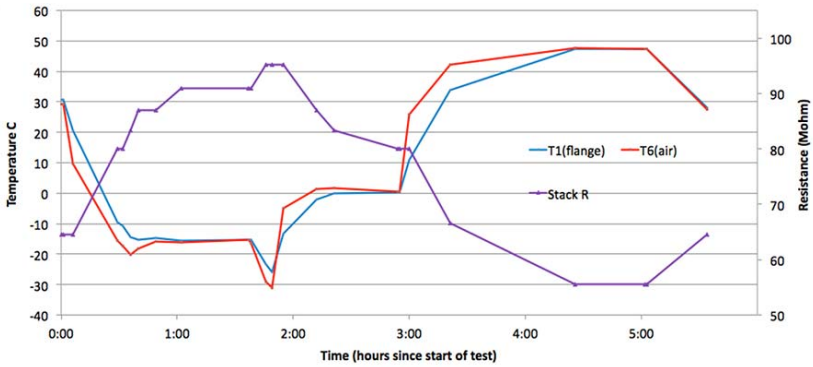


***Fig. 14.*** *Detector temperature and MCP resistance during thermal test of XS detector.*

We also used the SSL vibration table to vibrate both of the 50-mm and 100-mm detectors (without electronics) to the 14.1 g rms level specified by GEVS. Figure 15 shows the 100-mm detector backplate (air side) on the test fixture, and Table 1 shows the vibration spectrum levels applied to the detector. UV imaging performance was identical before and after vibration, showing this new detector design is ready for flight vibrations.

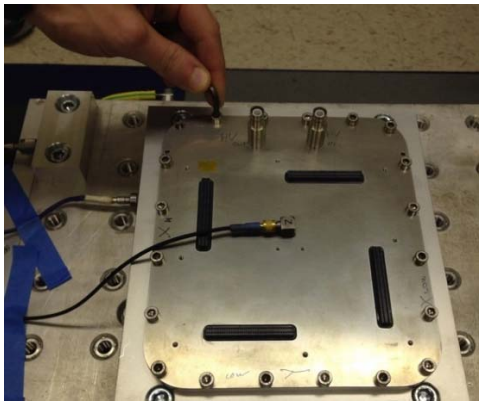

***Fig. 15.*** *100-mm XS detector mounted on vibration table at SSL.*

| Frequency (Hz) | $g^2$/Hz | dB/Octave |
|---|---|---|

| | | |
|---|---|---|
| 20 | 0.026 | 5.97 |
| 50 | 0.16 | 0 |
| 800 | 0.16 | -5.97 |
| 2000 | 0.026 | – |

***Table 1.*** *Vibration frequency spectrum (14.1 g rms).*

### *Radiation Testing of the CSAv3 and the HalfGRAPH2 ASIC*

To test the resilience of the new ASICs to TID, we spent two days at the University of Massachusetts Lowell Radiation facility. The facility allows exposure of microelectronics to $^{60}$Co gamma rays at controllable rates and durations, achieving a calibrated dose traceable to NIST standards using a calibrated Bruker Biospin dosimeter. For the CSAv3, we tested the ASICs both unpowered and battery-powered during the exposure, first in steps of 25-kRad dose, with performance testing in between. We measured bias current, pulse gain, and noise of every channel of the eight chips and did not detect a change (Fig. 16) or failure up to a TID of 486 kRad, more dose than we would expect for a mission to Jupiter. For the separate exposure of the HalfGRAPH2, our performance test consisted of driving the input with a linear voltage ramp and measuring the linear increase in the digital output codes for all channels, and again, did not see a change in performance to 236 kRad. We have not yet tested either ASIC with energetic ions to see if they suffer from single-event upsets (SEUs) or latch-ups.

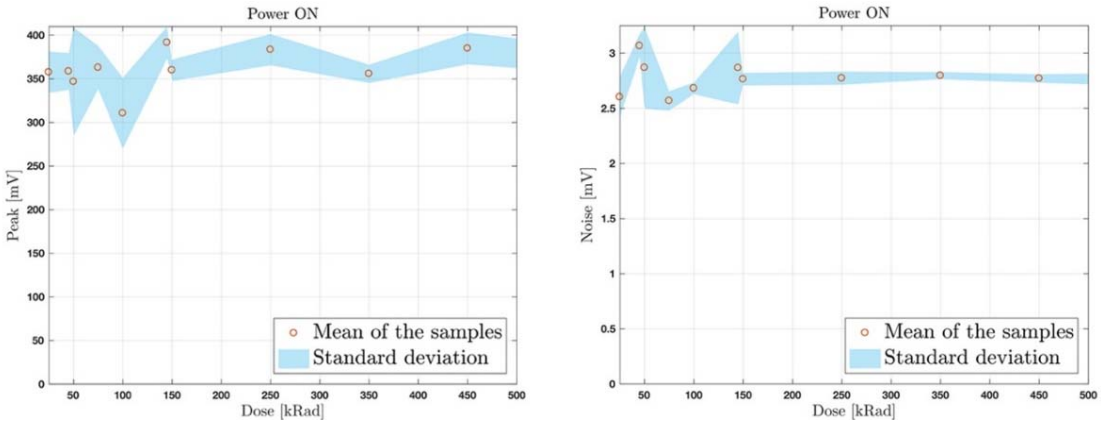


***Fig. 16.*** *Gain (left) and rms noise (right) of the CSAv3 CSA ASICs vs. TID from $^{60}$Co gamma rays. Six chips with 16 channels each were tested and the standard deviation was derived from the variation of the channels. Not all chips received the full dose.*

### *The 100 mm × 100 mm XS Detector*

The latest SAT program scales the XS technology to larger format size plus other improvements to increase its TRL. We double the size (quadruple the area) of a XS detector to 100 mm × 100 mm active area, while demonstrating high TRL with vibration and thermal tests. This larger size is not targeting a specific mission, but demonstrates a large-format design that can be scaled easily to a similar format while reducing risk. Along with a new detector mechanical design, we combine our working ASIC designs into a single ASIC (the "GRAPH" chip) using 130-nm CMOS technology to reduce readout volume, mass, and complexity. As such, we are converting all our sub-circuit libraries used in the 250-nm process HalfGRAPH2 to the TSMC 130-nm process, and then combining with the CSAv3 into the GRAPH ASIC (The CSAv3 was already designed in the 130-nm process). We also demonstrate the radiation hardness of the existing ASIC designs with energetic particles, and maintain this hardness in the new GRAPH ASIC.

### *The 100 mm × 100 mm Mechanical Design*

The brazed-body design (Fig. 17) is scaled up by a factor of ~2, with an output aperture below the MCPs of 103 mm while the active field of view is set by a 100 × 100 open mask of 25-µm thickness between top and bottom MCPs. It is designed to hold square Photonis USA MCPs up to 110 mm in size. The XS anode design (Fig. 18) is also scaled to 160 strips per axis, but with a slight increase in strip pitch from the 635 µm of the 50-mm anode to 645 µm for the 100-mm anode. This results in a 103 mm × 103 mm anode with enough strips at the edges to sample the 100-mm field of view fully. The anode outputs are now distributed on all four corners of the anode in a "pinwheel" fashion so the mechanical cutouts through the vacuum backplate can be more symmetric for increased strength. It also facilitates the electronics board layout where the GRAPH chips can be spread out on the printed circuit board.

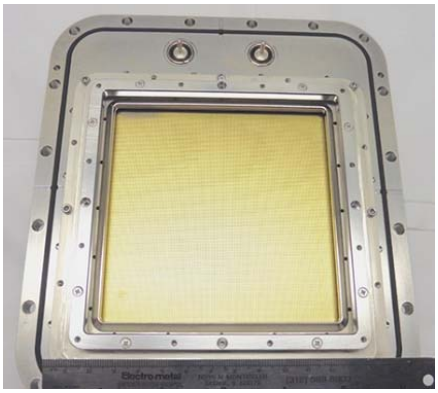

***Fig. 17.*** *View of windowless 100-mm XS detector mounted on a vacuum flange with two HV feed-throughs showing the XS anode (MCPs removed).*

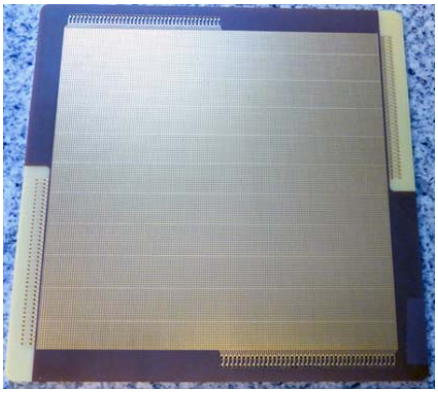

***Fig. 18.*** *Fabricated 100-mm XS anode. Note the four distributed output connectors along the edges of the anode.*

### *103-mm XS Anode*

We fabricated the new 103-mm square anode with the new pinwheel output arrangement using the same techniques of laser cutting and bonding of a polyimide top layer used with the 50-mm anode. Resistance and capacitive measurements were as expected, with about a 2× increase due to the doubled strip length. This should increase CSA readout noise from that of the 50-mm anode by only 50% given the baseline, no-load noise of the amps. Figure 18 shows the new, gold-coated anode.

### *100-mm Detector Brazed Body and Backplate*

The brazed body design is mostly a scaled-up version of the 50-mm design, but the body is more symmetric as the signal outputs are now coming off all four sides of the anode, so this must be accommodated by adding the cantilevered shelf to mount the MCPs directly over the anode center.

The backplate now has four cutouts to let the four signal connectors (80 channels each) through, again with an epoxied hermetic seal. The pinwheel design puts much more steel between the cutouts, increasing the strength of the backplate. We welded two commercial-off-the-shelf (COTS) safe HV (SHV) connectors to provide the MCP bias high voltage. Figure 17 shows the brazed body attached to the backplate with the XS anode showing (MCPs not installed).

### *GRAPH ASIC*

Given our success with the CSAv3 in 130-nm technology and design libraries, we are planning to combine the amplifier and digital converter on the same chip using this technology. Design techniques will be employed to shield the low-noise inputs from the high-speed digital outputs. However, to hedge our bets, we are using multiplexors to allow bypassing of the GRAPH CSA circuit in case the induced noise proves problematic. The resulting ASIC would then act like an improved HalfGRAPH, which could be used with the existing CSAv3.

Figure 19 is a simplified schematic with an overall 16-channel GRAPH ASIC design, including more detail for one channel and then more detail for one sampling cell (2048 analog samples per channel). Each GRAPH channel has an input CSA (which can be bypassed), a trigger circuit to detect a rising edge pulse, and an ADC whose outputs are multiplexed to fast LVDS lines to a downstream FPGA controller. Each channel has a trigger, and two consecutive triggers are OR-ed into a single output pin, signaling the FPGA of an event and on what channels the charge has landed. For each channel, the GRAPH core circuitry continuously samples the analog output of the CSA, storing the voltage on the sample cell capacitors. The timebase controls the sampling switches, and there are 64 samples per window, 16 windows per bank and 2 banks. After 2048 samples, the timebase overwrites the samples starting at the beginning. While one bank is being filled with new samples, the other bank goes through a Wilkinson conversion, whereby an analog linear ramp is input to a comparator while a digital register is being incremented with a grey-code binary counter. When the ramp voltage exceeds the stored sample voltage, the comparator output latches the counter, and the digital value is proportional to the input voltage, hence an ADC.

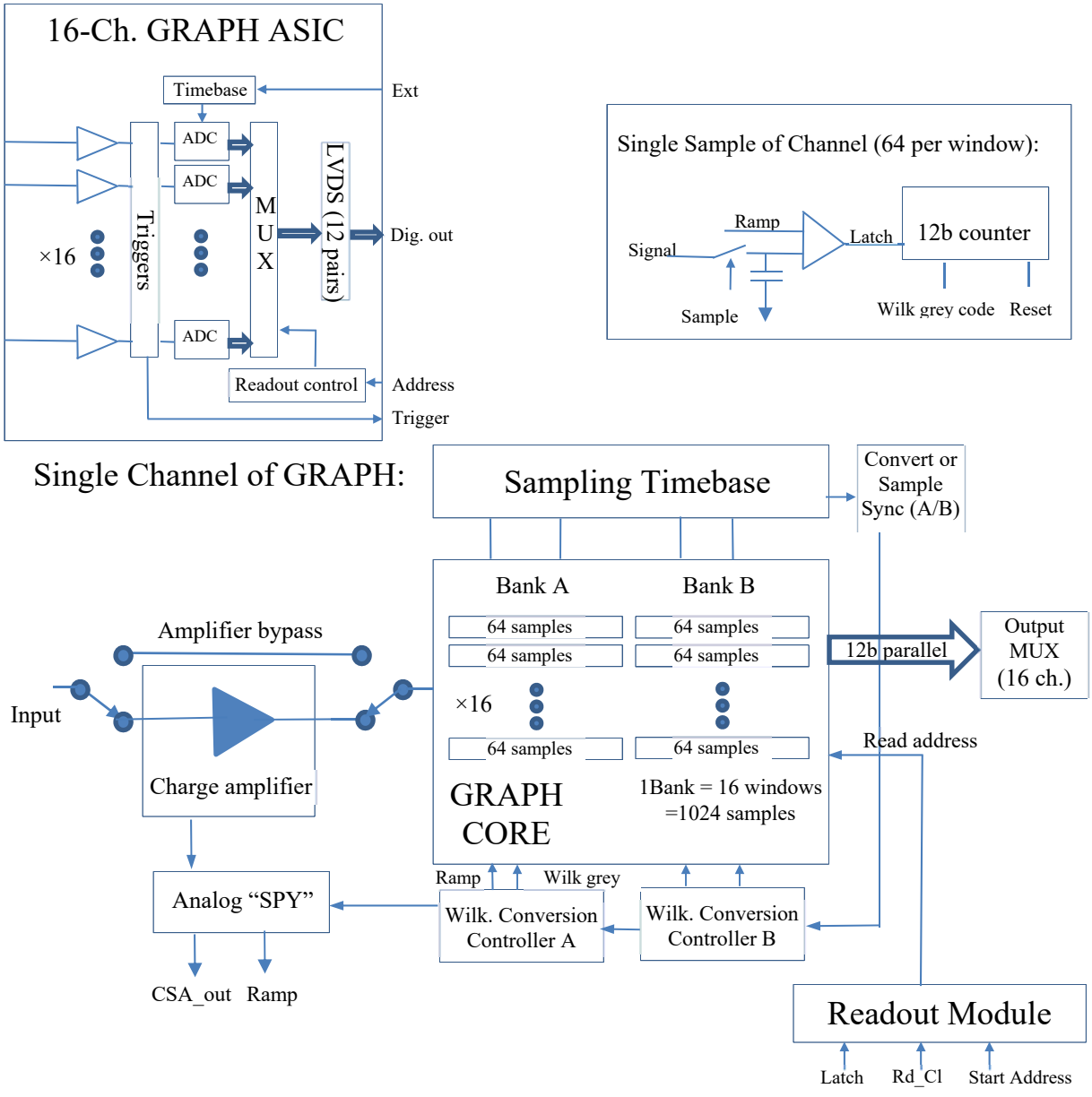

***Fig. 19.*** *Functional Schematic of GRAPH ASIC. Top left is the overall 16-channel ASIC where each channel has an amplifier and a Wilkinson ADC (top right), whose output is multiplexed to fast LVDS lines to a downstream FPGA controller. The bottom schematic is a more detailed description of a single channel showing the GRAPH core which samples the input analog signal, and converts to digital values whose registers are addressable. A more detailed description is found in the text.*

The other bank that is undergoing sampling has in its registers the digital values from the previous conversion, and can be read out. The FPGA instigates this process by sending the channel, window, and sample address serially to the readout control which transfers the data to the output MUX for fast transmission to the FPGA of a contiguous set of temporal sample values stored in the registers. While loading a new address via the serial port, the initially set value automatically increments. The timebase controls the ping-pong synchronization of the two banks, one sampling/readout while the other converting. The analog "SPY" output enables probing of the analog CSA outputs or ramps, useful for optimization of signal-to-noise ratio. Not shown are the slow serial interface to the FPGA used to set all static parameters of the chip.

## Path Forward

As of July 1, the GRAPH ASIC chip design is finished and undergoing final checks and simulations to the TMSC foundry at the end of July. Fabrication should take approximately three months. During that time, test boards will be built at the University of Hawaii to measure its performance, and readout boards that incorporate the new design will be started in Berkeley, taking advantage of the lower power and simplified layout, provided by the 2-for-1 decease in chip count.

This effort is directly transferable in the development of a 100-mm detector readout using the same logic as the 50-mm system scaled up by a factor of two in each dimension. In fact, some aspects are easier in that there are twice as many components, but four times the area. This might make the thermal design easier as well. Boards will have to be laid out and electronics boxes fabricated for the new size, this time incorporating methods for better heat extraction.

## References


[1] J. Vallerga, J. McPhate, A. Tremsin, O. Siegmund, R. Raffanti, H. Cumming, A. Seljak, V. Virta, and G. Varner, "*Development of a flight qualified 100 × 100 mm MCP UV detector using advanced cross strip anodes and associated ASIC electronics*," Proc. SPIE, **9905**, 99053F (2016)

[2] K. Hoadley, K. France, N. Nell, R. Kane, T.B. Schultz, M. Beasley, J.C. Green, J.R. Kulow, E. Kersgaard, and B.T. Fleming, "*The assembly, calibration, and preliminary results from the Colorado high resolution Echelle stellar spectrograph (CHESS)*," Proc. SPIE, **9144** (2014)

[3] J. Vallerga, R. Raffanti, A. Tremsin, O. Siegmund, J. McPhate, and G. Varner, "*Large-format high-spatial-resolution cross-strip readout MCP detectors for UV astronomy*," SPIE, **7732** (2010)

[4] X. Michalet, R.A. Colyer, J. Antelman, O.H.W. Siegmund, A. Tremsin, J.V. Vallerga, and S. Weiss, "*Single-quantum-dot imaging with a photon-counting camera*," Current Pharmaceutical Biotechnology, **10** (5), 543-558 (2009)

[5] F.B. Berendse, R.G. Cruddace, M.P. Kowalski, D.J. Yentis, W.R. Hunter, G.G. Fritz, O. Siegmund, K. Heidemann, R. Lenke, A. Seifert, and T.W. Barbee Jr., "*The joint astrophysical plasmadynamic experiment extreme ultraviolet spectrometer: resolving power*," SPIE Conference Series, **6266**, 31 (2006)

[6] A. Seljak, H.S. Cummings, G. Varner, J. Vallerga, R. Raffanti, and V. Virta, "*A fast, low power and low noise charge sensitive amplifier ASIC for a UV imaging single photon detector*," JINST, **Volume 12**, Issue 04, pp. T04007 (2017)

[7] A. Seljak, H.S. Cummings, G. Varner, J. Vallerga, R. Raffanti, and V. Virta, *"Prototype readout system for a multi Mpixels UV single-photon imaging detector capable of space flight operation*," JINST, **Volume 13**, Issue 02, pp. T02003 (2018)

**For additional information, contact John Vallerga:** *jvv@ssl.berkeley.edu*

# Ultrasensitive Bolometers for Far-IR Spectroscopy at the Background Limit

Prepared by: Charles M. (Matt) Bradford (JPL/Caltech)

## Summary

This is a three-year Strategic Astrophysics Technology (SAT) award begun in March 2018 (when funds were available to the PI). The aim is to demonstrate readiness for a flight program with the world's most sensitive bolometers: transition-edge-sensed (TES) devices which meet the requirement for background-limited spectroscopy from cold space telescopes.

We have developed a set of requirements and goals for our detector development program. We are working toward devices that:

- demonstrate a per-pixel noise equivalent power (NEP) less than $10^{-19}$ W Hz$^{-1/2}$ with a goal of $3\times10^{-20}$ W Hz$^{-1/2}$;
- provide sufficient speed of response, f3dB=5 Hz (requirement), 15 Hz (goal), to be useful in a range of instrument configurations for SPICA, the Origins Space Telescope (OST), and a potential NASA far-IR probe-class mission;
- are read out with a frequency-domain multiplexing scheme scalable to thousands of detectors at 50 mK and compatible with spaceflight; and
- can maintain high duty cycle in the face of cosmic-ray interactions in space.

The first challenge is the sensitivity, which requires very long and thin isolation legs for the bolometers. This has been our primary thrust thus far.

### Project highlight:

With a late start in FY 2018, we have developed designs for prototype arrays of a transition-edge-sensed (TES) bolometer. We demonstrated a new release process with these designs in the Microdevices Laboratory. We designed a cryogenic electronics system to support the testing, and specified and procured a new dilution refrigerator to house the experiment.

## Background

Far-IR wavelengths are uniquely well-suited to fundamental questions that guide NASA astrophysics such as: "How does the Universe work?" and "How did we get here?" Far-IR measurements are vital for probing the inner workings of galaxies, which are typically obscured by dust at optical wavelengths. The Spitzer and Herschel missions have shown us that the dust obscuration is so prevalent that most of the energy ever produced in galaxies by stars and accreting black holes through its history has been absorbed and re-radiated. Similarly, planets assemble from optically thick disks which cool primarily in the far-IR. Most of our information about the dust-obscured universe comes from broadband-imaging datasets. But these 2-D datasets fall short when it comes to providing astrophysical insight. Spectroscopy is a far more powerful tool, providing quantitative diagnostics to reveal the machinery at the heart of galaxies and forming planetary systems.

Astronomers are aware of this toolset, but sensitive far-IR spectroscopy has remained elusive because it requires advanced, exquisite detector sensitivities in the far-IR, a regime which does not benefit from the commercial/industrial infrastructure. Sensitive far-IR detectors and readouts must be developed and purpose-built by NASA scientists and technologists for far-IR astrophysics.

This work on low-noise-equivalent-power (NEP) detector development is directly applicable to future far-IR space missions such as SPICA [1] and the Origins Space Telescope (OST)[2]. These missions feature cryogenic telescopes, which when combined with dispersive spectrographs at the background limit (hereafter referred to as BLISS-type) create powerful spectroscopic facilities with 1–4 orders-of-magnitude sensitivity improvement over the current state of the art. Figure 1 shows these possible gains, along with a concept for SPICA, the nearest-term opportunity for sensitive far-IR spectroscopy, and the quantitative sensitivity gains possible. This advance will bring far-IR sensitivities into parity with those of powerful flagship programs at shorter and longer wavelengths, JWST and ALMA, but providing unique access to the most dust-enshrouded star formation and black hole growth in the universe's first billion years.

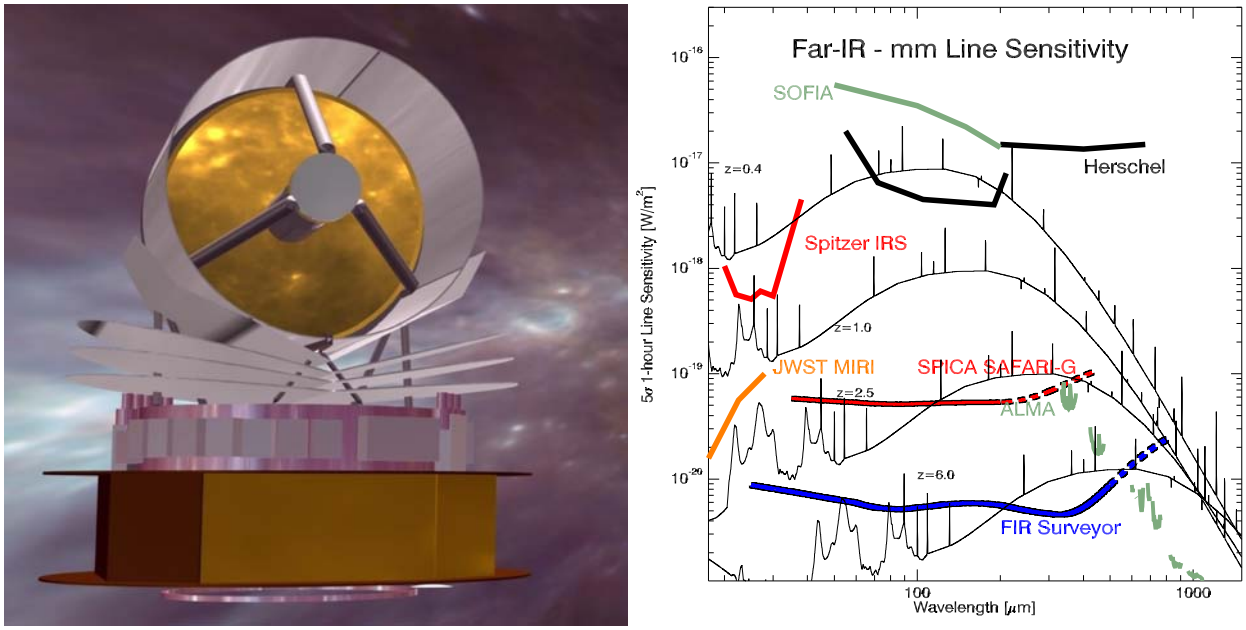


***Fig. 1.*** Left: *SPICA concept, a 2.5-meter telescope actively cooled to below 8 K, with a planned five-year lifetime at the Earth-sun L2 halo orbit.* Right: *Far-IR spectral sensitivities. A spectrometer on a cold telescope will be 100–1000 times more sensitive than present-day far-IR facilities, and observing speed scales as the inverse square of the plotted sensitivity. The SAFARI curve assumes detector NEP of $1\times10^{-19}$ W Hz$^{-1/2}$, the requirement adopted for this program. OST (previously the Far-IR or FIR Surveyor) sensitivity plotted here assumes a 4×6-m telescope with detectors operating at $2\times10^{-20}$ W Hz$^{-1/2}$, just a bit better than this program's goal sensitivity. Model galaxy spectra are over-plotted at a range of redshifts, from the epoch of reionization to the present day. In addition to the fine-structure lines, these spectrometers also have excellent sensitivity to broad mid-IR features such as the polycyclic aromatic hydrocarbon (PAH) bands—mid-IR fluxes are scaled to show the sensitivity when binned to R=100.*

The per-pixel sensitivity requirement described above exceeds the state of the art for flight far-IR bolometers (flown on the SPIRE instrument on Herschel) by a factor of ~300. We will achieve this sensitivity increase through a combination of lower temperature (we target 60-80-mK detector operation cooled with a 50-mK bath) and more extreme isolation leg geometry (we are baselining 1000-micron-long by 0.4-micron wide by 0.25-micron wide bolometer legs). The lower temperature requires development of new superconducting material, and the extreme isolation legs require new fabrication procedures. These have been the focus of our work in FY 2018. An additional key challenge we are beginning to address is integrating the new detectors with a superconducting multiplexing (MUX) readout system, which enables arrays with thousands of pixels. For this we are collaborating with a detector group in SRON (the Netherlands Institute for Space Research) that has developed an RF frequency-domain multiplexer (f-MUX), shown in Fig. 2.

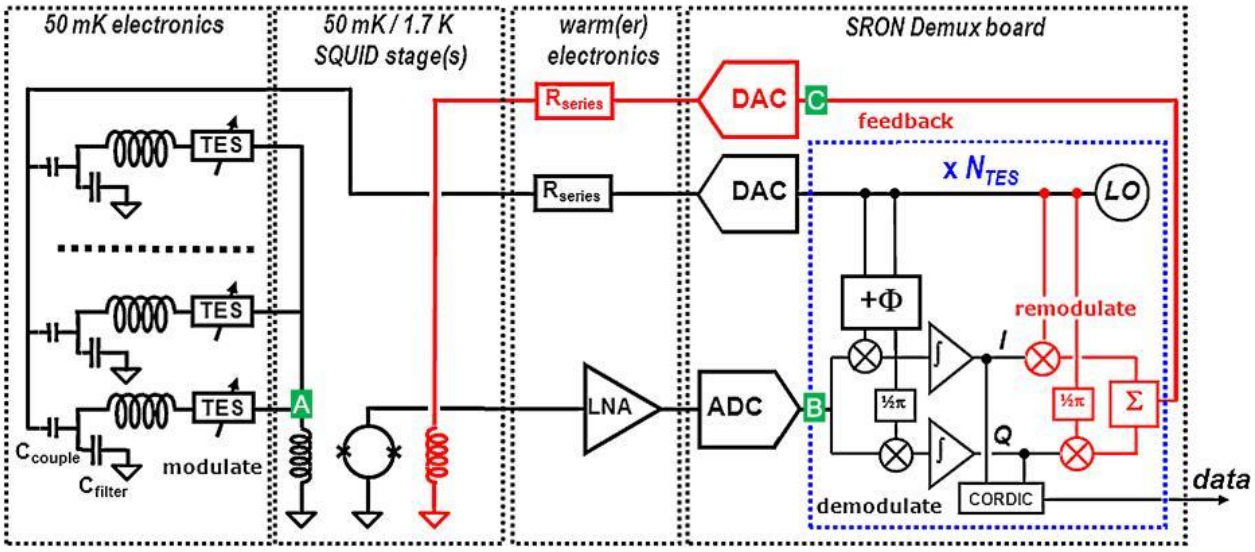


***Fig. 2.*** *Schematic of the frequency-domain multiplexer we will use to read out the TES bolometers. The schematic is provided by our partners at SRON [3], but this readout is similar to that being used for the bolometer instruments for the South Pole Telescope (SPT) [4] and Polarbear. A comb of bias frequencies is sent on a single line, with each frequency accessing a single TES through an LC resonator. Currents are summed at a Superconducting Quantum interference device (SQUID) input, and a baseband feedback system actively nulls the SQUID flux to maintain linearity. Our ultimate goal is to demonstrate this system at 176× multiplexing format, but our first step underway now is an 18-channel system read out pixel by pixel with a single-tone RF bias.*

## Objectives and Milestones

Our high-level objectives are presented above in the first paragraph of the report. We have developed a strategy for achieving these goals. Our initial testing will use a dark test package (we call v0) with an 18-channel passive-LC-filter chip from our SRON collaborators, and a new prototype bolometer array we are building. This package will be cooled in a new refrigerator to 50 mK, and biased with a benchtop RF source measured with a commercial SQUID system. This will allow us to debug stray light and stray RF problems, as well as develop experience with the f-MUX system. We will then push to a larger-format (176×, as envisioned for SPICA SAFARI) MUX demonstration, also dark v1-D. The work will culminate with optical sensitivity measurements with this array package, but including feedhorns coupling to the bolometers.

We have identified the following milestones with target completion dates:

- Specify and order test facility cryostat (Completed March 2018, upon receipt of funding);
- Develop new wet-release process for bolometer structures (Completed June 2018, see below);
- Develop design for RF cables, custom filter boards, order components, and test equipment (Completed July 2018);
- Design v0 mechanical test enclosure and fabricate (underway, expect September 2018, see below);
- Commission fridge and begin R vs T testing of bilayer films (delivery expected in August, testing underway in October 2018);
- Begin TES testing with v0 setup in cryostat (November 2018);
- Demonstrate dark NEP at or below $2\times10^{-19}$ W $Hz^{-0.5}$ and ≥ 50% yield with v0 setup (April 2019);
- Design v1 focal plane package, including MUX chips, backshorts, feedhorn coupling, flight-like design (February 2019);
- Procure/build multi-channel f-MUX warm electronics in collaboration with SRON. (May 2019);
- Dark-test v1 package underway with multi-channel electronics (June 2019);

- Demonstrate with v1 package NEP ≤ $2\times10^{-19}$ W $Hz^{-0.5}$ (goal $1\times10^{-19}$) and ≥ 50% yield; understand yield (December 2019);
- Verify expected cosmic-ray interaction using v1 package (March 2020); and
- Test optically v1 package underway with cryogenic blackbody; demonstrate optical efficiency ≥ 70% with no feedhorn impact on array yield (June 2020).

## Progress and Accomplishments

Since our funding arrived in March 2018, we completed the first three milestones described above. Figures 3, 4, and 5 show our new prototype bolometer structures under development in the micro-devices lab. Developing a wet-release process is essential to practical low-NEP devices, because our previous dry-plasma-etched bolometers, while they demonstrated sufficient thermal isolation and NEP, had excess heat capacity causing large (~1 sec) time constants. The challenge of the wet-release is that liquid solvents tend to destroy the fragile structures as they emerge. We are exploring both a range of wax-mounting/demounting schemes and release-support buttresses which can be removed with a laser trimmer after release. As Fig. 4 shows, a viable scheme has emerged.

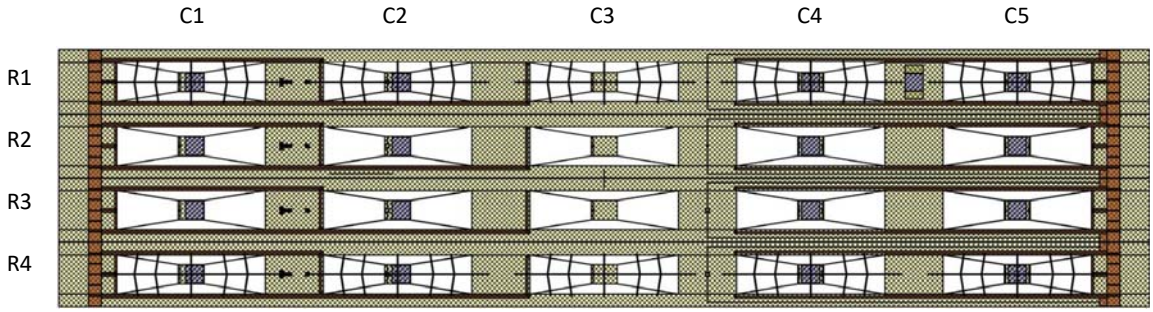


| | C1 | C2 | C3 | C4 | C5 |
|---|---|---|---|---|---|
| R1 | TES; beam-straight, 0.18 x 0.4 x 1000 $um^3$ | TES; beam-meander, 0.18 x 0.4 x 2000 $um^3$ | Small TES; beam-straight, 0.18 x 0.4 x 1000 $um^3$ | JTD; beam-straight, 0.18 x 0.4 x 1000 $um^3$ | JTD; beam-meander, 0.18 x 0.4 x 2000 $um^3$ |
| R2 | TES; beam-straight, 0.18 x 0.4 x 1000 $um^3$ | TES; beam-meander, 0.18 x 0.4 x 2000 $um^3$ | Small TES; beam-straight, 0.18 x 0.4 x 1000 $um^3$ | JTD; beam-straight, 0.18 x 0.4 x 1000 $um^3$ | JTD; beam-meander, 0.18 x 0.4 x 2000 $um^3$ |
| R3 | TES; beam-straight, 0.18 x 2 x 1000 $um^3$ | TES; beam-meander, 0.18 x 2 x 2000 $um^3$ | Small TES; beam-straight, 0.18 x 2 x 1000 $um^3$ | JTD; beam-straight, 0.18 x 2 x 1000 $um^3$ | JTD; beam-meander, 0.18 x 2 x 2000 $um^3$ |
| R4 | TES; beam-straight, 0.18 x 2 x 1000 $um^3$ | TES; beam-meander, 0.18 x 2 x 2000 $um^3$ | Small TES; beam-straight, 0.18 x 2 x 1000 $um^3$ | JTD; beam-straight, 0.18 x 2 x 1000 $um^3$ | JTD; beam-meander, 0.18 x 2 x 2000 $um^3$ |

***Fig. 3.*** *Mask layout notes for first prototype TES array. We are exploring both meandered and straight beams, and devices with and without post-release laser trimming approach to aid in the survival of the fragile devices.*

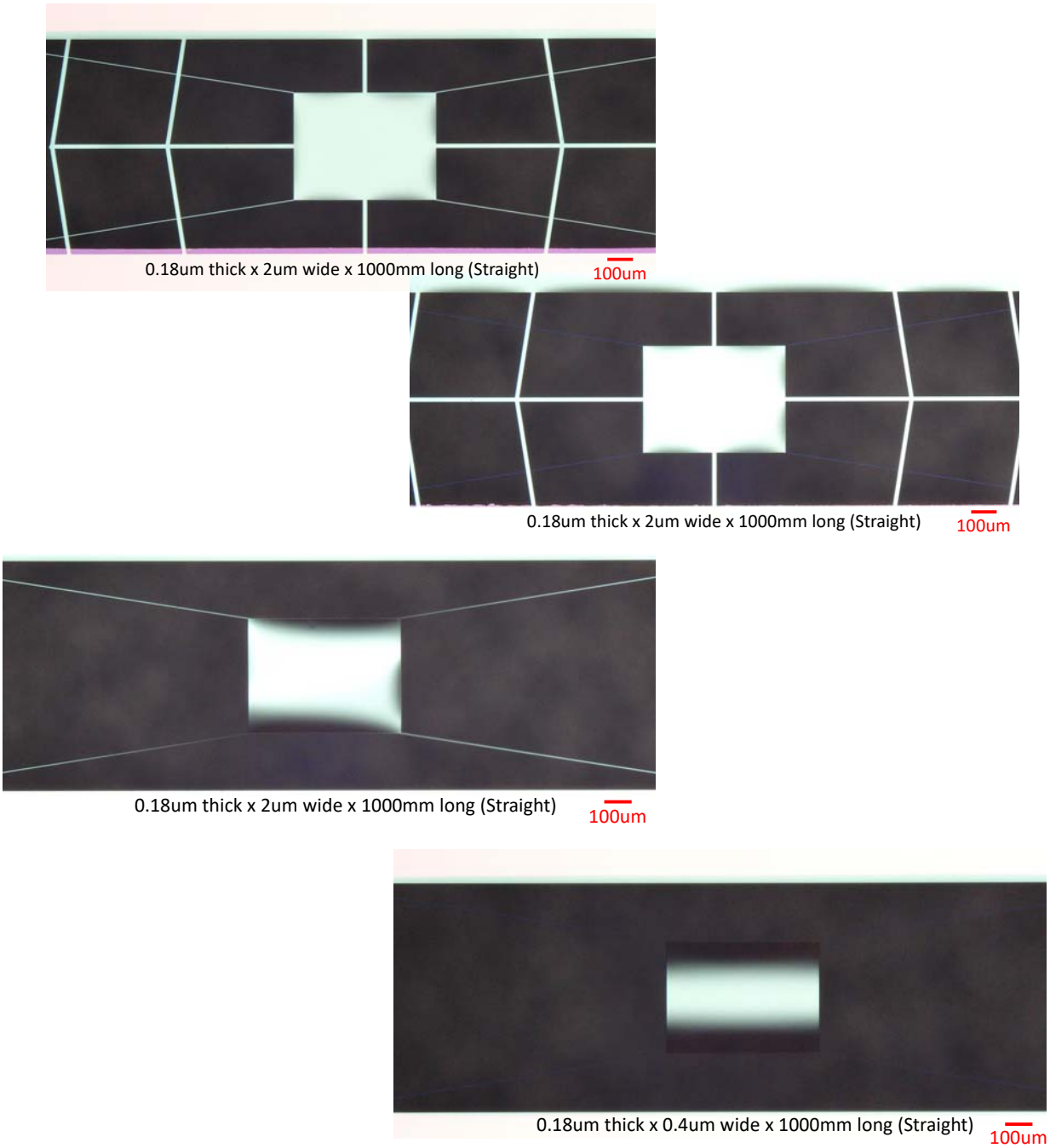


***Fig. 4.*** *Example bolometer test structures after release. Devices shown with buttresses both before (above) and after (below) laser trimming of support buttresses.*

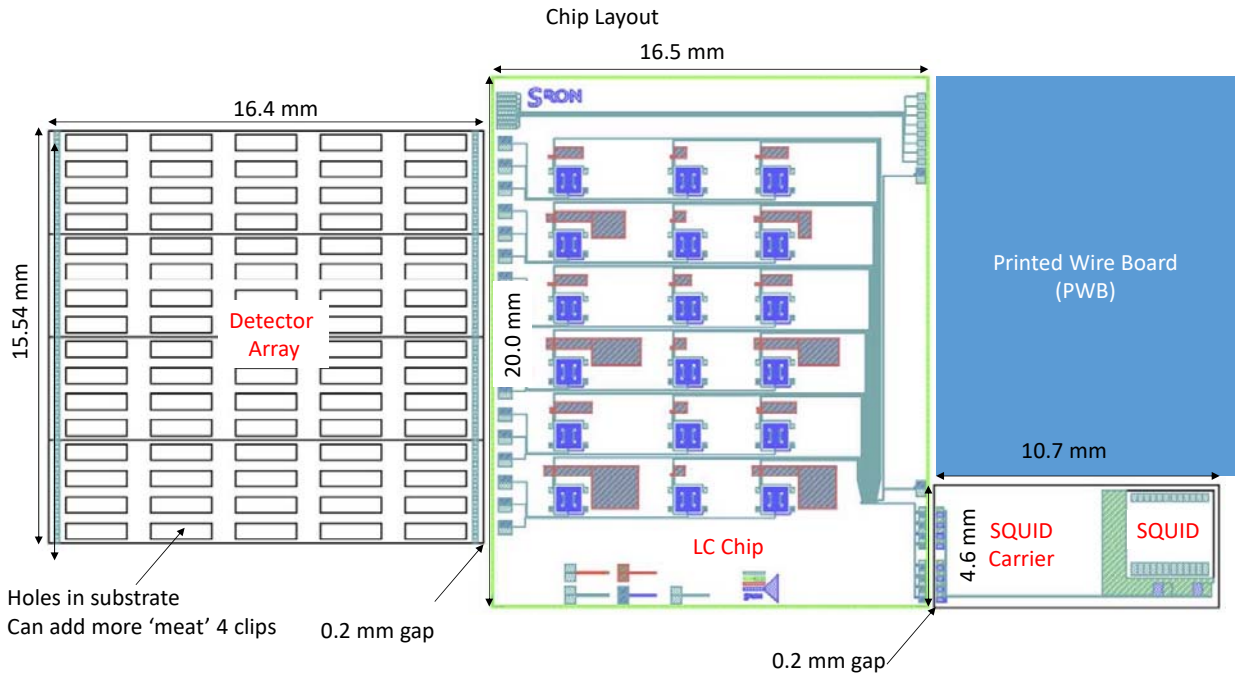


***Fig. 5.*** *Layout of our v0 bolometer test experiment. The detector array and SQUID carrier are fabricated in the microdevices lab at JPL. The LC chip was built by our collaborators at SRON. The printed wire board (PWB) includes an MDM connector to a loom of twisted-pair wires. The SQUID will be from Magnicon (a commercial SQUID vendor), and includes its own readout system outside the cryostat. RF interference is mitigated using double-pole RC filters on each conductor as it comes through the PWB, and the aluminum enclosure includes a partition near this filter array to separate the 'noisy' region where the cable enters the box from the 'clean' volume where the bolometers are.*

Another key accomplishment since onset of funding in March has been to design the initial bolometer test apparatus (layout in Fig. 5). This assembly will be housed in an aluminum box and cooled to 50 mK in our dilution refrigerator. The electrical system consists of four chips interconnected with wire-bonds: the bolometer array on a silicon die, the existing 18-channel LC chip from SRON, a custom SQUID carrier chip patterned on silicon, and a custom PWB which interfaces with the twisted-pair cable loom from the warm side of the cryostat. All these elements have been designed and are being fabricated (or procured, in the case of the PWB).

In addition to the v0 experiment box shown in Fig. 5, the cryostat also has a filtered breakout PWB at the warm vacuum shell of the cryostat. This filtered board also uses a partition galvanically connected to the cryostat jacket, so that the jacket forms an RF-tight Faraday cage with all signals passing through double-pole filters.

## Path Forward

Still underway in FY 2018 are delivery and commissioning of the refrigerator (expected August 2018), and the first measurements of resistance verses temperature (R vs T) for thermistor films (unreleased). By the end of FY 2018, we will have a full box mechanical design to accompany the v0 functional chip layout (Fig. 5), so we expect to measure bolometers early in FY 2019.

## References

[1] P. Roelfsema et al., "*SPICA – a large cryogenic infrared space telescope Unveiling the obscured Universe*," Publications of the Astronomical Society of Australia, SPICA Special Issue (2018)

[2] C. Battersby et al., "*The Origins Space Telescope.*," Nature Astronomy. **v.2** (August 2018)

[3] R. Hartog, M.D. Audley, J. Beyer, D. Boersma, M. Bruijn, L. Gottardi, H. Hoevers, R. Hou, G. Keizer, P. Khosropanah, M. Kiviranta, P. Korte, J. Kuur, B.-J. Leeuwen, A.C.T. Nieuwen- huizen, and P. Winden, "*Low-noise readout of TES detectors with baseband feedback frequency domain multiplexing*," Journal of Low Temperature Physics, **167(5)**, 652–657 (2012)
[4] M.A. Dobbs, M. Lueker, K.A. Aird, A.N. Bender, B.A. Benson, L.E. Bleem, J.E. Carlstrom, C.L. Chang, H.-M. Cho, J. Clarke, T.M. Crawford, A.T. Crites, D. I. Flanigan, T. de Haan, E.M. George, N.W. Halverson, W.L. Holzapfel, J.D. Hrubes, B.R. Johnson, J. Joseph, R. Keisler, J. Kennedy, Z. Kermish, T.M. Lanting, A.T. Lee, E.M. Leitch, D. Luong-Van, J.J. McMahon, J. Mehl, S.S. Meyer, T.E. Montroy, S. Padin, T. Plagge, C. Pryke, P.L. Richards, J.E. Ruhl, K.K. Schaffer, D. Schwan, E. Shirokoff, H.G. Spieler, Z. Staniszewski, A.A. Stark, K. Vanderlinde, J.D. Vieira, C. Vu, B. Westbrook, and R. Williamson, "*Frequency multiplexed superconducting quantum interference device readout of large bolometer arrays for cosmic microwave background measurements*," Review of Scientific Instruments, **83(7)** (2012)
[5] A.D. Beyer, M.E. Kenyon, P.M. Echternach, T. Chui, B.-H. Eom, P.K. Day, J.J. Bock, W.A. Holmes, and C.M. Bradford, "*Ultra-sensitive Transition-Edge Sensors for the Background Limited Infrared/Sub-mm Spectrograph (BLISS)*," Journal of Low Temperature Physics, p. 143 (December 2011)

**For additional information, contact Matt Bradford:** matt.bradford@jpl.nasa.gov

# Raising the Technology Readiness Level of 4.7-THz Local Oscillators

Prepared by: Qing Hu (MIT)

## Summary

The 63-μm (4.744 THz) [OI] fine-structure line is an important spectral line for astrophysics observations. Despite the great potential, however, astrophysical observation of the [OI] line has rarely been performed because the 4.744-THz frequency is beyond the reach of most implemented local oscillators (LOs) in sensitive heterodyne receivers involving cryogenic mixers. In this three-year NASA Strategic Astrophysics Technology (SAT) project, we plan to raise the Technology Readiness Level (TRL) of THz quantum-cascade lasers (QCLs) for LO applications to 5 or beyond, bridging the "mid-TRL gap" between a promising enabling technology and a mission-ready component. The project started in March 2016 and is planned to conclude in February 2019.

The objective will be achieved by developing antenna-coupled 3rd-order distributed feedback (DFB) lasing structures, and in parallel, designing and growing high-performance quantum-cascade gain media with peak frequency around 4.7 THz. By the end of the project, we will develop single-mode DFB lasers with frequency within 10 GHz of the target 4.744-THz line, continuous wave (*cw*) output power of ~5 mW, wall-plug power efficiency (WPE) of ~0.5% at an operating temperature of ~40 K, and beam patterns narrower than 10×10 degrees[2].

The project will be carried out in the Principal Investigator's (PI) laboratory at MIT, with the molecular beam epitaxy (MBE) wafers provided by Dr. John Reno at Sandia National Laboratories through a user agreement.

During the previous year, we completed the design of antenna-coupled 3rd-order DFB structures, and generated fabrication masks based on the design. We completed the fabrication process and tested the devices. The lasing frequency (4.74x THz) and power levels (>1 mW) already meet our final goal. However, the peak frequency of the gain medium is too far from 4.744 THz, so device performance suffered. The maximum operating temperature is only ~30 K, which does not meet the requirement of an actual observatory, but it is sufficient for lab testing at ~10 K. Several devices have been shipped to our collaborator at SRON to test their components (beam splitters and hot-electron bolometer, HEB, mixers) for the recently initiated the Gal/Xgal U/LDB Spectroscopic/Stratospheric THz Observatory (GUSTO) project. We have also developed a novel scheme to electrically tune the frequency by ~10 GHz (this is at a different center frequency of ~3.9 THz, but the method can also be applied to 4.7 THz once the gain medium is available).

## Background

The 63-μm (4.744 THz) [OI] fine-structure line is the dominant cooling line of warm, dense, neutral atomic gas. Because of its great intensity in high-UV photodissociation regions (PDRs) and shocks, the [OI] 63-μm line is superior for probing regions of massive star formation and the centers of galaxies. It is a unique probe of PDRs, shock waves from stellar winds/jets, supernova explosions, and cloud-cloud collisions. These radiative and mechanical interactions shape the interstellar medium of galaxies and drives galactic evolution. The size scale of the interactions can excite [OI] emission over many parsecs. Moreover, the emission regions are often complex, with multiple energetic sources processing the environment. Spectrally resolved observations of the [OI] line with a heterodyne receiver array will allow users to disentangle this convoluted interaction and permit the study of the energy balance, physical conditions, morphology, and dynamics of these extended

regions. In this way, such a receiver array will provide new and unique insights into the interrelationship of stars and gas in a wide range of galactic and extragalactic environments.

This project mainly addresses NASA's Strategic Subgoal 3D, "*Discover the origin, structure, evolution, and destiny of the universe, and search for Earth-like planets*." It also addresses NASA's Strategic Subgoal 3A, "*Study planet Earth from space to advance scientific understanding and meet societal needs*"; and NASA's Strategic Subgoal 3C, "*Advance scientific knowledge of the origin and history of the solar system, the potential for life elsewhere, and the hazards and resources present as humans explore space*." The development will significantly reduce the risk of several current and future suborbital projects such as GUSTO, a long-duration balloon (LDB) payload. The proposed systems this project will develop include an eight-element heterodyne receiver array for the 4.744-THz [OI] line.

DFB structures are required to generate robust single-mode lasing output. Currently, 1st-order, 2nd-order, and 3rd-order DFB lasers have been demonstrated (the grating period of an nth-order DFB grating is n times the half-wavelength in the gain medium). Among these, the 3rd-order DFB structures show the greatest promise for LO applications, because of their compact size and good beam patterns. Despite the promise of 3rd-order DFB lasers, the phase mismatch limits total length to less than 1 mm so the beam is still quite divergent. In addition, the low extraction efficiency yields a low WPE of 0.1%. In this SAT project, we plan to further develop this promising technology by developing the following.

- Perfectly phase-matched 3rd-order DFB lasers, to generate even narrower beam patterns and higher output power levels;
- Novel antenna-coupled 3rd-order DFB structure to increase WPE; and
- Better-performance gain medium, peaked at 4.74 THz.

## Objectives and Milestones

The project objectives are to develop single-mode DFB lasers with frequency within 10 GHz of the target 4.744-THz line, *cw* output power level greater than 5 mW, WPE ≥0.5% at an operating temperature of ~40 K, and beam patterns narrower than $10 \times 10$ degrees$^2$. The annual milestones are listed in Table 1.

| Year | Milestones |
|---|---|
| Year 1 (3/2016 – 2/2017) | • Complete the design of perfectly phase-matched 3rd-order DFB lasers aimed for ~4.7 THz<br>• Develop a high-yield dry-etching process using inductive-coupled plasma (ICP) to achieve clean and smooth sidewalls with high aspect ratios<br>• Grow ~3 MBE wafers based on improved QCL designs<br>• Fabricate devices using a combination of dry and wet etching |
| Year 2 (3/2017 – 2/2018) | • Continue to improve the fabrication process for higher quality and higher yield<br>• Grow ~3 MBE wafers based on improved designs<br>• Develop perfectly phase-matched ($n_{eff}$ = 3.00 ± 0.02) 3rd-order DFB with a modest value of $\alpha_m \approx 2$ cm$^{-1}$ to ensure a robust single-mode operation and $\eta_{WPE} \approx 0.1\%$<br>• Design phase-matched 3rd-order DFB structures integrated with half-wave antennas |
| Year 3 (3/2018 – 2/2019) | • Grow ~3 MBE wafers based on improved designs<br>• Develop phase-matched 3rd-order DFB coupled with integrated antennae with a more aggressive value of $\alpha_m \approx 10$ cm$^{-1}$, achieving $\eta_{WPE} \approx 0.5\%$ with ≥ 5 mW power at ~40 K. The phase matching should be good enough for a long device for the high output power and with beam divergence ≤ $10 \times 10$ degrees$^2$ |

***Table 1.*** *Milestones of this SAT project.*

## Progress and Accomplishments

Prior to the beginning date of the current SAT project, we successfully developed a single-mode 3rd-order DFB laser that lases within 3 GHz of the target 4.744-THz [OI] line [1]. Although the power level is lower

than desired due to imperfect phase matching and the lack of integrated antennas (which as discussed above is pursued in the SAT project), it is adequate to pump a single-element HEB mixer. One device was integrated with the Stratospheric Terahertz Observatory (STO-2) LDB observatory. Unfortunately, the control electronics of this device were damaged by the sun during the flight, so no data was obtained.

The design of novel antenna-coupled, perfectly phase-matched 3rd-order DFB structures requires clever analysis and accurate numerical validation, which is what we accomplished during the first year of the project. Fabrication of the designed structures requires a sophisticated combination of dry and wet etching, which started in the past three months. The design and growth of high-performance THz gain media is also a highly challenging process. Aided with sophisticated numerical packages including Schrödinger and Poisson solvers, we completed the design of quantum-cascade structures and three MBE wafers were grown. The growth was carried out by Dr. John Reno at Sandia National Laboratories. Sandia has all the required equipment, and Dr. Reno has a long track record in the growth of record-setting THz gain media.

The design of high-power and single-mode DFB lasers requires innovative thinking and detailed numerical simulations, and both were accomplished following a long history of innovation and technical know-how in the PI's group. We completed the design of antenna-coupled 3rd-order DFB structures and generated fabrication masks based on the design. We also designed quantum-cascade gain structures with the center frequency around 4.7 THz. Three MBE wafers were grown based on the design, but the growth took place during the end of the MBE machine cycle. As a result, the doping level is significantly off so the performance was poor in operating temperature and output power levels. We will regrow these three structures in August 2018 when the MBE machine is back online and will carry out the fabrication and device characterization shortly afterward. We do not anticipate any change of direction in the project. We are on track to achieve our milestones as shown above and anticipate achieving our objectives.

## Path Forward

At this stage, we expect our remaining work will closely follow the annual milestones listed above.

## Reference

[1] J.L. Kloosterman, D.J. Hayton, Y. Ren, W. Kao, J.N. Hovenier, J.R. Gao, T.M. Klapwijk, Q. Hu, C.K. Walker, and J.L. Reno, "*Hot electron bolometer heterodyne receiver with a 4.7-THz quantum cascade laser as a local oscillator*," Appl. Phys. Lett., **102**, 011123 (2013)

**For additional information, contact Qing Hu:** *qhu@mit.edu*

# Advancing Focal Plane TRL for LiteBIRD and other Next Generation CMB Space Missions

Prepared by: Adrian Lee (PI; UC Berkeley and Lawrence Berkeley National Laboratory); Shawn Beckman, Julian Borrill, and Benjamin Westbrook (UC Berkeley); Kam Arnold (UC San Diego); Nils Halverson (University of Colorado, Boulder); Hannes Hubmayr (NIST); Chao-Lin Kuo and Keith L. Thompson (Stanford University); and Aritoki Suzuki (Lawrence Berkeley National Lab)

## Summary

This three-year technical development project started in October 2017. The project's goal is to increase the Technology Readiness Level (TRL) of superconducting mm-wave detectors and readout electronics for a cosmic microwave background (CMB) space mission, with a focus on application to the LiteBIRD mission. This mission envisions a focal plane with thousands of detectors spanning 15 spectral bands – two orders of magnitude more than the most recent CMB space mission. This project's technology development goals are necessary to realize the next-generation CMB focal plane.

The US team is working as part of the LiteBIRD international collaboration, led by Masashi Hazumi. In the US, there are five partner institutions: The University of California Berkeley, The University of California San Diego (UCSD), The University of Colorado Boulder, Stanford University, and the National Institute of Standards and Technology (NIST) in Boulder, CO.

**Project highlight:**

A key technological requirement for the detectors is control of their sensitivity to cosmic rays. We have demonstrated that our detector array design is fairly insensitive to energy deposition from ionizing particles in the bulk silicon, which is a positive step toward achieving the requirement on dead-time due to cosmic-ray interactions in flight.

## Background

The Cosmic Microwave Background (CMB) has been a gold mine for cosmology. The temperature fluctuations measured by the COBE, WMAP, and Planck space missions revolutionized our understanding of cosmology, ushered in the era of precision cosmology, and form the basis for much of today's standard cosmological model. The CMB gives us such fundamental information about the universe since it is emitted at a time very close to the Big Bang, 0.003% of the current age of universe.

A next-generation CMB imager mission, such as LiteBIRD or PICO, will dig into the next archeological layer by measuring the polarization anisotropy of the CMB. All previous missions were optimized for temperature measurements, but the polarization contains new messengers that inform us on the beginning and evolution of the universe. At the very first moment of the universe, space itself is thought to have undergone an exponential expansion. This exotic but simple idea called Inflation is compelling since it explains simultaneously basic conundrums about the universe such as: why is the entire sky the same temperature even though the regions we see would not naively be thought to be causally connected? Why is the geometry of space flat (Euclidean)?

Theory suggests that there is one measurement that positively detects Inflation as the correct model for the beginning of the universe – to see the swirling fingerprints of "B-mode" polarization in the

CMB. If we are able to see this signature, we would not only have a clear identification of Inflation, but could also measure the energy scale of Inflation and be able to narrow in on the precise model for Inflation. Even if a signal is not seen, we will eliminate an entire class of Inflation models and thereby change the direction in the search for the physics at work at the beginning of the universe.

The US is participating in two imager mission concepts, LiteBIRD led by JAXA, and PICO, a Probe-class NASA mission study. Our PCOS investigation focuses on TRL advancement with the specific LiteBIRD mission concept as a focus, but all the technologies are leading candidates for PICO and other future CMB mission concepts. The LiteBIRD mission is one of two candidates in the "Strategic Large Mission" category in JAXA (along with Solar Sail), and a downselect to one mission is scheduled late in 2018.

The focal-plane array technology required for LiteBIRD has been matured for ground-based observations but requires adaptations to achieve the TRL required for a space mission. The list of areas for advancement include:

i. The detector array response to cosmic rays at L2 (the likely orbit for a CMB space mission) needs to be understood. If the predicted deadtime due to cosmic rays would significantly reduce science yield, the arrays need to be redesigned with features to mitigate the effect of cosmic rays.
ii. The detector arrays must be tested to see if they would survive launch vibration, and modified if required.
iii. The transition-edge sensors (TESs) must be adapted to the lower optical power they would receive in a space-borne telescope which is straightforward engineering.
iv. The frequency-domain readout electronics that our team has developed must be adapted to the longer cable lengths expected in a spacecraft.
v. Techniques to develop simulations of the relatively large data set generated in an all-sky mission with thousands of detectors have to be developed.

As will be described in detail below, our investigation will address each of these areas to advance the TRL of the detector arrays, readout electronics, and data simulation. Detector array performance will be evaluated using focused testing such as with radioactive sources to mimic cosmic-ray events and shake-table tests to simulate launch vibration. We will iterate on the design of the detectors, readout electronics, and data simulation pipeline to progress from TRL in the 3-4 range to TRL in the 5-6 range over the three-year program.

## Objectives and Milestones

The objectives of this research are to increase, in parallel, the TRL of focal-plane superconducting detectors and readout electronics for the JAXA LiteBIRD CMB mission and other CMB space missions. The milestones identified in the proposal to do this work are shown in Table 1 below. Good progress is being made toward the initial milestones. Details are given below.

| Date | Deliverable |
|---|---|
| 2018-09 | All necessary testing facilities validated |
| 2018-09 | Initial designs for TRL-4 demonstration of technology all complete |
| 2019-03 | Produce supporting documents for JAXA System Requirements Review (SRR), including both technology requirements and instrument simulations based on those requirements |
| 2019-09 | Demonstrate TRL 4 of all focal-plane and cryogenic readout technology |
| 2019-09 | Demonstrate acceptable level of magnetic-field and vibration sensitivity |
| 2020-03 | Demonstrate cosmic-ray mitigation appropriate for detectors |
| 2020-03 | Demonstrate end-to-end simulations of instrumental systematic effects, at their demonstrated levels in observations |

| | |
|---|---|
| 2020-09 | Demonstrate TRL 5 or 6 of all focal-plane and cryogenic readout technology |

**Table 1:** Milestones identified in original proposal.

- ***2018-09: All necessary testing facilities validated:***
  - The test cryostat at UC San Diego that will be used for development of the LiteBIRD cryogenic readout components is cryogenically fully operational. Wiring to support the DfMux development for LiteBIRD has been designed and ordered, and will be installed in time to meet this milestone;
  - The test cryostat at UC Berkeley that will be used for development of LiteBIRD detectors has been ordered. It will be delivered in January 2019. Until that time, other cryostats already validated at UC Berkeley are being used for testing; and
  - The test cryostat at Stanford University is in the design phase. A 100-mK fridge has been identified and will soon be ordered. We have decided to delay acquisition of this cryostat since it will not be needed until later in the program.
- ***2018-09 Initial designs for TRL-4 demonstration technology all complete.*** Key issues for technology development described in the proposal are addressed in more detail below:
  - Detector cosmic-ray sensitivity: we have demonstrated the ability to measure events from a radiation source, and have designed several mitigations to test. The sub-task on cosmic-ray sensitivity is complete. Demonstration is underway.
  - Detector vibration sensitivity: vibration tests of existing hardware similar to that proposed for LiteBIRD has been successfully completed. However, no specific TRL development hardware has been produced. We are awaiting agreement with our international partners on the focal-plane mechanical layout to build these modules. Work on this layout is underway.
  - Detector magnetic field sensitivity: constructing Helmholtz coils and related test equipment to characterize detector response to known magnetic fields. We plan to achieve the milestone in 2018-09 with LiteBIRD-like detectors.
  - Cryogenic detector readout system: the cryogenic readout system has been re-designed to include a superconducting quantum interference device (SQUID)array amplifier at the 0.1-K focal-plane stage. This design is complete, and some testing has occurred. Further testing is underway. On the topic of cryogenic readout, this milestone is complete, and now demonstration is underway.
- ***2019-03: Produce supporting documents for the JAXA SRR, including both technology requirements and instrument simulations based on those requirements.*** While this milestone is scheduled for 2019-03, the US team actually has to support a JAXA Phase A1 Exit Review around 2018-09. We are making progress toward this goal first.
  - Technology requirements: working with our international partners, we have detailed the instrument requirements to level 3, and are currently detailing the US deliverable requirements to level 5. That requirements breakdown will be delivered by 2018-09.
  - Instrument simulations: with focal-plane design expertise, we have supported trade studies for the instrument optical design and updates of the projected instrument sensitivity. We will define a baseline design before 2018-09, and support simulations of that design including the sensitivity of the instrument and the effect of instrumental uncertainties on the data.
- ***2020-03: Demonstrate end-to-end simulations of instrumental systematic effects, at their demonstrated level in observations.***
  - Simulation framework performance: we have ported the Time-Ordered Astrophysics Scalable Tools (TOAST) simulation and reduction framework to the new flagship supercomputer at the National Energy Research Scientific Computing Center (NERSC), and begun to optimize this novel architecture.

- Simulation of systematic effects: we have used simulations of realistic, correlated detector noise to optimize our scan strategy parameters, including investigating our robustness to catastrophic half-wave plate failure.

Other milestones in table 1 are discussed in the "Path Forward" section at the end of this document.

## Progress and Accomplishments

In this section, we report on progress and accomplishments on Cosmic-Ray Deadtime Mitigation, Focal-Plane Design, Bolometer Design Optimization, and Data Simulation.

### *Cosmic-Ray Deadtime Mitigation*

The LiteBIRD mission requirement is to limit data loss from cosmic-ray interactions in the focal plane to 5%. To achieve this requirement, our team is first developing an understanding of energy propagation mechanisms in our detector wafers. Our current understanding includes two primary energy transport mechanisms. First, energy deposition in the silicon substrate generates ballistic phonons which penetrate the thin detector layers, producing both ballistic and diffusive lateral phonon propagation to the TES. Second, Cooper pairs in the niobium ground plane are broken either directly by the incident particle, or by diffuse phonons. The resultant quasi-particles then recombine to create diffuse phonons near the TES that are subsequently absorbed.

To verify these mechanisms, a test facility and analysis toolkit for cosmic-ray mitigation testing have been developed at UC Berkeley over the last 12 months. This test setup uses an Americium-241 alpha-particle source to be accurately positioned in three dimensions over a test chip cooled to 250 mK. The source provides a 5.5-MeV alpha particle accompanied by a 60-keV gamma ray to simulate energy deposition into our focal plane via cosmic rays (see Fig. 1 for example alpha events). The alpha particle is capable of penetrating the silicon nitride and niobium surface layers when incident on the detector-side of our device wafers, and will stop in the substrate when incident on the substrate-side.

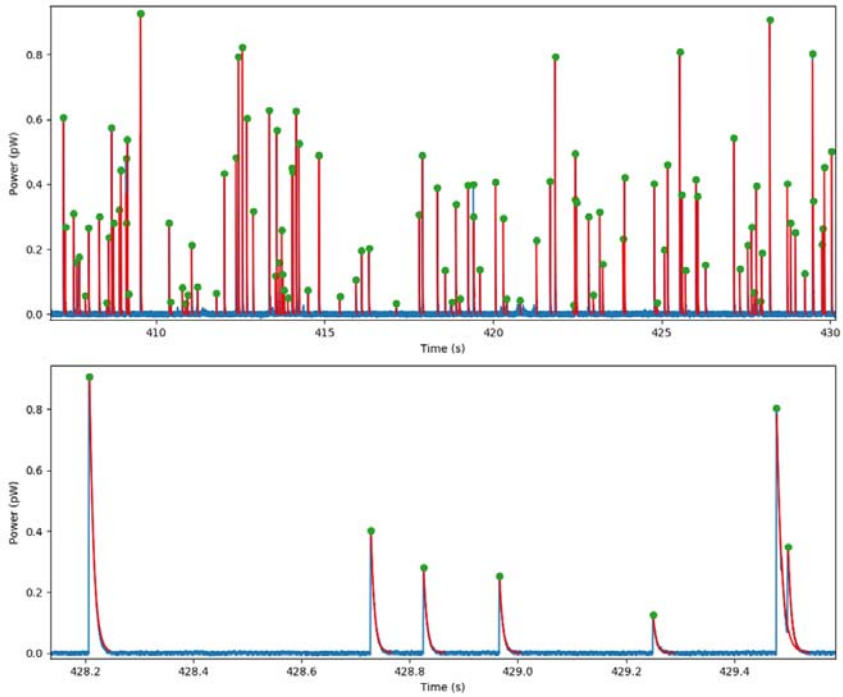


***Fig. 1.*** *Timestreams of Americium-241 alpha events on the detector side of the small detector array with pulse fits displayed.* Top: *A timestream of data of 22-second duration showing the rate of interaction and pulse height*

*variation.* Bottom: *A zoom-in of 1.5 seconds of data showing the rapid rise and slower fall times of the pulses. The fall times are consistent with the thermal time-constant of the TES detectors.*

We can compare events from illumination of the two sides of the detector chip to distinguish between transport mechanisms originating in the surface layers vs. in the substrate. We find that the hit rate given by alpha particles impacting the substrate-side of our test chips is nearly identical to the background hit rate, setting an upper limit on detection of the backside alpha interactions. The data are consistent with the hypothesis that ballistic phonons created in the substrate by 5.5-MeV alpha particles do not transmit energy to the TES appreciably when compared with mechanisms originating in the detector-side surface layers. When testing with alpha particles incident on the detector side of our test chips, we have verified that the primary energy transport mechanisms have a mean free path of 1 - 2 mm.

In future testing, we plan to continue to investigate energy transport mechanisms. Also, we have designed and built test detectors that have features to mitigate energy propagation to the TES which we plan to test in the coming year. Current tests have been done at 300 mK, but when the Berkeley 100-mK test facility is operational, we can test the bulk thermal response of the entire detector array to energy deposition by ionizing radiation.

### *Focal-Plane Design*

In collaboration with LiteBIRD teams from Japan and Europe, we have been optimizing telescope configurations and focal-plane configurations to maximize science return for a given set of instrument resources [2 ,3, 5]. We optimize the focal-plane configuration to achieve required sensitivity at all frequency bands, meet optical coupling requirements, minimize the number of detectors to relax readout requirements, and minimize the number of detector modules to reduce mass and cost. An example of a focal-plane design is shown in Fig. 2. This new design has fewer wafers compared to the 2016 NASA concept study report. The new focal plane has higher sensitivity because it has less focal-plane space taken up by mounting hardware. We are in the early stage of this re-optimization process, and the international collaboration is studying various trade-offs to ratify a new baseline design.

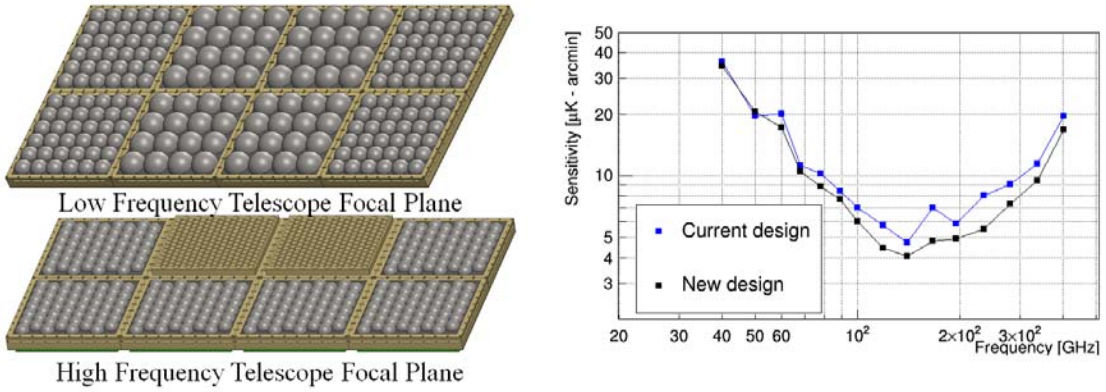


***Fig. 2.*** Left: *Example of re-optimized focal planes.* Right: *Sensitivity comparison between the current baseline design and the new design.*

### *Space-Optimized Bolometers*

A technical requirement of our Technical Development program is to realize TES bolometers optimized for space. We have taken two significant steps toward realizing such detectors. First, we developed AlMn films optimized for 100-mK operating temperature with suitable resistance to be coupled to the baseline frequency-division SQUID multiplexer. Second, we designed and are soon to fabricate bolometer prototypes that use these AlMn films and are space-optimized.

To satisfy the L1 science requirement to constrain inflation and the resulting L2 sensitivity requirement, LiteBIRD will use arrays of TES bolometers operated at 100 mK, with a target superconducting transition temperature $T_c$=170 mK [4]. An additional constraint to the sensor design is compatibility with the readout multiplexer. For the frequency-division multiplexer (fMUX) used in LiteBIRD, the required sensor impedance is ~1 Ohm. LiteBIRD is the first CMB experiment to use the combination of 100-mK bolometers and R = 1 Ohm sensors, and therefore TES film development is required.

By use of 90-nm-thick, 220-ppm AlMn films we have realized films that cover the needed parameter space in $T_c$ and R. We demonstrated high spatial uniformity in the superconducting transition temperature, Tc, across the wafer. This uniformity is essential to achieve consistent sensitivity of the detectors for LiteBIRD and other next-generation CMB polarization satellite missions. Figure 3 shows a mean $T_c$ ~ 170 mK and a peak-to-peak variation that is 6% within a 100-mm diameter wafer, the planned wafer size for LiteBIRD. This level of uniformity enables a tight distribution in detector NEP across the array.

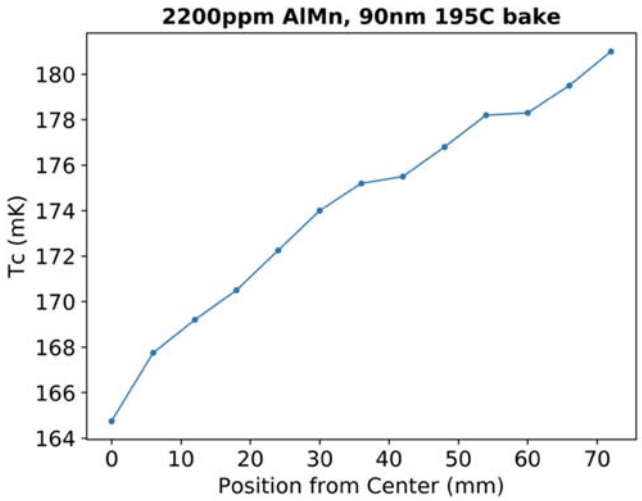


***Fig. 3.*** *AlMn films developed for LiteBIRD achieve the target Tc and exhibit 6% peak-to-peak uniformity across the planned 100-mm diameter wafer.*

Second, UC Berkeley and NIST co-fabricated a detector test chip to meet LiteBIRD specifications. A photograph of the bolometers is shown in Fig. 4. The bolometer designs span a leg-length range of 250 to 2000 μm in order to cover the range of saturation powers required for the medium-frequency (MF) pixels to be fabricated at Marvell Nanofabrication Facility. A second design iteration is underway and will likely provide us with baseline designs to achieve the specifications of the bolometers for all the MF wafers.


***Fig. 4.*** *Photograph of a LiteBIRD test chip fabricated at UC Berkeley with fabrication support from NIST for the AlMn TES. Results from initial test show that these bolometers are with a 10% of the $T_c$ target and a factor of 2 of the normal resistance targets.*

Finally, we designed space-optimized bolometers. We plan to fabricate detector chips with several variations on the bolometer shown in Fig 5. The aim of the fabrication splits is to span the saturation-power requirements of LiteBIRD and probe the thermal circuit of these devices for stability. Maximizing the instantaneous sensitivity of the detectors given the low photon-loading of space dictates the need for low-thermal-conductance bolometers. For LiteBIRD, the smallest saturation power (the total power which the bolometer can support, a quantity directly proportional to the thermal conductance) is approximately 100 fW. In previous work, TES bolometers optimized for a space-based spectrometer, with parameters similar to what is required for LiteBIRD, have been realized on the single pixel level [1]. More recently and within our own collaboration, TES bolometers optimized for balloon-based observation using 300-mK refrigeration has been demonstrated [2]. The bolometer design shown in Fig. 5 builds on these results; the main difference being optimization for 100 mK as opposed to 300-mK refrigeration.

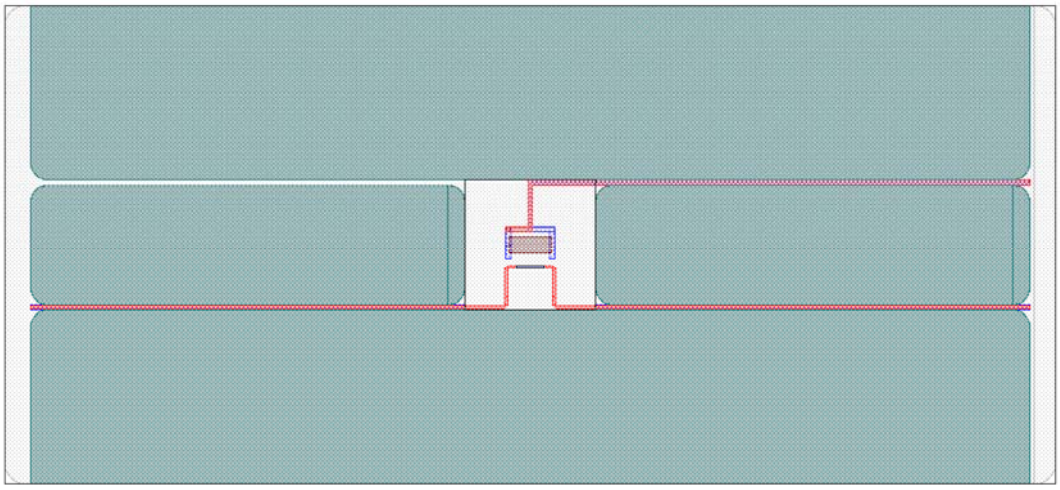

***Fig. 5.*** *Space-optimized TES bolometer design. The four long thermally isolating legs achieve low saturation power, yet are mechanically robust. The size of the central bolometer island is 150 μm x 150 μm.*

### *Cryogenic readout design*

To achieve the requirements on the detector readout, the SQUID array amplifier used to amplify the detector signals needs to be operated at lower temperature and closer to the detectors. We designed

a readout circuit with the SQUID array amplifiers at the detector focal plane (Fig. 6), and have begun initial tests at 250 mK. Tests at 100 mK will commence soon.

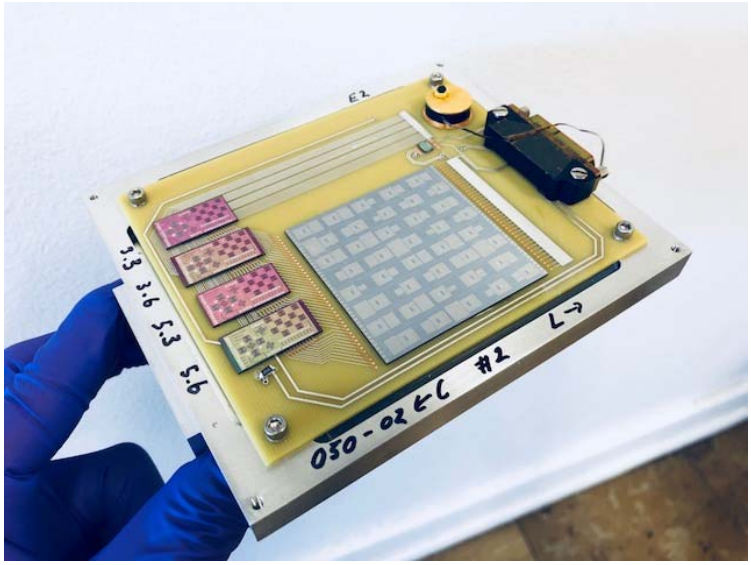

***Fig. 6.*** *Image of cryogenic readout test circuit with SQUID array amplifier, inductor/capacitor board, and bolometer test chips.*

### *Thermal Calculations*

In support of new collaborators in Europe who will focus on the sub-K cooler and high-frequency telescope (HFT) telescope design, Co-I Thompson re-calculated the thermal cooling power requirements of the sub-4-K stages for various focal-plane options for the low- and high-frequency LiteBIRD telescopes. Many of these choices are interdependent, so that e.g. choice of telescope with its f-ratio affects the physical size of the focal plane, even in the absence of a pixel-count change, thus changing the structural support thermal loading as well as the radiative loading on the cold stages. In the coming year, we plan to converge on mature designs with space thermal experts at the SSL at Berkeley.

### *Detector Test Systems*

At UC San Diego, A BlueFors dilution refrigerator cryostat was procured and is cryogenically functional. This will be the primary LiteBIRD cryogenic readout test facility. It is being outfitted with full wiring now. In parallel, we started some testing in this cryostat that does not require the full wiring.

At Stanford University, Co-I Thompson has been designing the optical-test cryostat in preparation for detector testing. It will have internal sources for measurements of optical beams, optical efficiency, integrated sidelobe power, and polarization. The test facility will also have a light-pipe option for spectral-response measurements for both an FTS source and a filtered (e.g., using thick grill filters) thermal source. Helmholtz coils around the cryostat will support magnetic-field-sensitivity testing up to ~100 Hz. A 100-mK fridge will be ordered soon. The time-scale for coming on-line should be by the beginning of 2019.

At Berkeley, A Blu-Fors dilution refrigerator was ordered, with delivery expected in January 2019. A new cryostat section was designed with sufficient size to hold the entire Low-Frequency Telescope (LFT) or High-Frequency Telescope (HFT) focal planes. This refrigerator will be the main test platform for full focal-plane integration tests.

### *Time-Domain Data Simulations*

LiteBIRD's ability to achieve its scientific goals will depend on precise control of both statistical and systematic uncertainties. Statistical uncertainties require us to gather a sufficiently large dataset, but this then poses a host of computational challenges. Systematic uncertainties require us first to design the mission so as to minimize them at the outset, and then to design, implement, validate, and verify strategies to mitigate whatever is left in the data analysis. Generating and reducing synthetic realistic data – both in volume and complexity – is therefore a mission-critical capability. For LiteBIRD we are extending the TOAST CMB data simulation and reduction software, originally developed and deployed by the Planck mission, to the scale and realism required by LiteBIRD.

At Berkeley, Co-I Borrill's team has ported TOAST to the newest NERSC supercomputer, Cori. Built on the Xeon Phi Knights Landing cores, each Cori node supports up to 272 threads, requiring a high level of vectorization to achieve good performance. We have fully instrumented the code, identified a number of performance bottlenecks, and addressed these sufficiently for the code to scale to the full system's 600,000+ cores.

At Stanford University, new postdoctoral hire Giuseppe Puglisi has been doing simulations on 1/f noise contributions to LiteBIRD-like scanning CMB satellites, with and without polarization modulators, and for ranges of satellite spin rates and 1/f knees. In coordination with other collaborators in the LiteBIRD project, he has identified some key issues that need to be addressed, such as the distribution of pixel orientations in the focal plane. He is also beginning to address systematics questions with regard to gain variation.

## Path Forward

As described in the Objectives and Milestones section, so far, we are on track to meet our early project milestones and deliverables shown in Table 1. Our path forward for the remaining work continues to adhere to the plan described in the proposal. The major remaining work, by project milestone, is outlined below, with notes on current progress where applicable.

- All necessary testing facilities validated (due 2018-09)
  - Fabricate and commission UCSD test cryostat
    - Delivered and cryogenically operational. Ordered readout wiring.
  - Fabricate and commission UC Berkeley test cryostat
    - Ordered; delivery expected January 2019
  - Fabricate and commission Stanford test cryostat
    - Design completed and construction beginning
- Initial designs for TRL-4 demonstration technology all complete (due 2018-09)
  - Design detector cosmic-ray-sensitivity test program
    - Complete; demonstration is underway.
  - Design detector vibration-sensitivity test program
    - Awaiting agreement with our international partners on the focal-plane mechanical layout
  - Design detector magnetic-field-sensitivity test program
    - Constructing Helmholtz coils and related test equipment to characterize detector response to known magnetic fields; tests planned for later in 2018
  - Redesign cryogenic detector readout system and devise test program
    - Complete, demonstration is underway
- Produce supporting documents for JAXA SRR (due 2019-03)
  - Finalize technology requirements
    - Completed draft instrument requirements to level 3; currently detailing the US deliverable requirements to level 5; working with international partners to finalize requirements
  - Develop instrument simulations to validate requirements

        - Supporting trade studies for the instrument optical design and updates of the projected instrument sensitivity; after baseline design is finalized, will support simulations of that design including the sensitivity of the instrument and the effect of instrumental uncertainties on the data
    - Develop interface control documents (ICDs)
        - Drafting ICD matrix; when baseline design is finalized, will begin draft ICD documents for the US deliverables
    - Develop validation plan
        - Working with international partners, develop validation plan for US deliverables
- Demonstrate TRL 4 of all focal-plane and cryogenic readout technology (due 2019-09)
    - Design/fabricate/test single-pixel LF/MF/HF detectors and optical coupling
    - Design/fabricate/test low-fidelity LF/MF/HF detector modules
    - Design/fabricate/test low-fidelity focal-plane-tower mechanical assembly
    - Complete TRL-4 demonstration on redesigned cold readout
- Demonstrate acceptable level of magnetic field and vibration sensitivity (due 2019-09)
    - Work with Japanese and European partners to define launch vehicle/spacecraft/instrument magnetic-field and vibrational environment
    - Iterate on detector/module/focal-plane design and shielding to reduce magnetic-field and vibration sensitivity to meet requirements
    - Iterate on cold-readout design and shielding to reduce magnetic-field and vibration sensitivity to meet requirements
- Demonstrate cosmic-ray mitigation appropriate for detectors (due 2020-03)
    - Work with Japanese and European partners to define anticipated cosmic ray flux at L2 and finalize requirements
    - Iterate on detector design/fabrication/test using in-lab radioactive source
    - Irradiate mature design with proton beam at HIMAC facility in Japan
- Demonstrate end-to-end simulations of instrumental systematic effects (due 2020-03)
    - Work with Japanese and European partners to conduct simulations to finalize scan strategy, use of half-wave plate (HWP) and inform hardware requirements for US deliverables
    - Finalize hardware requirements
    - Characterize detector and readout optical and electrical contributions to systematics
    - Incorporate measurements into high-fidelity simulations including detector, telescope, and HWP imperfections, representative sky model, and mission optimization
- Demonstrate TRL 5 or 6 for all focal-plane and cryogenic readout technology (due 2020-09)
    - Design/fabricate/test LF/MF/HF full detector arrays, optical coupling, and detector modules
    - Conduct magnetic-field/vibration/cosmic-ray tests on full modules
    - Design/fabricate/test high fidelity focal-plane-tower mechanical assembly
    - Integrate, test, and demonstrate detector module, cold readout, and focal-plane-tower assembly

# References


[1] A.D. Beyer et al., "*Ultra-sensitive transition-edge sensors for the Background Limited Infrared/Sub-mm Spectrograph (BLISS)*," Journal of Low Temperature Physics, **167.3-4**, 182-187 (2012)

[2] A. Suzuki et al., "*The LiteBIRD Satellite Mission: Sub-Kelvin Instrument*," Journal of Low Temperature Physics, in press (2018)

[3] T. Matsumura et al., "*LiteBIRD: Mission Overview and Focal Plane Layout*," Journal of Low Temperature Physics, **Vol. 184**, Issue 3-4, pp 824-831 (2016)

[4] C. Hill et al., "*BoloCalc: a sensitivity calculator for the design of Simons Observatory*," arXiv:1806.04316

[5] B. Westbrook et al., "*Development of the Next Generation of Multichroic Antenna-Coupled Transition Edge Sensor Detectors for CMB Polarimetry*," Journal of Low Temperature Physics, **Vol. 184**, Issue 1-2, pp 74-81 (2016)

**For additional information, contact Adrian T. Lee:** Adrian.Lee@berkeley.edu

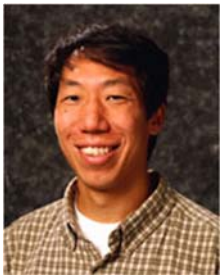

# Development of a Robust, Efficient Process to Produce Scalable, Superconducting Kilopixel Far-IR Detector Arrays

Prepared by: Johannes Staguhn (JHU)

## Summary

The funding for this two-year project started January 1, 2018. The primary objective of the project is to demonstrate a versatile scheme to connect two-dimensional superconducting detectors and cold-readout electronics through a separate silicon structure with superconducting through-wafer vias. The team consists of a number of experienced scientists and technicians: S. Harvey Moseley, Ari Brown, Ed Wollack, Karwan Rostem, Elmer Sharp and Steve Maher (NASA/GSFC); Gene Holton (NIST-Boulder); and Kent Irwin (Stanford University).

**Project highlight:**

We have designed all components needed to test the most crucial technical parameters required for the proposed delivery of a complete detector array. Production of test chips for metal interfaces and test detector arrays has begun.

## Background

The far-IR band is uniquely suited to study the physical conditions in the interstellar medium from nearby sources out to the highest redshifts. Incoherent superconducting bolometers are a high-sensitivity, Far-IR imaging and spectroscopy technology for many future suborbital and space missions, including the Origins Space Telescope (OST). Such missions require robust, high-sensitivity detector arrays with several $10^4$ pixels, high focal-plane filling factors, and low cosmic-ray cross-sections, operating over the entire far-IR regime.

These arrays could consist of smaller sub-arrays, if those are tileable. The transition-edge-sensor-(TES) based Backshort Under Grid (BUG) array architecture, which our group has fielded in a number of far-IR cameras, is a good candidate to meet these requirements: BUGs are tileable; and with the integration of the SQUID multiplexer, scalable beyond wafer sizes; they provide high filling factors (> 90% at 1-mm pixel pitch), and are designed to have low cosmic-ray cross sections. Individual BUG arrays have been demonstrated in the HAWC+ camera on SOFIA to provide background-limited performance for suborbital far-IR applications. However, the production of BUGs with integrated readout multiplexers has many time- and resource-consuming process steps. In order to meet the requirement of robustness and production efficiency for future arrays, we developed a new method to provide the superconducting connection of BUG detectors to the readout multiplexers or general readout boards behind the detectors. This approach should allow us to produce reliable, very large detector arrays for future far-IR missions.

## Objectives and Milestones

The aim of this project is to develop and streamline the fabrication processes required to produce background-limited large far-IR arrays with large pixel numbers (~$10^5$). We will achieve this goal by

combining mature detector and readout technologies from our previous work, to fabricate a robust, close-packed, high-sensitivity bolometer array with reliable high-quantum-efficiency absorbers that operates over the entire far-IR range, and can be efficiently and reliably produced. The simplified process will integrate detector arrays through superconducting bonds to a cold readout multiplexer. It is very versatile in its applications, since it will allow the mating of TES detectors to time-domain, frequency-domain, microwave, and code-division multiplexers.

The main objectives will be achieved by meeting the following goals:

a. Develop a novel BUG architecture in which the superconducting through-via process is separated from detector production, improving production speed and reducing risk; and
b. Produce background-limited 5-kilopixel arrays suitable for the far-IR spectrometer Super-HIRMES.

For the latter we will additionally:

c. Refine our AlMn process for quickly and reliably fabricating TES with highly predictable and uniform transition temperatures (less than 5% variation) across the entire wafer; and
d. Refine a standard process for reliably fabricating impedance-matched and robust absorbers for the entire far-IR wavelength range, which are not susceptible to room-temperature aging.

## Progress and Accomplishments

***1. Through-wafer vias*:**

The existing through-wafer via process involves placing the vias directly on the detector device wafers, which is extremely challenging technically. This is primarily because the vias need to be filled with a polymer that is planar with the silicon membranes to within a micron, so that subsequent micron-scale lithography is not compromised. In order to circumvent this challenge, we have moved the vias to a separate substrate (Fig. 1), which relaxes the tolerances on the lithography and greatly simplifies the detector fabrication process. Furthermore, in order to increase the through-wafer via fabrication throughput, we have not filled the vias.

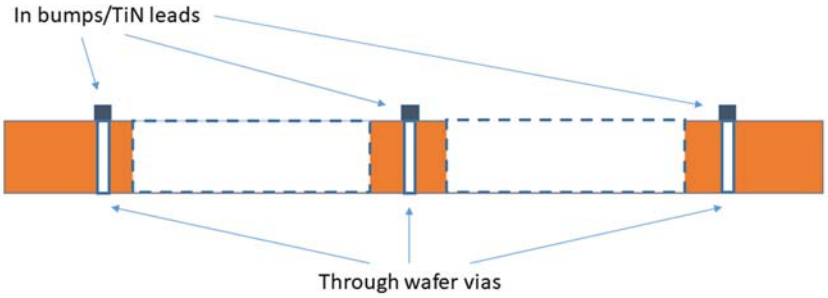


***Fig. 1.*** *Schematic of the through-wafer via substrate. The dashed rectangles are regions where the silicon will be removed so that light can pass through, which will be located directly below the optically active region of the bolometric detectors.*

The primary technical challenge associated with this new approach involves patterning superconducting traces and indium bumps on the through-wafer via substrate. We have addressed this challenge by developing two novel patterning processes.

The first process, used to etch metallic traces on a via-containing substrate, involves using a two-layer etch mask. The first layer consists of an anti-reflection coating and the second consists of a dry-film resist, which is laminated on the wafer. The dry-film resist is photolithographically patterned and the anti-reflection coating is reactive-ion etched. In contrast with a conventional spin-on resist, a dry-film resist can effectively cover the vias.

The second process, used to lift off the indium bumps on a via-containing substrate, involves using a two-layer lift-off mask. The first layer consists of positive photoresist and the second consists of a dry-film resist; and the lift-off mask is patterned in a similar manner as the etch mask described above.

Figure 2 shows the smallest features, 20 μm, which can be reliably patterned using the first process. If we conservatively allow for a 20-μm buffer region around the patterned features, in this case superconducting TiN leads, our novel process will permit fabrication of bolometric detector arrays with a BUG architecture and a filling fraction of ~94%.

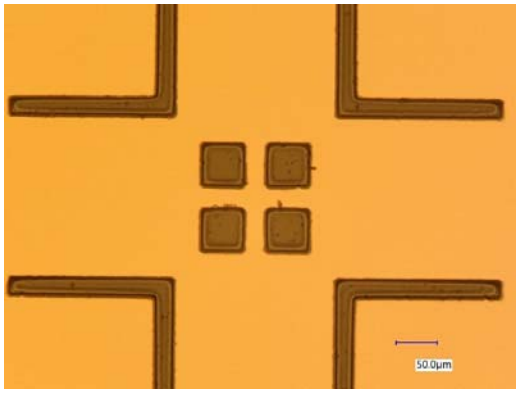


***Fig. 2.*** *Micrograph of a dry-film-resist etch mask.*

Figure 3 shows the smallest indium bumps, 20 μm, which can be reliably be lifted off a substrate containing through-wafer vias, our second process. As in the case of all patterned features fabricated on the through-wafer via substrate, the size of the bumps will limit the optical-filling fraction of the focal plane bolometric detector arrays. Bump placement μμcan be as close as 5 μm away from the vias, illustrating the versatility of this process.

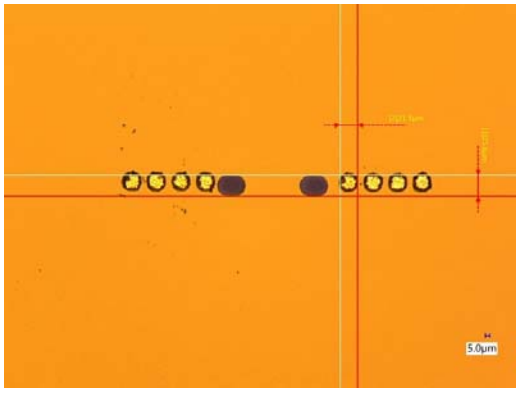


***Fig. 3.*** *Micrograph of two groups of four 4-μm tall indium bumps next to two through-wafer vias. The silicon wafer in which the vias were micromachined was ~0.4 mm thick.*

We have begun production of these test structures. We have also developed a novel metal-patterning process (Fig. 4). This process involves using a combination of laminated dry-film resist and sprayed-on positive photoresist to lift off traces from a wafer which contains through-wafer vias. This avoids the need of filling the vias, which is a high-risk process. It also avoids the need to use corrosive chemicals for patterning the metal.

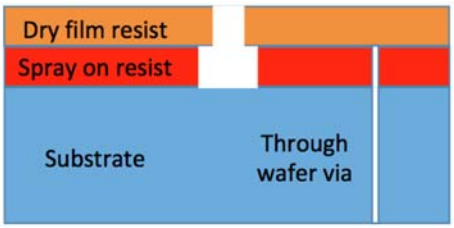


***Fig. 4.*** *Lift-off mask used to pattern metal on through-wafer via containing substrates.*

### *2. Metal-metal test chips:*

We have designed test boards to test all required metal-metal interfaces (e.g., In, $Mo_2N$, and TiN) and metal interfaces (e.g., $Mo_2N$/In, TiN/In) for superconducting transition temperature and critical current density. The boards also enable tests of In bumps with four different dimensions. There are 12 unit-cells on a single wafer.

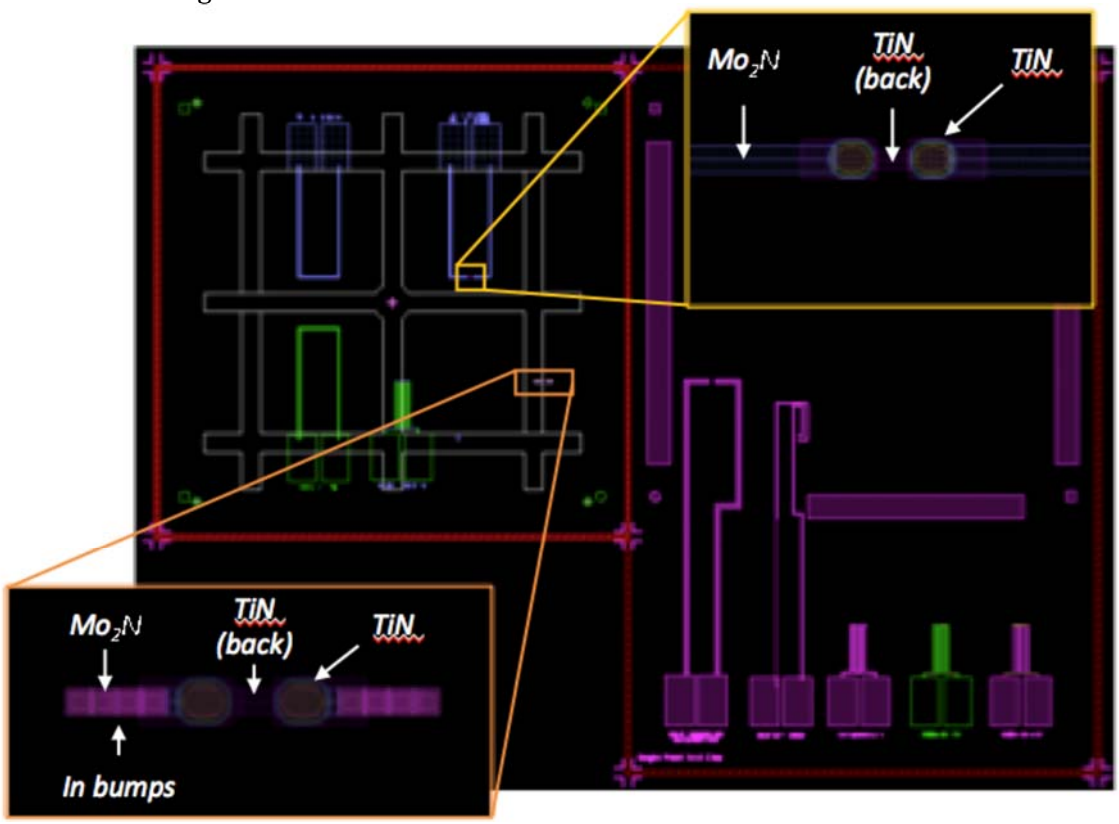


***Fig. 5.*** *Mask layout for a single "unit cell" test device. The die on the left can be flip-chip bonded onto the die on the right.*

### *3. Detector Array*

We have designed our first TES detector pixels which will provide us with the capability to test thermal conductance though the detector legs that provide the required sensitivity. The test chip also contains features that let us measure the thermalization within the membrane. Figure 6 shows an image of the test array, which will go into production soon. We decided to use either Molly-Silicite or Niobium-Silicyte. Patterning will be used to tune for the right impedance.

***Fig. 6.*** *Layout of the test array*

### *4. Detector landing wafer*

While we only proposed to mate the new detector to a SQUID multiplexer, we are also investigating a more flexible solution to mate the detector to a wafer that contains a fanout to any type of multiplexer. Figure 6 shows a sketch of the architecture used to connect a detector array with the (multiplexer-)readout chips. As shown, the wafer can be folded so that the chips will be behind the detector, allowing for tilability. Figure 7 shows how this scheme will look physically.

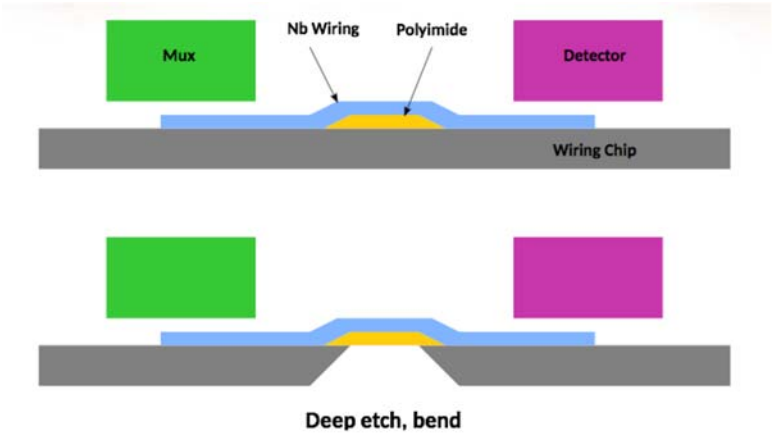


***Fig. 6.*** *With the ability to etch away a section of the wafer below the polyamide, part of the wafer can be flipped under the other part, positioning it under the array.*

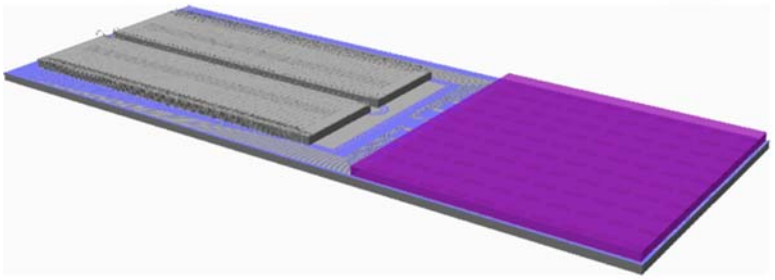

***Fig. 7.*** *CAD image of the wafer with detector array (right) and multiplexer chips (left). All connections are made with superconducting materials.*

## Path Forward

In the remainder of Year 1, we plan to:

- Develop a through-wafer via substrate fabrication process, refine double-bond hybridization; prepare for device tests; and
- Carry out a first iteration of detector fabrication and tests/characterization and deliver uWave SQUID multiplexers – completion timeframe: 12/2018

In Year 2, we will start production of the final flight array. Laboratory test measurements will be used to verify its performance.

**For additional information, contact Johannes Staguhn:** *johannes.staguhn@nasa.gov*

# High-Efficiency Continuous Cooling for Cryogenic Instruments and Sub-Kelvin Detectors

Prepared by: James Tuttle (NASA/GSFC)

## Summary

This is a three-year development effort, which began in January 2017. Its goal is to advance the Technology Readiness Level (TRL) of a multi-stage magnetic cooling system, which will continuously cool detectors to 0.05 K and reject heat to 10 K. The device, based on adiabatic demagnetization refrigerators (ADRs), will have high thermodynamic efficiency and will simultaneously cool optics continuously at 2–4 K. It will exceed the cooling requirements of all currently conceived future space missions with cryogenic detector arrays. With a heat-rejection temperature of 10 K, it will be compatible with recently demonstrated extremely-low-vibration mechanical coolers. Since ADRs have no moving parts, it will enable an essentially vibration-free 300-to-0.05-K cooling system.

The development team is a group of technologists at NASA/GSFC with a wealth of experience in spaceflight and laboratory ADRs. In fact, this group developed and demonstrated the technology being advanced here. During the first 18 months of this effort, they produced a designed-for-flight single-stage 10-to-4-K ADR and completed extensive performance testing on it. In addition, they made good progress on the design, fabrication, and procurement of parts, equipment, and supplies to make a second such stage. This was in preparation for assembly and testing of a two-stage 10-to-4-K continuous ADR in late 2018.

## Background

Several past, and many future, astronomical instruments require cooling to sub-Kelvin temperatures to obtain high sensitivity. Newer generations of detector arrays need several μW of cooling at temperatures of 0.05 K and lower. Previous long-life space missions used single-cycle cooling devices with modest cooling power, but these sub-Kelvin refrigerators are no longer adequate. As detector technology matures and array size grows larger, demand has increased for higher cooling power and lower operating temperatures. Presently, several astrophysics flagship mission concepts require cooling of large superconductor-based focal planes to sub-Kelvin temperatures, including the Origins Space Telescope (OST), Lynx, Probe of Inflation in Cosmic Origins (PICO), and Galaxy Evolution Probe (GEP). Instrument design studies for all these missions, including three different OST instruments, are currently incorporating our ADR technology in their designs. In addition, the development team for the Japanese mission, LiteBIRD, has expressed interest in this technology. Sub-Kelvin energy-resolving detectors would also enhance the Habitable Exoplanet Observatory (HabEx) and Large UV/Optical/Infrared (LUVOIR) mission concepts. High-cooling-power, high-efficiency, high-duty-cycle sub-Kelvin coolers are required for the next generation of sensitive instruments. Both Cosmic Origins (COR) and Physics of the Cosmos (PCOS) Program Annual Technology Reports (PATRs) listed sub-Kelvin cooling as technology gaps ("*High Performance Sub-Kelvin Coolers*" and "*High-efficiency cooling systems covering the range from 20 K to under 1 K,"* respectively).

Sub-Kelvin temperatures in space are produced by a combination of mechanical cryocoolers at the upper-temperature end and specialized sub-Kelvin coolers operating from a few K to less than 0.05 K. There are several ways to produce this low temperature: ADRs, dilution refrigerators, and a combination of sorption cooling and adiabatic demagnetization. An ADR, having a thermodynamic

efficiency close to Carnot, is the most efficient way to produce sub-Kelvin temperatures. It provides cyclic cooling by raising the magnetic field in a paramagnetic material, removing the resulting heat from the material, and then cooling it by reducing the field. Our team invented a method to produce high-heat-lift continuous cooling with a multi-stage continuous ADR (CADR). We demonstrated a TRL-4 CADR with 6.5 μW of continuous cooling at 50 mK, a significant improvement over the 0.7 μW cooling provided for about 40 hours per cycle on Astro-H/Soft X-ray Spectrometer (SXS). That CADR can alternatively provide 31 μW at 100 mK compared to the 0.2 μW of cooling achieved on Planck. The CADR rejects its heat to a cryocooler at temperatures as high as 4.5 K.

In addition to detector cooling, several proposed far-IR space observatories require telescopes to be at 2–6 K to limit self-emission. This is much colder than the ~30 K that can be achieved via passive cooling, as in the James Webb Space Telescope (JWST). This technology need is listed in the COR PATR ("*Advanced Cryocoolers*"). The combination of a highly reliable mechanical cryocooler reaching 10 K and a CADR cooling from 10 to 4 K will provide a low-input-power solution to fill this technology gap.

Many space observatories require extremely stable pointing. The CADR, which has no moving parts, is vibration-free, but it is just part of a cooling chain. Currently, the CADR rejects its heat at 4 K, limiting the choice of upper stage coolers to linear piston cryocoolers. Jitter caused by such coolers has been a problem for recent astrophysics missions. Miniature turbo-Brayton coolers offer a solution to this problem, as was demonstrated by the 70-K cooler for the Hubble Space Telescope (HST) Near Infrared Camera and Multi-Object Spectrometer (NICMOS) instrument. There are difficulties extending this technology to 4 K, but an engineering unit has recently demonstrated significant cooling power at 10 K. Thus, extending the CADR heat rejection temperature from 4 to 10 K will enable sub-Kelvin detectors in observatories with tight pointing requirements.

Figure 1 shows our full CADR schematically. The left side of the image is the four-stage 4-to-0.05-K CADR. The stages are thermally connected in series via heat switches. The first stage, on the very left, remains continuously at 0.05 K. The other stage temperatures rise and fall as the heat switches open and close in a sequence that pumps heat from the cold source to the continuous 4-K stage. The 10-to-4-K CADR is on the right side. It consists of two parallel stages, which alternatively cool the 4-K stage and warm up to just above 10 K to dump heat to the cryocooler. Each magnet in the system has its own ferromagnetic shield to minimize its stray magnetic field and to enhance the field inside the magnet bore. The entire system is surrounded by a second shield, which further reduces any field fluctuations caused by the magnets. Figure 2 (left) shows a preliminary conceptual design with the overall shield cut away for clarity, and (right) a cross-section of our designed-for-flight 10-to-4-K ADR stage. The 10-K magnet is shown inside its ferromagnetic shield, with the salt pill suspended inside the magnet bore.

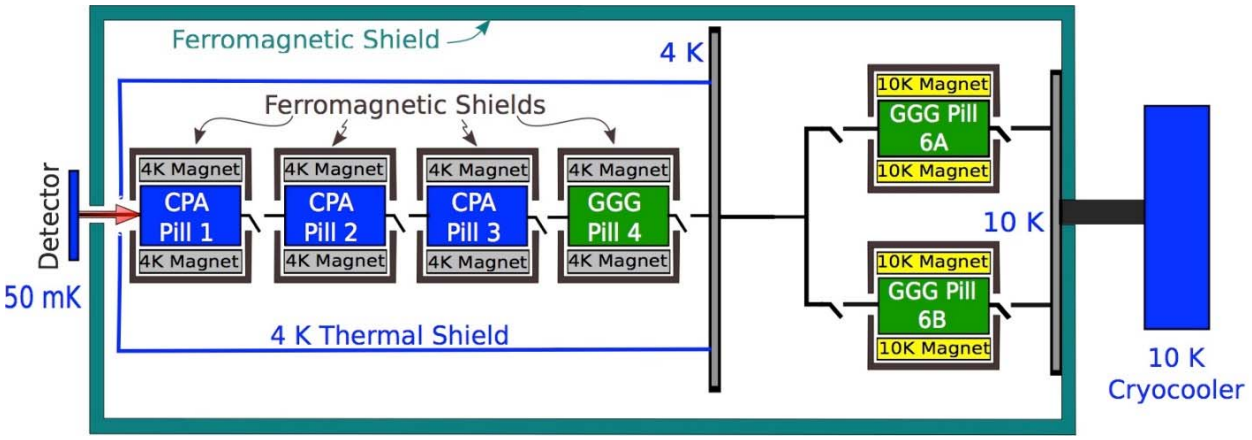


***Fig. 1.*** *A schematic representation of our 10-to-0.05-K CADR.*

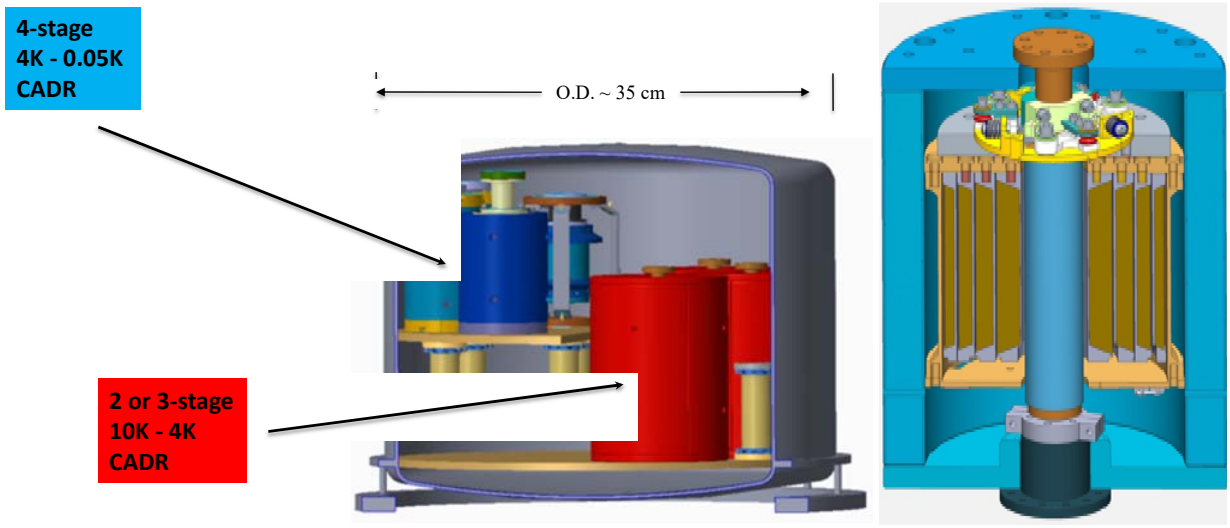


***Fig. 2.*** Left: *A preliminary layout of the full CADR with the overall magnetic shield and thermal straps cut away for clarity (OD, outer diameter).* Right: *A cross-section view of our designed-for-flight 10-to-4-K ADR stage. The 10-K magnet is shown inside its ferromagnetic shield, with the salt pill suspended inside the magnet bore.*

Our development plan is to demonstrate a single-stage 10-to-4-K ADR in Year 1, a two-stage 10-to-4-K CADR in Year 2, and a 10-to-0.05-K CADR in Year 3. In addition, we will develop an overall magnetic-shielding scheme which nearly eliminates any nearby field fluctuations caused by our CADR operation. The complete system will be tested before and after vibration to demonstrate TRL 6.

## Objectives and Milestones

Our first major milestone was met early in Year 2, when we demonstrated a single-stage 10-to-4-K ADR. This device includes a unique 10-K magnet, developed several years ago under NASA's Small Business Innovative Research (SBIR) program. It also includes a passive gas-gap heat switch configured to work from 10 to 4 K, a ferromagnetic shield for the magnet, a paramagnetic salt pill inside a metal can, and a thermally isolating suspension system for the salt pill.

By the end of Year 2, we will meet our second major milestone by demonstrating continuous cooling at 4 K using a two-stage 10-to-4-K CADR. This will include two shielded 10-K magnets with salt pills suspended in them, two passive and two active gas-gap heat switches, and thermal straps connecting the pills and switches. It will require a customized control algorithm to keep the 4-K temperature constant to within 0.001 K. The target cooling at 4 K will be greater than 20 mW.

By the end of Year 3, we will assemble a flight-worthy version of our laboratory 4-to-0.05-K CADR and integrate it with the 10-to-4-K CADR. The resulting 10-to-0.05-K CADR will be surrounded by an overall magnetic shield to keep external field fluctuations below 5 μT. Our third major milestone will be met in the third quarter of Year 3, when this assembly will be performance-tested, with a target of at least 5-μW of cooling at 0.05 K and better than 1-μK root-mean-square (rms) temperature stability at that temperature. We will then subject it to a vibration test chosen to envelope the acceptance levels expected for future cryogenic space missions. The final major milestone will be a successful post-vibration performance test by the end of Year 3.

## Progress and Accomplishments

During the period between mid-2017 and mid-2018, the team accomplished the Year-1 goal, and made significant progress on items required to stay on schedule in Years 2 and 3.

We fabricated parts and assembled a designed-for-flight single-stage 10-to-4-K ADR. Figure 3 (left) shows components of the salt pill assembly, and (right) the Kevlar suspension system used to hold this pill assembly inside the 10-K magnet. We installed the ADR in a cryostat and performed extensive testing on it in early 2018. Figure 4 shows the ADR before and after installation in the cryostat. In each test, we operated the ADR through a complete cooling cycle. First, we fully charged the magnet and waited until the salt pill cooled back to 10 K. Then, we rapidly lowered the magnetic field, bringing the salt pill to its operating temperature of 4 K. At this point we established a feedback control loop which slowly ramped down the magnetic field to keep the pill at 4 K until the field reached zero. At this point the "hold time" at 4 K was completed, and we ramped the magnet back up to its full field, beginning a new cycle.

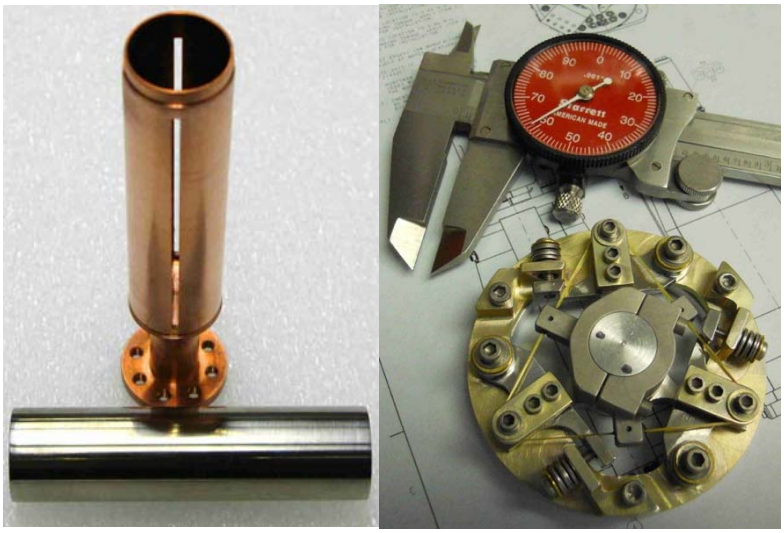

***Fig. 3.*** Left: *The copper housing which contains the salt pill in the 10-to-4-K ADR, and the stainless-steel shell which surrounds it.* Right: *A modular Kevlar-suspension element used to support the salt pill inside the 10-K magnet.*

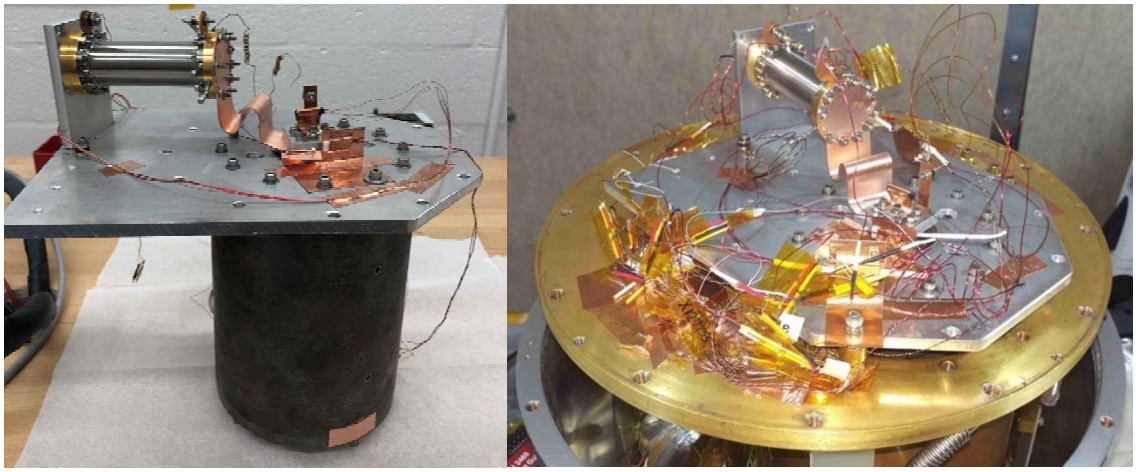

***Fig. 4.*** Left: *The single-stage 10-to-4-K ADR.* Right: *The ADR installed in a cryostat for testing.*

This was performed several times with different constant-power values applied (while at 4 K) to a resistive heater mounted on the salt pill. The parasitic heat load leaking into the salt pill from the 10-K stage exactly matched the calculated contribution from the open heat switch and the pill's isolating suspension system. Also, the pill was able to absorb 2.4 Joules of heat at 4 K, independent of applied power values within the range relevant for system performance. This indicates that our salt pill assembly remains isothermal even when absorbing the maximum power that it will see.

We then studied the speed with which we could re-cycle the ADR after its magnetic field reached zero. We used the maximum practical magnet ramp rate, and we were able shorten the cycle time by not waiting until the salt pill had cooled to 10 K. The 4-K cooling energy depends on the temperature at which we began the magnet's rapid de-magnetization. Thus, our tests provided a correlation between 4-K cooling energy and total recycle time. In our eventual two-stage continuous 10-to-4-K ADR, two identical stages will operate in parallel. While one stage holds the constant 4-K temperature, the other stage will be recycled. Thus, the 4-K hold time will be equal to the recycle time. The total 4-K cooling energy divided by the hold time is the maximum heater power that our two-stage ADR can absorb continuously, and calculations using our cycle data predicted a power of about 13 mW. Finally, we demonstrated that we could cycle in 132 seconds and then hold the pill at 4 K for 132 seconds while absorbing 13 mW.

The target cooling power for the 10-to-4-K CADR is 20 mW, of which less than 1 mW will be absorbed from the 4-to-0.05-K CADR subsystem. Our testing indicates that our existing design will fall short of that goal, and we performed extensive studies to determine the causes. One contributor is the heat capacity of the metallic parts which cycle between 4 and 10 K along with the salt pill. Of these, the stainless-steel fasteners and the thick stainless-steel flange on the heat switch's cold end are most significant. We expect to be able to increase our cooling capability by 1 – 2 mW by thinning this flange and switching to titanium fasteners.

We also discovered a subtle error in our performance prediction based on the published magnetization data for the gadolinium gallium garnet (GGG) salt. It turns out that for a cylindrical pill in a solenoid magnet, the magnetization is not uniform, and there is an effective de-rating of the salt's cooling performance. We updated our model to account for this, and it now predicts our measured performance quite well. We learned that other researchers in this field have made the same error, and we plan to publish our results with an explanation of this effect. We also started a parallel study of the feasibility of making salt pills from a different salt, gadolinium floride, with higher cooling capability per unit volume. This material is only available to us as a powder, however, so we would need to compress it into small pills to be stacked inside our copper salt pill bus. Depending on the thermal conductivity of the compressed powder, we might need to include some additional copper parts between the pills to enhance the heat conduction. Summer students are assisting us with this study, and it is independent of our baselined development effort.

Our team members performance-tested a 4-to-0.05-K CADR built for an external customer for laboratory use. This system used many components identical to those planned for use in our overall CADR, so the testing was very relevant to our planned activities in 2019. The test cryostat included a cryocooler which produces significant vibrations, and these got worse as the cooler's operational hours rose. When the vibrations were at their worst, significant heating was seen in the coldest two stages of the CADR. Temporarily shutting off the cooler eliminated this heating, confirming that the vibrations caused the heating. While this would not be expected for a space-flight cryocooler, it certainly impacted the lab testing of this particular CADR. We suspect that the heating occurs in the Kevlar strings used to suspend these stages, and we initiated a study to verify this. Summer students are assisting with this test, in which we have suspended a dummy mass and will vibrate it at cryogenic temperatures using a voice coil. Figure 5 shows a preliminary test configuration installed in a cryostat. Tiny thermometers installed at the midpoints of the Kevlar strings will measure any temperature rises due to vibration, and we will correlate these rises with any measured heat reaching the suspended mass. Preliminary testing at room temperature looks promising and indicates that we should be able to resolve the heating effects once the system is cooled to 4 K.

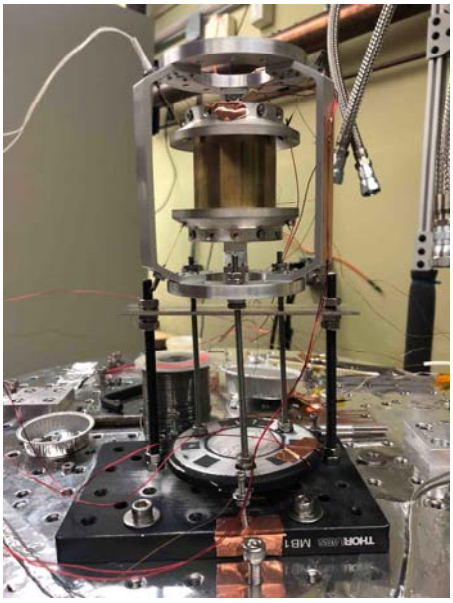

***Fig. 5.*** *An experiment which will study the heating of our CADR's low-temperature stages due to cryocooler vibrations.*

In parallel with this work, our team initiated procurement of the new 10-K magnets, and we expect the first to arrive this summer. We also procured nearly all the supplies and equipment needed for the remainder of the research effort. Most of the ADR parts needed for the 10-to-4-K CADR are already being fabricated by outside machine shops, and the remaining drawings will soon be submitted as well.

In July, 2017, we presented a paper describing this work at the Cryogenic Engineering Conference in Madison, Wisconsin. Our paper was well-received by the cryogenics community, and many conference attendees expressed support for this technology being available for future space missions. In May, two members of our team participated in a preliminary design study for the Origins Survey Spectrometer instrument being proposed for OST. The baselined cooling system for this instrument includes our 4-to-0.05-K subsystem, providing another potential customer for this technology.

## Path Forward

In the second half of Year 2, we will produce a second stage for the 10-to-4-K CADR and integrate it with the existing stage. We will performance-test the CADR to meet our Year-2 milestone. In parallel, we will continue to fabricate parts needed for the 4-to-0.05-K CADR in Year 3, as well as the overall magnetic shield. In Year 3, we will proceed with our original development plan, as described above.

**For additional information, contact James Tuttle:** *james.g.tuttle@nasa.gov*